AD NUMBER

AD280809

NEW LIMITATION CHANGE

TO

Approved for public release, distribution unlimited

FROM

No Foreign

AUTHORITY

DTRA Ltr., 6 May 99

AD 280 809

10 October 1962

TRANSMISSION AND SCATTERING PROPERTIES OF THE LOS ANGELES, CALIFORNIA ATMOSPHERE IN AUGUST AND SEPTEMBER 1960

by
E. R. Schleiger
J. R. Nichols
F. I. Laughridge

U.S. NAVAL RADIOLOGICAL DEFENSE LABORATORY
SAN FRANCISCO 24, CALIFORNIA

USNRDL-P7463

RADIATION EFFECTS BRANCH
R.S. Alger, Head

NUCLEONICS DIVISION
W.E. Kreger, Head

This research supported by the Defense Atomic Support Agency.

Requests for copies of this report should be submitted to ASTIA, Arlington Hall Station, Arlington 12, Virginia.

ADMINISTRATIVE INFORMATION

I. Background of Work

During the past several years, this Laboratory has prosecuted a project "Measurement of Attenuation Parameters for Real Atmospheres" sponsored by the Defense Atomic Support Agency (formerly Armed Forces Special Weapons Project). The primary objective of this project was to measure the attenuation coefficients for thermal radiation reaching a target from a 4π source, and the secondary objective was to determine the angular scattering diagrams of real atmospheres for radiation in the visible and near infrared regions of the spectrum as a function of wavelength and atmospheric properties.

II. Authorization and Funding

This work was authorized by the Defense Atomic Support Agency under RD 30 59, WEB No. 12.007 and funded under Budget Project 99 allotment 178 60 and 61. Details of this work can be found in the U.S. Naval Radiological Defense Laboratory FY 1961 Technical Program as Program A-2, Problem 7.

III. Description of Work

During FY 1959 equipment was designed, fabricated, and used to determine the radiation attenuating properties of clear atmospheres at the Nevada Test Site. In FY 1960 the equipment was modified and measurements made in atmospheres with overcast cloud conditions at the same location. In FY 1961 after further equipment modification, measurements were made in the summer atmospheres of Los Angeles, California. The results of the FY 1961 measurements and a discussion relating them to the earlier NRDL studies are contained in this report.

Eugene P. Cooper
Eugene P. Cooper
Scientific Director

E.B. Roth, CAPT USN
Commanding Officer and Director

ABSTRACT

Measurements of peak irradiances have been made in Los Angeles, California, nighttime atmospheres at distances from 0.90 to 6.77 statute miles from a Xenon flashlamp radiating uniformly in all directions. The measurements were made at wavelengths 0.40, 0.50, 0.77 and 0.88μ (microns) with receiver fields of view up to 64 degrees half-angle. From these data attenuation coefficients were calculated for collimated transmission and aureoled transmission (4π source and flat receiver facing the source). Also calculated for aureoled transmission were values of R, the ratio of "scattered-in" radiation to direct radiation received by the flat receiver at various distances from the source. Angular scattering diagrams and attenuation coefficients for scattering were measured for radiation of wavelengths 0.40, 0.45, 0.50 and 0.55μ. Relations between these optical characteristics of the atmosphere and meteorological characteristics such as visibility, relative humidity, and contaminant contents were examined. Investigations of transmission variability with respect to both time and space were made. Curves were prepared from these and other experimental data showing transmittances of four typical atmospheres as a function of range for the case of flat receivers and radiation from a 4π black body source at 6000 degrees K.

SUMMARY

The Problem:

The amount of thermal radiation delivered to a given receiver from the fireball of a nuclear explosion depends on the transmittance of the atmosphere as a function of wavelength, the spectral distribution of the radiation, the receiver field of view, the range, the albedo of the terrain, and the amount and height above the ground of clouds present. The purpose of this experiment was to determine the range of transmittance values of the Los Angeles nighttime atmosphere during the months of August and September 1960.

The Findings:

A Xenon flashlamp 4π source and mobile photomultiplier receivers with adjustable fields of view and filters are used to determine attenuation coefficients for collimated transmission and aureoled transmission (4π source and flat receiver) and for calculating R, the ratio of "scattered-in" to direct irradiance, at source-receiver distances ranging from 0.90 to 6.77 statute miles. A polar nephelometer is used to obtain angular scattering diagrams and attenuation coefficients for scattering for radiation of wavelengths 0.40, 0.45, 0.50 and 0.55μ in the Los Angeles nighttime atmosphere. For 26 test nights during August and September 1960, 50% of the measured attenuation coefficients for collimated transmission of 0.50μ radiation are in the range 0.52 to 0.88 $mile^{-1}$; 50% of the measured attenuation coefficients for aureoled transmission of 0.50μ radiation are in the range 0.32 to 0.58 $mile^{-1}$. Values of R are found to increase with distance on both clear and cloudy nights with one exception in which clouds at 1,000 feet are accompanied by a maximum in the R versus distance curves for radiation of wavelength 0.77 and 0.88μ. Weak correlations are found between attenuation coefficients and visibility, and between attenuation coefficients and the contaminants NO_2, CO, and particulate matter (K_m).

ACKNOWLEDGMENTS

The authors express their thanks to the following who actively participated in the experimental work of the project and without whose efficient assistance and many helpful suggestions the measurements could not have been made: M. J. Boone, C. P. Butler, R. J. Jenkins, E. W. Jones, W. J. Parker, and R. L. Rudkin. Thanks are also due Professor Gilbert F. Kinney of the Naval Postgraduate School at Monterey, California, who assisted in the analysis of absorption data, J. E. Stone AT-1, USN, who participated in equipment preparation for the experiment, and C. F. Smith and R. W. Westover, who assisted in data reduction. Permission to reproduce the Mt. Wilson photograph of Sirius was kindly granted by Dr. I. S. Bowen of the Mt. Wilson and Palomar Observatories.

The performance of these measurements in a metropolitan area required the cooperation and assistance of many governmental agencies, private organizations and individual citizens. In all cases, this assistance was provided in a most generous manner, and although the persons concerned are too numerous to be individually named, their help is most gratefully acknowledged. Special mention is due the staff of the Los Angeles Air Pollution Control District who provided contaminant data and valuable advice, United States Weather Bureau personnel at the Los Angeles International Airport and at the Los Angeles downtown station who furnished daily weather sequences, and the management and staff of radio station KRKD for making available a site for the light source and providing electrical power for its operation. During the experiment and throughout the preparation of this report, Dr. M. G. Gibbons and W. J. Parker contributed many valuable suggestions concerning both experimental procedures and theoretical considerations. Their assistance is greatly appreciated.

CONTENTS

LIST OF TABLES

LIST OF ILLUSTRATIONS

REPORT OF INVESTIGATION

INTRODUCTION

Experimental measurements of nighttime transmission of visible and near infrared radiation from a 4π source to an uncollimated receiver have been made during recent years in the San Francisco Bay Area, in the San Joaquin Valley and in Yucca Flat at the Nevada Test Site.[1,2,3,4] This report describes the results of similar measurements made at night in Los Angeles, California, during August and September of 1960.

EXPERIMENTAL ARRANGEMENT

The equipment used in this investigation was essentially the same as that described in the report of the Nevada Test Site Study of February 1960.[4] A few modifications were made to meet new operating requirements of the Los Angeles area and to remedy deficiencies which became apparent during the previous study.

Two types of measurements were made. Transmission of the atmosphere was measured by means of a 4π light source and two mobile receiving stations. Angular scattering characteristics were determined by a polar nephelometer.

The 4π radiation source was a General Electric FT-617, Xenon-filled flashlamp flashed automatically at 2 minute intervals by discharging through it a 1200 mfd capacitor charged to a potential difference of 3750 volts. The flash duration was approximately 5 milliseconds. Figure 1 shows the lamp as mounted on top of the one-ton panel truck which was substituted for the trailer used in the Nevada Test Site experiments. The controls and power supply system for the lamp were contained inside the truck.

Measurements of irradiance at different distances from the lamp were made by two mobile receiving stations (Figure 2) each mounted in a Metro-type van.

The measuring system used in each receiving station consisted of a photomultiplier with auxiliary apertures and filters and an oscilloscope with vertical amplifier input connected across the photomultiplier load resistor. The peak height of the photomultiplier current pulse produced by the light flash was measured by observing the resulting oscilloscope trace. Earlier investigations[1] showed that the peak height of the trace is just as satisfactory as the area under the trace as an indication of the amount of energy from the light flash incident on the photomultiplier. The oscilloscope was triggered by the action of the same light flash on an E. G. G. fiducial marker focused on the light source. The fiducial marker contains a sensitive photomultiplier and thyratron circuit which produces a trigger pulse at the very beginning of the light flash. Oscilloscope deflections for each lamp flash were observed visually and recorded by the observer.

The field of view "seen" by the photomultiplier in each detector was limited by a fixed artificial horizon and by adjustable stops above the horizon with semi-circular apertures. The aperture sizes could be varied to permit fields of view of 4, 8, 16, 28, 44, and 64 degrees half-angle. In addition to the apertures, the field-of-view device was equipped with a removable occulter, also semi-circular in shape, but subtending only 2 degrees half-angle. The occulter was used to blank out the central portion of the field of view and thus eliminate the line-of-sight radiation from the source. A sighting telescope was used to point the field-of-view device at the source. Tests made during the study indicated that the sighting method could center the source in the aperture system with a tolerance of ± 1/2 degrees half-angle. Four different photomultiplier-filter combinations were used to provide irradiance measurements in four different spectral regions centered at 0.40, 0.50, 0.77 and 0.88 microns. The two shorter wavelength spectral bands were obtained with a Dumont 6292 photomultiplier (S-11 surface) and Wratten filters No. 39 and No. 65. The two long wavelength bands were obtained with a Dumont 6911 photomultiplier (IR surface) and Wratten filters No. 16 and No. 87. Figure 3 contains four curves showing the product obtained for each photomultiplier-filter combination response when multiplied by the estimated spectral distribution of the flash lamp output. The filter transmissions and photomultiplier responses used in these curves were from manufacturers'

data. The spectral distribution assumed for the lamp is that shown[5] in the literature as typical for a high voltage Xenon lamp. It is recognized that the operating voltage (3750 volts) used on the project lamp is higher than that used for the referenced data. However, in the absence of more applicable data the referenced distribution curve has been used. The chief effect of increased operating voltage at this range would be to shift the minimum in the lamp's spectral distribution curve towards longer wavelengths. This shift would have only negligible effects upon the shape of the combined curves for the two filter-photomultiplier combinations having the shorter wavelength responses. In the case of the two longer wavelength combinations the effect of the shift would be to narrow the band width somewhat without affecting the location of the peaks.

The Pritchard polar nephelometer described earlier[3,4,6], was again used to determine angular scattering characteristics of the Los Angeles atmosphere. This instrument measures the intensity of light scattered from a collimated beam at angles ranging from 10 to 170 degrees at 5 degree intervals--the angles being measured from the forward direction of the beam. Wratten filters 39, 47, 65, and 16 used in the nephelometer in combination with a Dumont K-1448 photomultiplier tube with an S-11 surface made it possible to obtain the above mentioned scattering data for four different spectral bands of widths approximately 0.2 μ and peaks at wavelengths of 0.40 μ, 0.45 μ, 0.50 μ, and 0.55 μ.

Figure 4 shows the location of the light source and the observation stations which were used during the experiment. The numbers which are shown with each station identification indicate the distance in statute miles between station and light source (left hand number), and the station elevation in feet (right hand number). In this report the word "mile" will be understood to mean statute mile.

The particular area used for the tests was selected because it was believed to be the area most likely to have the heavy nighttime haze and smog through which the measurements were desired. The light source was located on the top of a hill adjoining radio station KRKD in Highland Park, approximately 3 miles NE of downtown Los Angeles. Figures 5 and 6 show a panoramic view of the test area as seen from the source. This source location was chosen because it was centrally located and high enough to be seen from many places in the area but low enough so that it would be within the haze layer most of the time. It furthermore fulfilled other important requirements in that it was easily accessible by automobile, had available electric power (thus obviating

the use of the gasoline powered generator), provided an area for safe daytime storage of the truck, and was far enough removed from private homes so that the flashing light would not be considered objectionable by neighboring residents. The sites for the observation stations were selected so as to provide several stations along each of three different lines or ranges radiating out from the source. The Highland Park range extending NE from the source included the four stations Southwest Museum, Springvale, Poppy Peak, and Kenworthy; the Los Angeles River range extending NW from the source included the four stations Fernleaf, Allesandro, Cadman, and Griffith Park; the downtown Los Angeles range SW of the source included the three stations Lacy, Elysian Park, and Ft. Moore.

The Highland Park and Los Angeles River ranges were quite similar topographically -- both being located in shallow valleys. The more distant stations in both of these ranges were situated in areas which were less densely populated than those surrounding the central stations. The downtown Los Angeles range extended over a relatively flat terrain bounded on one side by the hills of Elysian Park. In general, the nighttime haze in the downtown area appeared to be somewhat more severe than that in the other two areas, but the difference was never obviously great and in many cases could not be detected at all. One local smoke source was apparent - an incinerator approximately one-half mile southwest of the Lacy station which was in operation six nights of the week. Although smoke from the incinerator stack was often observed, there were no clearcut indications that it caused anomalous results. On those occasions when the incinerator was shut down during the course of a test run, comparisons between data taken before and after the shutdown gave no indication that the incinerator had a significant effect. On a few nights when irradiance measurements were being taken at the Lacy Street station, wind shifts brought the smoke down to the ground in the immediate vicinity of the truck, but even in these conditions there was no apparent effect on irradiance levels. It is therefore believed that although the smoke from this source undoubtedly contributed to the overall haze condition, it had no localized effects on irradiance measurements which would distort the attenuation calculations.

Figures 7 through 13 show views of the source as seen from several of the observation stations. The sites for the observation stations were, for the most part, vacant lots or public grounds which provided a direct line of sight to the light source, with a minimum of obstructions and interfering light sources within the 64 degree half

angle field of view. The availability of such locations in a metropolitan area such as Los Angeles is not great and so it was found necessary to use a few sites in which the field of view was not completely clear of obstructions. These obstructions, however, filled only a small percentage of the field and were not of a highly reflecting nature as can be seen from typical examples in Figures 10 and 11. It is believed that their effect was negligible.

EXPERIMENTAL AND DATA REDUCTION PROCEDURES

The procedures used in this study were, in general, the same as those used and discussed in previous reports.[3,4] The following sections summarize the methods and describe in some detail any procedural changes that were made.

At any given station, with any given photomultiplier-filter combination, peak irradiance values from successive light flashes were measured with various fields of view with and without the occulter. Figure 14 shows photomultiplier response plotted as a function of field of view in two typical runs -- one with and one without the occulter. The fields of view used in these runs were typical of the procedures followed in the preliminary phase of the investigations. As is discussed below, this procedure was changed somewhat for the latter part of the experiment. The photomultiplier response is expressed as the peak value of the photomultiplier current pulse produced by the light flash as observed on the oscilloscope trace. The data represented by the lower set of points in Figure 14 were obtained with the 2-degree half-angle occulter in place to blank out the direct or line-of-sight radiation. Thus the curve which has been drawn through these points represents all of the "scattered-in" radiation except for that portion blocked out by the 2-degree occulter. For this reason the curve has been drawn to intercept the X-axis at field of view 2 degrees half-angle. The "scattered-in" radiation which was blocked out by the occulter can be restored by raising the observed curve to pass through the origin as shown by the dotted line. The dotted line curve when extrapolated to the 90-degree half-angle field of view gives the irradiance due to the scattered-in radiation which would be received from the 4π source by a flat receiver or target. This is called I_{sc}, the irradiance due to "scattered-in" radiation, and is represented by the plotted triangle.

The upper set of circles in Figure 14 show irradiance values without the occulter in place and thus include both the direct or line-of-sight radiation and the "scattered-in" radiation. The scatter of

these points and their poor fit to the shape of the lower curve are the results of fluctuations in atmospheric transmission of the direct portion of the radiation. The curve which has been drawn through the upper set of points lies above the lower dotted curve by an amount equal to the average irradiance resulting from the direct radiation. Thus the intercept of this upper curve at 0 degrees field of view is called I_d and represents the irradiance due to direct or line-of-sight radiation. The extrapolated value of this curve at the 90-degree half-angle field of view represents the irradiance due to both the direct and the "scattered-in" radiation which would be received from the 4π source by a flat receiver or target. This irradiance value is called I_{tau}, the aureoled irradiance. Both I_d and I_{tau} are plotted as triangles on the upper curve.

From the examination of many such curves obtained during the preliminary runs in the Los Angeles area, it became apparent that the "scattered-in" irradiance curves had characteristics in common which could be used to simplify data taking. The lower portion of the curve from 0 to 4 degrees field of view was for all practical purposes straight and the slope of the curve gradually decreased as the field of view increased. More specifically, the average slope between 64 and 90 degrees half-angle was estimated to be 0.7 of the slope from 44 to 64 degrees half-angle. Assuming these characteristics to apply to all curves made it possible to extrapolate the "with-occulter" responses to the 90-degree half-angle field of view from data taken at only the 4, 44 and 64-degree half-angle fields of view. Irradiance measurements without occulter (direct plus "scattered-in") were necessary at only the 64-degree half-angle field of view since the vertical separation of the curves (I_d) could be determined by an average of readings at any desired field of view. The reduction in the required number of fields of view made it possible to take a larger number of readings at each field of view. This result was believed highly desirable in view of the variabilities of the Los Angeles atmosphere. Accordingly, the following schedule of observations was used for each photomultiplier-filter combination: 64, 64, 64, 64, 64_o, 64_o, 4_o, 4_o, 44_o, 44_o, 64_o, 64_o, 64, 64, 64, 64 degrees half-angle, where the subscript o indicates that the 2-degree half-angle occulter was in place. The large number of 64-degree readings with and without occulter were taken because these were the most important readings in establishing the I_d and I_{tau} values, and also because the 64-degree readings without occulter customarily had a wide spread. As was indicated above, the 4-degree readings with occulter and the assumed X-axis intercept at 2 degrees half-angle field of view were used to establish the amount the curve should be raised to restore the "scattered-in" radiation

blocked out by the occulter. The 44-degree reading with occulter was used in conjunction with the 64-degree reading with occulter to establish the curve slope for extrapolation to 90 degrees half-angle field of view. Beginning and ending each run with a series of 64-degree half-angle field of view readings made it possible to evaluate the over-all constancy of the atmospheric transmission characteristics during the run. In several cases marked changes in atmospheric conditions were detected by comparisons of these readings. In such cases the data were discarded since extrapolation of the curve of irradiance versus field of view pre-supposes constant atmospheric conditions over the time period during which the data were taken.

Data taken over the same time period by each of the two mobile receivers located at two different stations make possible the determination of I_d and I_{tau} values for the same photomultiplier-filter combination at two different distances from the source. Knowing I_d for a given wavelength at distances D_1 and D_2 from the source make possible the calculation of the attenuation coefficient σ_t for that wavelength as follows:

$$\sigma_t = \frac{1}{D_2 - D_1} \ln \frac{(I_d)_1 D_1^2}{(I_d)_2 D_2^2}$$

Where $(I_d)_1$ and $(I_d)_2$ are the direct irradiance values (described above as I_d) at distances D_1 and D_2 from the source; the D_2^2 and D_1^2 terms are introduced to remove the inverse square effect of distance on irradiance; and σ_t is the sum of the absorption coefficient and scattering coefficient applicable to a collimated beam in which attenuation occurs as a result of absorption and scattering out. This method of computing σ_t from irradiance measurements at only two stations differs from that previously used.[3,4] In the earlier studies the quantity $\ln I_d D^2$ was plotted as a function of D where I_d was the measured irradiance (direct radiation) at each of the observation stations -- as many as eight or nine different observation stations being used in a single night. The negative slope of the straight line connecting these plotted points was then taken as σ_t for the atmosphere concerned. In order that this slope method be valid there should be no appreciable changes in optical characteristics of any part of the atmosphere being measured during the entire test period. In the Los Angeles atmospheres such constant conditions did not often last for the required several hours. Using the above described two-station method, data for the determination of σ_t could be obtained in 32 minutes for a given photomultiplier-filter combination. Thus on each test night in Los Angeles the general

procedure was to make several σ_t determinations for each of the wavelengths concerned. Each σ_t value obtained was representative of the atmosphere between the two stations being used for the particular half hour during which the data were taken. On most nights all of the attenuation measurements were made at a single pair of stations although on some occasions two pairs of stations were used.

The procedures described above have all referred to σ_t determinations. The attenuation coefficient σ_{tau} for the case of aureoled transmission, that is, for the case of a 4π source and a flat receiver, was calculated in the same manner using the irradiance I_{tau} instead of I_d. The measuring data used to compute I_{tau} were obtained at the same time as those used to compute I_d and thus each σ_{tau} value has a companion σ_t value representative of the same atmosphere. It should be pointed out that in the method used to compute σ_{tau} it is assumed that σ_{tau} is independent of distance. From preliminary measurements made in Los Angeles at four distances from the source (maximum 6.77 miles) it was found that the points obtained from a plot of $\ln I_{tau}D^2$ versus D lay on a straight line within the limits to be expected under the conditions of atmospheric variability which prevailed during the experiment. Earlier experiments [3,4] in the desert atmosphere indicated the same independence of σ_{tau} with respect to D for distances up to approximately 17 miles. The same results were found for the relationship between $\ln I_dD^2$ and D and thus the coefficient σ_t has also been assumed independent of distance -- an assumption which is generally made in the literature.

Since the calculation of σ_{tau} or σ_t required that comparisons be made between irradiances measured by photomultiplier systems in the two different trucks it was necessary to have a calibration factor expressing the ratio between sensitivities of the two systems.[3,4] This factor was obtained experimentally by locating the two trucks side by side and making simultaneous determinations of I_{tau} and I_d for each photomultiplier-filter combination in the two trucks. The ratios between the I_{tau} obtained by a system in one truck and the I_{tau} obtained by the same photomultiplier-filter system in the other truck were used to normalize the I_{tau} irradiance value obtained on one system to that of the other. In the same manner a normalizing factor was found for the I_d measurements. The calibration process was repeated approximately once each week and average factors determined at the end of the test period. A discussion of the deviations of the calibration factors is contained in a later section of this report. Checks made in an earlier study[3] showed that the angular response of the photomultiplier-filter combinations differed slightly from a cosine dependence on incident angle. Corrections for this non-cosine angular response have also been made in all calculations.

Polar nephelometer data were taken at least once each evening. The data were usually taken at one of the receiving stations, although on several nights a series of readings were taken on the rooftop of the Air Pollution Control District Building in order to check correlations between atmospheric contamination and atmospheric scattering. The nephelometer data were used to construct angular scattering diagrams and to calculate σ_{sc}, the attenuation coefficient due to the scattering out of the light in a collimated beam. The angular scattering diagram is a plot of $B(\phi)/B(10^{o})$ versus ϕ where $B(\phi)$ is a quantity proportional to the volume scattering function of the atmosphere concerned. The volume scattering function is in turn defined as the amount of radiation scattered per unit solid angle in the direction ϕ per unit irradiance and per unit volume of the beam. The attenuation coefficient due to scattering was calculated from an integration of the scattering function over all angles. A more detailed description of the methods used in these two processes has been given in an earlier NRDL report.[3]

It should be pointed out that both the angular scattering diagrams and the σ_{sc} values are representative of the local atmosphere during the short time period in which the nephelometer readings were taken - whereas the attenuation coefficients obtained from data with the flash lamp and receivers are representative of a much larger atmosphere over a much longer time period.

Meteorological data were furnished to the project by U. S. Weather Bureau personnel and consisted of temperature, relative humidity, visibility, cloud cover, and wind data at the Los Angeles International Airport and Burbank Airport; temperature and relative humidity reports from the downtown Los Angeles office; and upper air data (temperature, relative humidity, and inversion height) from the Santa Monica soundings. The locations of these sources are shown respectively by the letters A, B, C, and D on the insert map of Figure 4. Atmospheric contaminant data provided by the Los Angeles Air Pollution Control District consisted of the results of measurements of the following contaminants at the downtown Los Angeles station: NO, NO_2, CO, SO_2, O_3, total oxidant, and particulate matter. Standard methods of chemical analysis were used for the contaminant measurements except for the particulate matter (particles smaller than 40 microns) which was determined by an optical reflectance method.[7] The K_m unit in which the particulate content is expressed is defined as

$$K_m = 10 \log_{10} \left(\frac{R_o}{R}\right)$$

Where R is the reflectance of a white filter paper of 1 cm^2 area through which 1 m^3 of the air under test has been passed and R_o is the reflectance of the filter paper before the air has passed through it.

TEST RESULTS

Weather and Contaminant Data

Table 1 shows details of the weather and contaminant data reported during each nightly test run. The entries are believed self-explanatory except that a comment should perhaps be made on the column labeled "Test Range." The visibilities in this column are estimates which were based on observations made by the operators of the receiving station, observations made from the light source location at the beginning and end of the test period, and the Meteorological Range which was computed from the measured σ_{sc} by the expression[8]

$$MR = \frac{3.912}{\sigma_{sc}}$$

The reliability of nighttime estimates of visibility is always open to question even when made by trained meteorological observers under the best of conditions. The values shown as range estimates are no exception to this statement. It is believed that they can be satisfactorily used to provide visibility trends during a single night and even from one night to another. Their absolute values, however, should be considered only as indicating a general range. Tolerances of ±40% should probably be assigned to these visibility estimates.

Attenuation Coefficients

Figures 15 through 18 show the individual σ_t values obtained on each of the test nights--each sheet containing the data for a single wavelength. Figures 19 through 22 and 23 through 26 show the same sort of presentation of σ_{tau} and σ_{sc} respectively. The encircled points are values obtained with clouds over the test range. From these data have been constructed the histograms of Figures 27 through 29 showing the number of values falling within consecutive σ intervals of width 0.10 $mile^{-1}$.

Attenuation coefficients for absorption (σ_{abs}) were calculated as the numerical difference between σ_t and σ_{sc}.[3,4] Results are shown in Figure 30 for the wavelength 0.50μ. The numerical values of these absorption coefficients are believed to indicate order of magnitude

only. There are two reasons for this lack of confidence. First, the magnitude of σ_t and σ_{sc} are not appreciably different and thus σ_{abs}, the difference between them, will contain magnified effects of the uncertainties in either σ_t or σ_{sc}. Second, the σ_{sc} value for any given wavelength is representative of a given point in the atmosphere over a short period of time, whereas the σ_t value is determined by over-all atmospheric conditions between light source and receiver over approximately one-half hour, and thus the difference of these two quantities would be representative of atmospheric absorption only if the atmosphere were uniform with respect to space and time--a condition which did not often exist during the study.

It should be noted that the attenuation coefficient values shown in these data (Figures 15 through 30) are representative of atmospheric conditions ranging from very clear (visibility 15+ miles) to heavy haze and/or light fog (visibility 3 miles). Also included are several nights in which clouds were over the range. Table 2 is a tabulation of the various operating nights by general weather classification types.

From the data of Figures 15 through 26 it will be seen that there appears to be a somewhat cyclic pattern in the attenuation coefficients consisting of a gradual increase in coefficients from the beginning of the test period to a maximum on 19 August, a rapid decrease to minimum values on 22 August followed by two more cycles of gradual increases followed by sharp decreases to minimum values on 4 September and again on 21 September. Partial explanations of this cyclic behavior can be seen from the data of Tables 1 and 2. The night of 22 August, on which the first minimum in σ values occurred, had low stratus cloud overhead, but of greater importance was the atmospheric clarity below the clouds (visibility estimated 8 miles). The "scattering-in" effect of the low clouds is believed of secondary importance since the σ_t and σ_{sc} values, neither of which should be affected by the presence of a cloud cover, are also very low on this night. The next minimum in σ values which occurred on 4 September is very readily explained by a markedly clear atmosphere with very good visibilities. Actually the difference between the observed visibilities of 22 August and 4 September is greater than would be indicated by a comparison of the attenuation coefficients for those two nights. A possible explanation of this discrepancy is that the downtown atmospheres in which the attenuation coefficients were measured may not have differed much from one another on the two nights in question, but the over-all atmospheric conditions outside the rather small measuring area on 22 August were not as clear as those of 4 September, thus producing the difference between observed visibility conditions. The relatively low σ_{tau} values on 21 September are

believed to be at least partially the result of a "scattering-in" effect of the low clouds reported on that night, since the σ_t and σ_{sc} values did not show as marked a decrease as the σ_{tau}. The nights during which noticeably high values of σ_{sc}, σ_t, and σ_{tau} occurred (16, 18, 19, 26, and 27 August) were nights with low visibilities and, in the case of 26 and 27 August, low clouds as well.

The relatively large number of zero values for σ_t and σ_{tau} at $\lambda = 0.88\mu$ (Figures 18 and 22) actually includes a number of negative values. The largest negative values obtained were $\sigma_t = -0.20$ and $\sigma_{tau} = -0.21$ mile^{-1}, but most of them were in the range 0 to -0.10 mile^{-1}. The -0.20 and -0.21 mile^{-1} values were obtained on a night when some difficulties were encountered because of photomultiplier saturation by a very bright moon and so may not be true values. The small negative values are believed to have no significant physical meaning other than to indicate that in the atmospheres concerned the attenuation for the 0.88μ wavelength was so small that the measuring method could not reliably detect the difference between the irradiance level at the two different stations. Later sections will deal with this estimated precision at greater length.

The tendency of most of the histograms to show a double peak frequency distribution is believed to be a result of the weather pattern consisting of periods of stagnation during which the attenuation coefficients are relatively high followed by occasional periods during which the circulation pattern is such that the stagnant air is swept out and continuously replenished by cleaner, drier air in which the attenuation coefficients are relatively low. The change from one type of period to another takes place in a relatively short time and so the bulk of the attenuation measurements were made in one or the other type of atmosphere.

Because of the nature of the frequency distribution patterns of attenuation coefficients it was felt that the calculated average value would have little significance. Central halves of the distribution range were therefore established for each of the σ's as is shown on the histograms. Los Angeles visibilities for which the upper and lower limits of the σ_{tau} central ranges are typical are estimated to be 6 and 12 miles respectively.

Correlations Between Attenuation and Atmospheric Characteristics

In collimated atmospheric transmission measurements the attenuation coefficients are usually found to correlate well with observed

visibility. Since σ_{tau} is the most significant attenuation coefficient in transmissions in which a 4π source and flat receivers are considered, a plot of σ_{tau} versus estimated visibility has been prepared in Figure 31. The σ_{tau} values at $\lambda = 0.50\mu$ have been selected since of the spectral bands used, it is nearest the wavelength at which the spectral distribution curve of a nuclear weapon is a maximum. It will be noted that although the correlation is not as clear cut as might be hoped, there is a general grouping of the largest coefficients toward the smallest visibilities and vice versa. The points inclosed in circles are for data obtained when clouds were overhead. The arithmetic mean of σ_{tau} values for each visibility is shown by an x, and the dashed line has been drawn to fit these mean values. The visibility shown as 15+ miles was for the night of 4 September, an exceptionally clear night. The fact that three of the four σ_{tau} values were higher on that night than they were for some other nights with poorer visibility has no obvious explanation. It is possible that during the early part of the night there was sufficient residual haze in the downtown area to affect the measured attenuation coefficients but because of the rapid clearing in the outlying districts the over-all visibility was better than that indicated by the coefficients themselves. The fact that the last coefficient obtained that night was appreciably lower than the earlier values lends some credence to this explanation.

Attempts to relate σ_{tau} values to atmospheric relative humidity were not successful. Figures 32 and 33 show σ_{tau} versus surface relative humidity (downtown Los Angeles) for two wavelengths, and are typical of all data. Figure 34 shows σ_{tau} versus relative humidity aloft. The humidity aloft values are averages of surface humidity and humidity at the 800-ft level (elevation of the source). The 800-ft relative humidities were obtained from the Santa Monica upper air soundings taken at 1700 and 0500 hours PDST, linear interpolations between the morning and afternoon soundings being used to estimate the relative humidity values at the time of the attenuation measurements. Some correlation was found to exist between σ_{sc} and the Los Angeles surface relative humidity for all four wavelengths (Figure 35) and is of the expected form, that is, σ_{sc} increasing with relative humidity.

Figures 36, 37, 38 and 39 are plots of σ_{tau} at wavelength 0.50μ versus various measured contaminants. The data have been plotted at four different ranges of relative humidity in order to minimize any masking effect that varying relative humidity might cause. It will be seen that with the exception of the high humidity groups there can be found some slight increase in σ_{tau} with increasing contaminant content for the NO_2, K_m, and CO data, but no apparent relationship

with ozone content. The effect of the NO_2 can probably be expected because of the relatively high absorption of this gas for visible radiation.[9,10] Increasing particulate matter (K_m) should also be expected to increase atmospheric attenuation although the absence of detailed information concerning the constituents and size distribution of the particles makes impossible any more specific comments. CO has no significant absorption in the visible ranges and would not be expected to attenuate by scattering. Its relation to σ_{tau} is probably merely an indication that the conditions favorable to haze formation are also favorable to increasing CO content. The ozone amounts were so low at night that they are probably of no significance as indicators of optical characteristics of the atmosphere.

The reported contaminants of the Los Angeles atmosphere which might contribute to the absorption coefficient for light of wavelength $\lambda = 0.50\mu$ are ozone, nitrogen dioxide, and particulate matter. Chappius band absorptions were calculated for the observed ozone concentrations using reported [11,12] absorption coefficients for ozone at $\lambda = 0.50\mu$ but were found to be negligible. The reported nitrogen dioxide contents during the testing hours ranged from 0 to a maximum of 0.1 ppm. Absorption coefficients shown in the literature[9,10] indicate that a nitrogen dioxide content of 0.1 ppm could cause an attenuation coefficient due to absorption as great as 0.17 $mile^{-1}$. Thus the nitrogen dioxide appears to be a factor in atmospheric absorption, especially in view of the reported increase of the oxides of nitrogen with elevation in the Los Angeles atmosphere.[13] However, the plot of σ_{abs} at wavelength 0.50μ versus nitrogen dioxide shown in Figure 40 does not indicate any significant correlation between the two--probably because of the previously mentioned difficulty in obtaining representative σ_{abs} values from the data of this study. The difference between the path lengths of the "scattered-in" and direct radiation also complicates evaluation of the absorption process.

Evaluating the optical importance of the particulate contents (particles smaller than 40μ) in the Los Angeles contaminants is difficult because the value reported is not an absolute content and furthermore is not broken down into various constituents.[7] Typical values of particulate contents in the Los Angeles atmosphere shown in the literature vary widely[13,14,15] but according to Magill[15] the carbon and metal particles could account for 10 to 50% of the observed visibility decrease. More precise determinations of absorption coefficients and much more detailed contaminant analyses than were obtained in this experiment would be required for adequate investigation of this feature of the atmospheric contaminants.

Ratio of "Scattered-in" to Direct Irradiance

Figures 41 through 45 show relationships between R and the distance from the source, where R is the ratio between "scattered-in" irradiance and direct irradiance. In order to simplify the presentation, the data are shown only for wavelengths 0.40 and 0.88μ. The numerical R values for the intermediate wavelengths in almost all cases were found to lie between the values obtained for 0.40 and 0.88μ. It should be noted that different vertical scales have been used on the various sets of curves.

In Figure 41, R values have been plotted for 30 August, a night with relatively low visibilities and high R values. The large increase in R which took place between runs 1 and 3 (approximately 3 hours time differential) reflects the visibility reduction and attenuation coefficient increase which occurred during that time interval. Figure 42 is for 5 September, a night with high visibility and low attenuation coefficients. Here again the R values increased noticeably between the first and last runs of the test period. Figures 43, 44 and 45 are for 22 August, 27 August, and 7 September--all nights in which clouds formed or materially increased during the test period, thus providing a possibility of evaluating cloud effects. This evaluation of the modifying effect of the clouds can be made by comparing, for a given wavelength, the R curve obtained on the early run (before cloud formation) with the R curve obtained on the late run (after cloud formation). In making this comparison, however, consideration must be given to the changes which normally occurred in R between the early and late runs when cloud was not present. Thus on 22 August (Figure 43) although the values of R at a given distance for a given wavelength are somewhat higher after cloud formation than for an earlier run without clouds, the increases in R with clouds are not much different from the increases which were usually found as the night progressed on cloudless nights. The same comments can be made for the effects of the broken cloud at an estimated 1,000 ft on 27 August and the overcast cloud at 16,000 ft on 7 September (Figures 44 and 45, respectively), except that on 27 August the R versus distance curve for cloudy conditions and wavelength 0.88μ was found to have a maximum at a distance between 2 and 3 miles from the source. The 0.40μ wavelength curve also evidences some cloud effect on the same night, in that it is straight instead of tipping upward like the curve for the corresponding wavelength before cloud formation.

Clouds were present on four other nights but for the following reasons no attempts have been made to judge the influence of the clouds.

On 21 August the clouds were so variable in amount that no consistent pattern of effects could be expected. On 26 August low broken to overcast clouds formed but transmission characteristics were so variable on this night that reliable evaluations of cloud effect were not possible. On 8 September there were thin high clouds during one run, but the coverage was too small to be significant. On 21 September low clouds (broken to overcast) were present during the entire test period. Thus comparisons between cloudless and cloudy conditions could not be made for this night. Maxima were not observed in any of the R versus distance curves on this night.

The absence of any effect of high cloud on R as shown in Figure 45 was also observed in the desert experiments.[4] The variability of the low cloud effect on R was not expected, however. A possible explanation of it may be found in the nature of the low clouds themselves--which consisted of patches of high fog blown in from the ocean. The thickness and spacing of the clouds was quite variable and the cloud bottoms were very ragged. These are both characteristics which might be expected to produce variable results insofar as their light scattering effects are concerned.

Atmospheric Angular Scattering Diagrams

As indicated in the description of test methods, polar nephelometer runs were made on most of the nights during the investigation. The data thus obtained were used primarily for determinations of the coefficients of attenuation by scattering (σ_{sc}). The scattering diagrams which were plotted from these data were similar in shape to those found by other investigators for comparable atmospheres[3,4,5,6,7] -- that is, large ratio of forward scattering to back scattering and a minimum in the scattering function at an angle of approximately 120 degrees (measured from the forward direction of the projected beam). Figures 46 and 47 show angular scattering diagrams for several different Los Angeles atmospheric conditions. In Figure 46 are plotted the diagrams for three different nights, all with wavelength 0.50μ. The atmosphere in which the data for the 16 August curve were taken would probably be described as having light fog. The σ_{sc} value at this time and location (Southwest Museum) was computed from the nephelometer data to be 2.17 $mile^{-1}$. Measurements of transmission by the two-station method were discontinued that evening at about the same time because of the rapidly changing conditions. The value σ_t for wavelength 0.40μ was found to be 1.10 $mile^{-1}$ approximately one-half hour previously. Relative humidity was unfortunately not measured at the nephelometer site. The recorded value at the downtown Los Angeles station was 90%. The 4 September

curve was obtained in a dry, clear atmosphere with relative humidity 53% and a measured σ_{sc} value of 0.22 mile^{-1} at wavelength 0.50μ. The 22 September curve is for a moderately hazy atmosphere with relative humidity 71% and a σ_{sc} value of 0.50 mile^{-1} at wavelength 0.50μ. The three curves clearly show the effect of increasing humidity in increasing the ratios of forward scattering to back scattering. In Figure 47 have been plotted three angular scattering diagrams obtained at approximately one-half hour intervals on 22 September on the rooftop of the Air Pollution Control District building in downtown Los Angeles. This series of nephelometer data was taken to facilitate correlation between scattering coefficient and the conteminant measurements which were being made at the same building. However, since there was no very significant change in contaminants during the test period, no attempt has been made to relate the curve shapes to contaminant counts. Relative humidity values showed an increase during the night which is reflected by increasing ratios of forward scattering to side scattering and back scattering, as well as increasing values of σ_{sc}.

As was mentioned earlier, nephelometer measurements were made at four different wavelengths -- 0.40, 0.45, 0.50 and 0.55μ. The ratios of forward-to-backward scattering were generally found to increase with wavelength in agreement with the findings of others.[3,4,6] As was suggested by Gibbons,[3] a possible explanation of the nature of this wavelength dependency is that with increasing wavelength the relative contribution of molecular and small particle scattering to total atmospheric scattering decreases rapidly. Thus with increasing wavelength the increase in relative importance of large particle scattering (which is characterized by large ratios of forward to back scattering) has a greater effect than the reduction in the ratio of forward to back scattering which occurs for any given particle size.

Variability of Transmission

A well known optical characteristic of the earth's atmosphere is its variability--with respect to both time and space. This variability takes two general forms--variations in refractive index and variations in aerosol. Shimmer, twinkle, and scintillation which plague the astronomical observer as well as the surveyor are the result of rapid small-scale variations of the air's index of refraction along the observer's line of sight--the variations in refractive index occurring because of atmospheric turbulence primarily of a thermal nature.[18,19,20] The so-called heat waves seen above heated surfaces are a familiar example of refractive index fluctuations. Figure 48 gives an example of these effects. This photograph shows the collecting mirror of an

astronomical telescope as it was illuminated by a star with exposure time approximately 1/25 second. If the atmosphere were homogeneous the mirror would be uniformly illuminated instead of displaying the striations which result from refractive index variations. Variations in the type, size, and number of light-scattering and light-absorbing particles of the aerosol lead to another type of fluctuation in atmospheric transmission both with respect to time and space. These variations of the aerosol would appear to result from local topographical features and small scale meteorological phenomena.

The optical characteristics of the Los Angeles atmosphere were found to vary widely with respect to both time and space--the time variations occurring in the form of rapid unpredictable variations as well as in the form of gradual trends extending over several hours. Examples of the relatively slow moving changes can be seen in the plots of individual values of attenuation coefficients obtained during one night (Figures 15 through 26). Manifestations of the more rapid changes and the spatial fluctuations are found in the consecutive irradiance measurements of the unprocessed data. In order to obtain specific examples of these, several nights were devoted to measurements designed to show the variations in the optical characteristics of the Los Angeles atmosphere. The measurements were of two general types; namely, those made at a single observation station and those made simultaneously at two different stations.

Fluctuations in irradiance levels at four different points at a single observation station were observed by mounting four photomultiplier tubes in an arrangement so that they could be spaced at distances from each other varying from 4 inches to 11 feet. The photomultiplier tubes used were the same types as those used in the truck-mounted field-of-view devices, but for this experiment the tubes were removed from the trucks and mounted in small boxes with circular apertures providing fields of view of approximately 14 degrees half-angle. Two different combinations of filter and photomultiplier were used--one giving a peak response to the lamp output at 0.40μ, the other at 0.77μ. Voltage supplies and detection systems used were those of the observation trucks. The general procedure was to set the photomultiplier tubes and filters in the desired array, all four facing the light source, and then record the observed signals of each tube for at least fifteen consecutive lamp flashes. This process was then repeated with other desired array systems. The average of the responses was taken for each of the four filter-photomultiplier combinations in the array and a normalizing factor determined and applied to the individual responses so that the four averages would be identical, thus eliminating

the effects of tube sensitivity. Cross comparisons were then made between the normalized responses of the four combinations for each lamp flash. Figure 49 shows the four different arrays used at a single station. Table 3 shows random fluctuations of the normalized responses for one of the four different arrays as observed at the Griffith Park station on 20 September. In Figure 50 the average differences between the individual normalized responses are shown for all four arrays used on 20 September. The Griffith Park station was the most distant used in the study. Similar data obtained at shorter distances from the source displayed the same types of variations, but on a smaller scale.

Several conclusions can be drawn from Table 3 and Figure 50.

a. At a distance of 6.8 miles from the source the output from a single flash produces widely varying irradiance values at slightly separated points.

b. Over the range of separations tested (4 inches to 11 feet) the average variations between responses at different points do not change with amount of separation.

c. For 4-inch separations between detectors the variations along a horizontal plane are not significantly different from those along a vertical plane.

d. Average variations in irradiance at two separated points are much greater at wavelength 0.77μ than for wavelength 0.40μ.

The observed point-to-point fluctuations are more reasonably explained by refractive index fluctuations due to turbulence than by inhomogeneities of atmospheric particle size and distribution since the latter would require the existence of atmospheric cells of well defined boundaries having small areas normal to the line of sight and long dimensions parallel to it.

The apparent wavelength dependency of the variations is probably due to the fact that a larger fraction of "scattered-in" radiation in the 14-degree half-angle field of view is contained in shorter wavelengths. Since the effects of refractive index fluctuations (or atmospheric inhomogeneities) are averaged out in the "scattered-in" radiation, the shorter wavelengths should experience smaller magnitude fluctuations.

A second type of variability study was made by comparing irradiance values obtained from two different observation stations--the two stations

being located at approximately the same distance from the source but in different directions from the source. For these comparisons one observing truck was set up at each station and irradiance readings taken for a series of flashes. The photomultiplier-filter combinations and fields of view were the same as those used in the normal attenuation runs and the same calibration constants previously described were used to remove the effect of different sensitivities in the two truck systems. Since the two stations were not at exactly the same distance from the light source, additional corrections for inverse square attenuation and atmospheric attenuation were applied to the response at one of the two stations before direct comparisons were made between the responses at the two stations. The inverse square correction factor was simply the quotient of the squares of the two distances. The atmospheric attenuation correction was made by using an assumed attenuation coefficient based on measured values from comparable nights. Figures 51 through 62 show results of these comparisons. Figure 51, for example, shows relative irradiance values for wavelength 0.40μ at the Springvale and Ft. Moore stations for the night of 13 September. These data, and all other data in these comparisons, are for a field of view of 64 degrees half-angle, without occulter. Thus the irradiance values being compared represent both direct and "scattered-in" irradiance. The time interval between consecutive flashes was 2 minutes. However, between flashes 4 and 13 a time interval of 18 minutes elapsed (other readings were being taken during this period). The time interval between runs was only a few minutes. It will be noted that during the first two runs shown in Figure 51 the Ft. Moore irradiance values are significantly higher than those at Springvale but the difference between the two is far from uniform. During the first part of run 4 the differences between the two stations were negligible but 18 minutes later the irradiance levels at both stations were much lower and continued to decrease at Springvale while starting to increase again at Ft. Moore. Comparisons between the same stations for the 0.50μ and 0.77μ wavelengths (Figures 52 and 53) show similar fluctuations. In Figure 54, which shows the comparison for the longest wavelengths (0.88μ), the previously established relations are reversed, the atmosphere between source and Ft. Moore showing greater attenuation than that between source and Springvale. Figures 55 through 62 are comparisons between irradiance levels at the Allesandro and Ft. Moore stations for two consecutive nights. In these cases the shorter wavelength radiations again experienced significantly smaller attenuations in the atmosphere between the source and the Ft. Moore station than in the comparison atmosphere between source and the Allesandro station. For the longer wavelengths there is no consistent pattern of difference

except for the 0.88μ radiation on 17 September (Figure 58) in which case the Ft. Moore atmosphere displayed greater attenuation than the Allesandro atmosphere.

In describing the comparisons it was mentioned that an attenuation correction was made by use of an assumed attenuation coefficient. To insure that the comparisons were not being distorted by improper values of this correction, several calculations were made with various assumed values of coefficient. The results showed that the differences between the irradiances at the two stations could not be explained by any reasonable change in this coefficient. The effect of errors in the calibration factor used to correct for differences between instrument sensitivity in the two trucks was also examined. The average deviation from the mean in the series of weekly calibrations ranged from 5 to 9 percent for the four filter-photomultiplier combinations. The differences between irradiance levels at the two stations are for the most part larger than could be explained by calibration factor errors of this order of magnitude.

It thus appears that the differences between relative irradiance levels at the two stations are the result of real differences in the atmospheres intervening between the light source and the stations. To gain some idea of the magnitude of these differences in terms of attenuation coefficients, reference is made to the Ft. Moore-Allesandro comparison used in the above example of 17 September, wavelength 0.40μ, run 1, flash 13 (Figure 55). Assuming that σ_{tau} for the atmosphere between source and Ft. Moore had the value 0.33 $mile^{-1}$, the σ_{tau} value for the atmosphere between source and Allesandro would have to be 0.45 $mile^{-1}$ in order to produce the observed difference in relative irradiance level. This magnitude difference in σ_{tau} for the two areas is not at all unreasonable.

The wavelength dependency of these comparisons indicates that on the nights concerned the atmosphere between source and Ft. Moore in downtown Los Angeles apparently contained particles whose attenuating effects on the near infrared were noticeably greater than those of the particles in the other two atmospheres. The possibility of water vapor effects on these comparisons was considered by assuming relative humidity and temperatures of the Ft. Moore and Allesandro atmospheres to correspond to those recorded on 18 September for downtown Los Angeles and Burbank, respectively. The precipitable water contents in the two paths were calculated from these data to be 19.2 and 16 cm, respectively. The selective water vapor absorptions for these two water contents for the infrared window II (0.94 to 1.13μ) differ by only a few percent[21]

and thus there appears to be no possibility of differential water vapor absorption causing the observed irradiance differences. Aerosol particle distribution offers a much more plausible explanation since the relation between the extinction cross-section of a water droplet and the wavelength varies greatly with the droplet size--the term "extinction cross-section" being defined as the ratio between the luminous flux scattered by the droplet and the illuminance on the droplet.[22] For example, droplets of radius 0.8μ have an extinction cross-section for radiation of wavelength 0.88μ which is approximately 1.5 times as large as for radiation of wavelength 0.50μ but droplets of radius 0.5μ have an extinction cross-section for 0.88μ radiation which is only 0.7 times that for 0.50μ radiation.[23] Persistent differences between the aerosol spectrum of the Ft. Moore area and that of the Springvale-Allesandro area could undoubtedly account for the greater near infrared attenuations of the Ft. Moore atmosphere.

Reliability

Precise evaluations of the reliability of the data presented in this report are not easily made. The usual precautions were taken to minimize instrumental error. All electronic components were serviced and checked before, during and after the project. Oscilloscope calibrations were checked periodically during the experiment. The alignment between each field-of-view device and its sighting telescope was checked at the end of the first month of testing and was found satisfactory. Steady state photomultiplier current outputs were measured during periods of unusually large background lighting or if the data gave indication of saturation effects. At one station (Cadman Street) it was found necessary to mask a streetlight which caused saturation of one of the photomultipliers. To the greatest extent possible, preliminary processing of data was accomplished as taken in the trucks so that such sources of error as incorrect filter settings, field-of-view adjustments, and gain controls could be immediately detected and rectified. The best indication of instrumentation reliability is probably the series of calibration constants which represent the ratio of responses of companion equipment in the trucks as obtained by parking the two trucks side by side and observing the same light flashes. These calibrations were obtained weekly for each photomultiplier filter combination and for both aureoled and direct transmissions. Over the entire test period the average deviation from the mean for any given filter-photomultiplier combination ranged from 6 to 9 percent for direct transmission and from 5 to 9 percent for aureoled transmission. The effect which a 7 percent error in calibration factor would have on the calculated attenuation coefficient

varies with the magnitude of the attenuation coefficient and with the distance between test stations. Taking two actual runs as examples with σ_{tau} values of 0.20 and 0.81 mile^{-1} it was found that a 7 percent change in calibration factor would cause changes of 15 percent and 8 percent, respectively, in the calculated σ_{tau} values.

A second source of unreliability is the change in atmospheric transmission that occurs during the approximately half hour required for the accumulation of data for a given filter-photomultiplier combination. The data taken during this period establish the shape of the curve showing response versus field of view. Any atmospheric changes that occur during the time that the shape of the curve is being determined will affect the total aureoled transmission when the curve is extrapolated to the full 2π field of view and will affect the collimated transmission when the curve is extrapolated to the zero field of view. Persistent changes during a given run could be detected by comparing measurements taken at the beginning and end of the run with the same field of view, and if the changes were significantly large the data concerned were discarded. Short-lived atmospheric changes which did not last through the length of a run would not, however, be detected by this method but could still have an effect, especially since both observation stations would probably not experience the same changes. As was mentioned earlier, a series of eight readings without occulter and with field of view 64 degrees half-angle were taken with each filter--four at the beginning of the run and four at the end. To obtain some concept of the magnitude of the short-time changes, the average percent deviations from the arithmetic mean were calculated for these values for each run on eight typical nights--four nights with high attenuation coefficients and four with low coefficients. The overall averages of these deviations (expressed as percent of the arithmetic mean) for the eight nights were 6% for wavelengths 0.4 and 0.5μ, 8% for wavelength 0.77μ, and 7% for wavelength 0.88μ. The effects which errors of these magnitudes would have on calculated values of σ_t and σ_{tau} were also examined for several typical runs and were found to vary widely--the smallest being a 3% change in a σ_t value of 1.32 mile^{-1}, the largest being an 80% change in a σ_{tau} value of 0.03 mile^{-1}.

Considering the above factors it is estimated that the individual attenuation coefficients determined in this experiment have precisions ranging from $\pm$0.15 mile^{-1} for the large coefficients to $\pm$0.03 mile^{-1} for the small coefficient values.

These estimates describe the reliability of a given coefficient with respect to that particular segment of the nighttime Los Angeles

atmosphere being measured. The degree to which the given values represent the entire area is much more difficult to evaluate. Values of attenuation coefficients for collimated transmission between 0.23 and 0.55 microns have been measured for the Pasadena area by Dunkelman.[24] Values shown in his report for $\lambda = 0.40\mu$ in the month of September 1949 range from 0.64 to 1.77 $mile^{-1}$. Corresponding visual ranges calculated from the attenuation coefficients at $\lambda = 0.55\mu$ were 12 and 3.5 miles respectively. Figure 27 of this report shows the frequency distribution of σ_t, which is the coefficient corresponding to Dunkelman's collimated measurements. It will be noted that the central half range of the frequency distribution for σ_t at wavelength 0.40 μ lies within the range of Dunkelman's values. However differences were often observed between visibilities in the test area and those reported at nearby Burbank, and obvious differences in haze conditions in various parts of the area are often apparent. The general impression that was obtained during the experiment was that nighttime haze was less pronounced in the outermost regions of the test area except perhaps in the direction towards the ocean. Thus it is believed that the attenuation coefficients measured in this study represent the maximum nighttime values for the entire area for the time period concerned with the possible exception of the areas subject to frequent coastal fog.

Atmospheric Transmittance Curves

The four solid curves of Figure 63 have been prepared to show calculated transmittances of four typical atmospheres for the case of flat receivers and radiation from a 4π radiating black body source at $6000^{\circ}K$. The atmospheres are typical of those in which this study was performed and those at the Nevada Test Site where two earlier investigations were made by a group from this Laboratory.[3,4] Also shown in Figure 63 for comparison purposes are the four dashed curves from Figures 3-5A and 3-5B of TM 23-200.[25]

The characteristics of the atmospheres concerned were as follows:

a. Curve 1, Nevada desert atmosphere in February, clear skies, estimated visibility 65 miles, and water vapor content 3.5 g/m^3 (corresponds to 0.32 cm of precipitable water in a 1000-yard path length).

b. Curve 2, Nevada desert atmosphere in May, clear skies, estimated visibility 35 miles, and water vapor content 2.8 g/m^3 (corresponds to 0.25 cm of precipitable water in a 1000-yard path length).

c. Curve 3, Los Angeles, California, atmosphere in August and September, clear skies with light haze, estimated visibility 12 miles and water vapor content 11.8 g/m^3 (corresponds to 1.08 cm of precipitable water in a 1000-yard path length).

d. Curve 4, Los Angeles, California, atmosphere in August and September, clear skies with moderate haze, estimated visibility 6 miles and water vapor content 13.0 g/m^3 (corresponds to 1.19 cm of precipitable water in a 1000-yard path length).

In order to calculate the transmittance values the radiation spectrum of the black body was divided into 13 bands as follows: five bands corresponding to infrared windows II through VI,[21] four bands in the visible and near infrared representing the four photomultiplier-filter combinations used in this study, and four ultraviolet bands from 0.22 to 0.36μ. At any given range in a given atmosphere the transmittance value T was calculated as the sum

$$T = \sum_{i=1}^{13} T_i R_i$$

where T_i represents the atmospheric transmittance value in the i^{th} spectral band and R_i represents the fraction of the 6000°K black body radiation contained in the same band. The individual values of T_i used in the visible and near infrared bands were calculated from the experimental attenuation coefficients (σ_{tau}) obtained in these studies. In the infrared windows beyond 1μ T_i was calculated from water vapor absorption and extrapolated values of σ_{tau}. The water vapor absorptions were calculated from published data[21] relating infrared absorption and precipitable water--the latter being obtained from relative humidity and temperature records compiled during the project. The extrapolation of σ_{tau} from experimental data was made by the expression

$$\sigma_{tau} = C\lambda^{-0.7}$$

The exponent -0.7 is that which was previously suggested[26] for the wavelength dependency of σ_{sc} in the infrared region. The justification for the use of this value in extrapolating σ_{tau} into the infrared is that σ_{tau} is essentially the difference between a "scattering-out" and a "scattering-in" process and may therefore be expected to have a wavelength dependency similar to that of σ_{sc}. In the ultraviolet

bands, T_1 for the desert atmosphere was calculated from collimated attenuation coefficients shown in the literature[24] for the same desert area. A "scattered-in" correction was applied to the collimated coefficients by subtracting from them a value numerically equal to one-half the Rayleigh scattering coefficient. The numerical values subtracted ranged from a minimum of 0.06 $mile^{-1}$ for the ultraviolet band centered at 0.34μ to a maximum of 0.45 $mile^{-1}$ for the ultraviolet band centered at 0.23μ. In the Los Angeles atmospheres the attenuation coefficient for each ultraviolet band was the sum of an extrapolated σ_{tau} plus a calculated absorption by oxygen and ozone. The extrapolation used was a straight line extrapolation of a plot of ln σ_{tau} versus wavelength, where the σ_{tau} values were the Los Angeles experimental results obtained on those days selected as typical for the visibility and moisture conditions for which the curves were drawn. The difference between the TM 23-200 curves and those based on the experimental attenuation data is believed to be caused by the relatively low height of the source in the NRDL experiments which, as was explained by Gibbons,[3] results in an atmospheric attenuation somewhat between that of the air burst and surface burst curves of TM 23-200.

SUMMARY AND DISCUSSION OF NRDL ATMOSPHERIC ATTENUATION EXPERIMENTS

This report covers the last of five NRDL experimental investigations of attenuation properties of several different atmospheres. The previous investigations were in the San Francisco Bay Area,[1] San Joaquin Valley (ground to air measurements),[2] and at the Nevada Test Site.[3,4] In the first study[1] the emphasis was on the ratio between irradiance received from a 4π source by a flat receiver and that received by a collimated receiver. Using data obtained for wavelengths ranging from 0.40 to 0.9μ the above defined ratio for wavelength 0.55μ was estimated to have a maximum of 1.9 at a distance of 7 miles for an atmosphere with a 12-mile visibility. The presence of broken to overcast clouds was found to approximately double this figure. In the second study[2] the ground-to-air measurements were made in hazy atmospheres with approximately 10 miles visibility. From these measurements the ratio of "scattered-in" radiation to total radiation (wavelength 0.5μ and 45 degree half-angle field of view) was found to vary from 0.06 at 4000-ft range to a maximum of 0.165 at 12,000-ft range, then decreasing to 0.133 at 16,000-ft range. Longer wavelengths gave smaller ratios. For example, with $\lambda = 0.90\mu$ the ratios ranged from 0.038 at 4000 ft to 0.046 at 16,000 ft. The next two experiments were made at the Nevada Test Site - one in clear skies in May 1959[3] and the second in both clear and cloudy conditions in February 1960.[4]

In these two experiments a polar nephelometer was used to determine σ_{sc}, the coefficient for attenuation by scattering only. Measurements of σ_t, the total attenuation coefficient for collimated transmission, σ_{tau}, the total attenuation coefficient for aureoled transmission, and R, the ratio of "scattered-in" to collimated irradiance were also made. Table 4 has been prepared to provide a very brief comparison of the data obtained in the various experiments. For applications involving thermal radiation from a nuclear weapon the attenuation experienced by aureoled transmission (4π source and flat receiver) is of greatest interest. Thus the attenuation coefficient σ_{tau} is also of special interest. In the case of the San Francisco and San Joaquin Valley data, calculations of σ_t and σ_{tau} were not included in the reports but the difference $(\sigma_t - \sigma_{tau})$ could be calculated from the reported relationships between "scattered-in" and total radiation at specified distances. The significance of the term $(\sigma_t - \sigma_{tau})$ has been discussed at some length previously.[3] It may be thought of as representing a build-up coefficient resulting from the "scattering-in" process. Since σ_{tau} is not available from part of the NRDL data, the quantity $(\sigma_t - \sigma_{tau})$ has been used to evaluate the various NRDL experiments. Typical values of $(\sigma_t - \sigma_{tau})$ are therefore included in Table 4.

For wavelength 0.50μ (or in some cases 0.55μ), which approximates the effective peak wavelength of the spectral distribution of intensity of radiation from a nuclear weapon, typical values of $(\sigma_t - \sigma_{tau})$ may be established for three general types of atmospheres, namely; very clear (visibility 20 miles or more), light haze (visibility about 12 miles), and moderate haze (visibility about 9 miles). Thus the desert data would indicate a $(\sigma_t - \sigma_{tau})$ value of 0.04 $mile^{-1}$ for the very clear atmosphere. The San Francisco and San Joaquin Valley data lead to a $(\sigma_t - \sigma_{tau})$ value of 0.1 $mile^{-1}$ for the light haze condition. The Los Angeles results give $(\sigma_t - \sigma_{tau})$ as 0.25 $mile^{-1}$ for the moderate haze conditions. The effect of high thin clouds seems negligible. The effect of lower clouds is to somewhat increase the value $(\sigma_t - \sigma_{tau})$. The Nevada Test Site data which indicate an increase of about 25% (for 0.50μ wavelength) is believed most reliable in this respect since the Los Angeles data gave very inconclusive results with respect to cloud effects, while the San Francisco Bay comparisons which show an approximate doubling of $(\sigma_t - \sigma_{tau})$ by cloud coverage may have been distorted by other variables such as fog, smoke, and scattered clouds. If a single value is to be chosen for the cloud factor, a compromise at 1.40 seems reasonable for the case of low clouds.

It was hoped that the Los Angeles tests would provide opportunities for extensive measurements in smog atmospheres with visibilities as

low as 1 mile. This did not prove to be the case, however, because the intense smog of the daytime hours no longer existed by the time it was dark enough to begin the measurements. Estimated visibilities as low as 3 miles in haze and/or light fog were experienced during the nighttime tests and the dashed line of Figure 31 showing the approximate relation between σ_{tau} and estimated visibility for wavelength 0.50μ has been extended to a 2-mile visibility value. Assuming that the typical smog particles have the same size range as those of haze[27] the dashed line of Figure 31 can be used to estimate σ_{tau} values for visibilities in smog as low as 2 miles. In making these estimates, however, it should be kept in mind that the visibility values which were used in plotting the points are visual estimates of nighttime visibility and thus must be considered as only approximations.

CONCLUSIONS

The following objectives of this experiment have been accomplished. Using several wavelengths in the visible and near infrared spectral regions, angular scattering diagrams have been constructed and values of σ_{sc}, σ_t, σ_{tau}, and R determined for the entire range of atmospheric conditions prevailing in Los Angeles, California, during the nights of August and September 1960. For the type of nighttime atmospheres encountered in this period of the year in Los Angeles, numerical values of σ_{tau} can be very approximately estimated from observed visibility, the lack of reliability resulting for the most part from the difficulty in establishing nighttime visibility. Relative humidity and contaminant measurements in downtown Los Angeles were of little help in predicting nighttime values of σ_{tau}, although some correlations were observed between σ_{sc} and relative humidity. For the atmospheres and ranges concerned in this study the presence of high thin cloud or of low ragged cloud blown in from the ocean had little measurable effect on R or on any of the attenuation coefficients, including σ_{tau}.

Although the range of nighttime σ_{tau} values to be expected during a typical August-September period has been established, large fluctuations both with respect to time and direction from source will occur.

Curves showing atmospheric transmittance between a 4π black body source at 6000°K and a flat receiver facing the source versus slant range have been plotted for four typical atmospheres.

TABLE 1

WEATHER DATA AND CONTAMINANTS

		Los Angeles International Airport					Burbank Airport					Downtown Los Angeles		Test Range		Inversion* Ht., Ft.		Contaminants, Downtown Los Angeles						
Date	Time	Temp °F	R.H. %	Wind Knots	Vsby* Miles	Cloud* & Height	Temp °F	R.H. %	Wind Knots	Vsby* Miles	Cloud* & Height	Temp °F	R.H. %	Vsby* Miles	Cloud* & Height	1700 hours	0500 hours	NO ppm	NO_2 ppm	Oxidant ppm	CO ppm	SO_2 ppm	O_3 ppm	K_m*
8-11	2000	71	73	SW 7	12	○	80	56	ESE 5	35	H◑			15	○	400	500	0.00	0.03	-	10	0	0.03	1.5
	2100											72	75	15	○									
	2300	71	77	SSW 6	15	○	72	69	ESE 3	15	○	71	78	15	○			0	0.03	0	10	0	0.01	2.5
	0100	69	81	SSW 6	15	○	71	71	E 6	15	○	71	79					0	0.04	0	11	0	0.01	2.6
8-12	2000	67	87	WSW 8	8	7⊕	73	65	ESE 11	10	○					-	700	0	0.04	0	8	-	0.01	1.3
	2100											68	84	7	○									
	2300	65	90	W 7	8	9◑	68	70	ESE 3	8	○	67	87	7	○			0	0.04	0	6	-	0.02	1.8
	0100	62	93	WSW 7	5 HK	7⊕	67	81	ESE 4	8	○	66	88	7	○			0	0.03	0	6	-	0.02	-
8-14	2000	65	84	WSW 9	8	9⊕	71	66	ESE 9	40	○					1800	1050	0	0.02	-	18	-	0.01	1.4
	2100											65	87	10	○									
	2300	64	84	WSW 8	10	9◑	64	78	E 10	10	○	64	90	10	○			-	0.03	0	15	0	0.02	1.6
	0100	62	90	WSW 5	10	9◑	63	84	E 4	10	○	63	89	10	○			-	0.03	0	10	-	0.01	1.2
8-15	2000	67	69	W 8	8	○	70	41	S 7	10	○					1600	1350	0	0.03	-	13	-	-	1.5
	2100											66	78	8	○									
	2300	65	76	WSW 5	8	12◑	65	62	ESE 7	10	○	64	84	8	○			0	0.02	0.01	15	-	-	1.5
	0100	65	81	SSW 4	10	13⊕	63	71	ESE 6	8	○	64	81	8	○			0	0.03	0.01	11	-	-	2.0
8-16	2000	66	87	WSW 8	10	9⊕	68	76	S 3	8	○					2200	-	0	0.03	-	5	0	0.01	1.4
	2100											67	87	6	○									
	2300	66	90	NW 7	7	9⊕	64	87	SE 6	6 H	○	66	90					0	0.02	0.02	8	0	0.02	1.6
	0100	66	87	WNW 6	5 HK	10⊕	63	90	SE 5	3 F	4⊕	65	90					0	0.03	0.02	10	0	0.02	1.1
8-17	2000	65	90	WSW 6	5 HK	5⊕	73	64	ESE 8	10	●○					1300	1300	0	0.02	-	11	0	0.01	1.2
	2100											66	89	8	○									
	2300	64	93	WSW 7	3 HK	5⊕	66	81	ESE 7	8	○	65	92	6	○			0	0.02	0.02	10	0	0	1.6
	0100	64	93	SW 7	3 HK	5⊕	65	81	S 3	7	○	64	93					0	0.02	0.02	10	0	0.01	2.2

*NOTES: 1. Cloud symbols as follows: ○ = Clear, ◑ = Scattered, ◍ = Broken, ⊕ = Overcast. Heights given in hundreds of feet or as High (H), Medium (M), or Low (L).

2. K_m designates particulate matter smaller than 10 microns, expressed in units of reflectance of filter paper on which particles are deposited.

3. Inversion heights from Santa Monica upper air sounding.

4. Code to visibility obstructions: H = Haze, K = Smoke, F = Fog.

(Continued on page 30)

		Los Angeles International Airport					Burbank Airport					Downtown Los Angeles		Test Range		Inversion* Ht., Ft.		Contaminants, Downtown Los Angeles						
Date	Time	Temp °F	R.H. %	Wind Knots	Vsby* Miles	Cloud* & Height	Temp °F	R.H. %	Wind Knots	Vsby* Miles	Cloud* & Height	Temp °F	R.H. %	Vsby* Miles	Cloud* & Height	1700 hours	0500 hours	NO ppm	NO_2 ppm	Oxidant ppm	CO ppm	SO_2 ppm	O_3 ppm	K_m*
8-18	2000	67	87	WSW 8	8	O	84	45	WNW 6	50	O					1300	270	0	0.06	-	-	0	0	2.4
	2100											69	82	8	O									
	2300	65	93	SW 5	6 HK	O	69	73	ESE 7	15+	O	68	85	7	O			0	0.06	-	-	0	0	3.0
	0100	65	93	SSE 6	5 HK	O	68	76	E 6	10	O	67	87	4	O			0.04	0.06	-	-	0	0	3.2
8-19	2000	63	90	WSW 7	6 HK	7 ◍	73	62	ESE 8	12	O					427	919	0	0.03	-	-	0	0.02	1.3
	2100											66	83	6	O									
	2300	63	93	W 6	5 HK	6 ⊕	66	76	ESE 8	8	O	64	87	6	O			0	0.02	0	0	0	0	2.2
	0100	63	93	WNW 6	4 HK	7 ⊕	64	84	ESE 7	6 HK	O	63	91	5	O			0.02	0.02	0	-	0	0.01	2.0
8-21	2000	66	87	WSW 7	3 HK	9 ◍	70	59	ESE 5	12	120 ◍					660	3180	0.01	0.01	0.04	8	0.02	0.03	2.7
	2100											66	81		L ◐									
	2300	64	90	E 7	4 HK	O	65	78	ENE 6	6 HK	O	66	82	6	O			0.02	0.04	0.01	7	0.02	0.02	1.6
	0100	66	81	SE 8	12	17 ⊕	64	84	SSE 9	5 HK	10 ⊕	65	86	6	L◐ to ◍			0.01	0.02	0.01	7	0.01	0.03	1.4
8-22	2000	68	81	W 8	10	O	67	68	SSE 7	12	O					1970	3050	0	0.02	-	4	0	0.01	2
	2100											68	80	8	O									
	2300	66	81	SSE 3	8	10 ◍	63	84	SE 4	10	O	65	85	8	L ◍			0	0.03	0.01	4	0	0.01	2
	0100	65	84	NNE 3	12	18 ◐	64	81	E 4	8	19 ◐	65	85	8	L ◐			0	0.03	0.02	4	0	0	2.5
8-23	2000	68	81	WSW 9	8	O	70	59	S 5	10	O			8	O	1310	2760	0	0.03	-	3	0	0.04	2
	2100											68	79	8	O									
	2300	66	87	W 7	10	O	65	76	SE 3	8	O	66	82	7	O			0	0.05	-	3	0	0.01	1.5
	0100	64	93	[illegible]	10	O	64	81	ENE 5	7	O	65	83	6	O			0	0.04	-	3	0	0.02	2.5
8-26	2000	67	87	[illegible] W 10	6 H	11 ◍	68	68	S 6	10	O					1300	1210	0	0.04	-	8	0	0.03	1.4
	2100											66	86	6	O									
	2300	65	87	7	6 H	11 ◐	67	87	SSE 4	7	O	66	86	5	L ◍			0	0.01	0.03	7	0	0.03	1.3
	0100	65	87	W 5	7	20 ⊕	62	87	ESE 7	4 HK	7 ⊕	65	85	5	L ⊕			0	0.03	0.01	8	0	0.02	2.0
8-27	2000	65	87	WSW 9	7	9 ◍	66	66	SSE 6	8	O					790	2625	0	0.04	-	7	0	0.02	1.4
	2100											63	87	6	O									
	2300	63	93	WSW 7	8	9 ⊕	63	78	ESE 3	7	O	62	90	6	O			0	0.03	0.02	7	0	0.02	1.0
	0100	63	93	WNW 4	6 H	10 ⊕	61	87	ESE 5	5 H	O	62	93	3	L ◍			0	0.05	0.02	8	0	0	1.5

(Continued on page 31)

		Los Angeles International Airport					Burbank Airport					Downtown Los Angeles		Test Range		Inversion* Ht., Ft.		Contaminants, Downtown Los Angeles						
Date	Time	Temp °F	R.H. %	Wind Knots	Vsby* Miles	Cloud* & Height	Temp °F	R.H. %	Wind Knots	Vsby* Miles	Cloud* & Height	Temp °F	R.H. %	Vsby* Miles	Cloud* & Height	1700 hours	0500 hours	NO ppm	NO_2 ppm	Oxidant ppm	CO ppm	SO_2 ppm	O_3 ppm	K_m*
8-30	2000	65	84	WSW 10	7	○	72	51	ESE 6	15	○					950	Surface	0	0.04	-	8	0	0.01	1.7
	2100											65	83	8	○									
	2300	65	84	SSW 4	12	○	64	75	E 4	15	○	65	85	8	○			0	0.04	0	8	0	0	1.8
	0100	63	87	E 4	10	○	63	81	E 5	10	○	63	86	4	○			0	0.07	0	12	0	-	5.2
8-31	2000	65	84	WSW 9	12	○	70	55	ESE 10	15+	○					1020	Surface	-	-	-	6	0	0.01	1.5
	2100											66	77	10	○									
	2300	64	84	NNW 6	12	○	65	73	E 5	15	○	65	76	10	○			0.02	0.05	0	7	0	0.01	1.1
	0100	62	90	NW 4	15	○	64	75	ESE 5	15	○	65	73	10	○			0.02	0.05	0	7	0	0	1.1
9-1	2000	65	87	W 8	12	○	71	53	SE 7	15	○					20	Surface	0	0.04	-	7	0	0.01	1.8
	2100											66	81	8	○									
	2300	62	93	WSW 4	15	○	64	78	ENE 7	15	○	64	87	8	○			0.03	0.03	0	7	0	0.02	2.4
	0100	60	97	WNW 5	15	○	64	46	NW 8	15+	○	63	91	15	○			0.04	0.10	0	11	0	0.01	2.0
9-3	2000	72	62	SW 7	15+	○	80	42	ESE 6	50	○					520	Surface	0.04	0.02	0.01	8	0.01	0.01	3.9
	2100											75	51	15	○									
	2300	70	71	SSE 7	15+	○	74	48	ESE 4	15+	○	72	58	15	○			0.07	0.03	0.01	9	0.02	0.01	3.2
	0100	69	76	S 6	15+	○	72	53	ESE 4	15+	○	72	61	15	○			0.10	0.03	0.01	10	0.01	0.01	4.8
9-4	2000	72	64	WSW 13	15+	○	87	19	W 6	50	○					690	Surface	0	0.02	-	7	0	0.01	2.1
	2100											78	44	15+	○									
	2300	68	76	S 6	15	○	76	39	NNW 4	15+	○	72	58	15+	○			0.01	0.07	0	9	0	0.01	2.2
	0100	66	75	W 3	15+	○	71	51	ESE 5	15+	○	71	63	15+	○			0.02	0	0	9	0	0	2.8
9-5	2000	69	84	WSW 8	30	○	77	39	ESE 10	15+	○					950	Surface	0	0.05	-	7	0	0.03	1.7
	2100											75	50	12	○									
	2300	65	87	N 6	15	12 ◑	68	70	E 5	15+	○	69	75	12	○			0.01	0.03	0.02	7	0	0.01	2.4
	0100	64	90	WNW 4	15	○	67	57	W 3	15+	○	68	72	12	○			0.01	0.03	0.01	10	0	0	3.0
9-6	2000	64	90	WSW 9	5HK	6 ◍	73	57	ESE 10	15+	○					590	722	0.01	0.07	-	8	0	0.01	2.2
	2100											67	77	5	○									
	2300	62	97	W 7	4HK	6 ⊕	67	70	E 4	6 H	○	65	84	5	○			0.05	0.06	0.01	8	0	0.01	1.5
	0100	61	93	W 7	3HK	4 ⊕	66	63	WSW 3	7	○	63	90	4	○			0.05	0.06	0.01	9	0	0	2.8

(Continued on page 32)

		Los Angeles International Airport					Burbank Airport					Downtown Los Angeles		Test Range		Inversion* Ht., Ft.		Contaminants, Downtown Los Angeles						
Date	Time	Temp °F	R.H. %	Wind Knots	Vsby* Miles	Cloud* & Height	Temp °F	R.H. %	Wind Knots	Vsby* Miles	Cloud* & Height	Temp °F	R.H. %	Vsby* Miles	Cloud* & Height	1700 hours	0500 hours	NO ppm	NO_2 ppm	Oxidant ppm	CO ppm	SO_2 ppm	O_3 ppm	K_m*
9-7	2000	66	87	WSW 9	8	160 ⊕	75	47	ESE 6	15+	160 ⊕					750	Surface	0	0.07	-	9	0	0.03	2.7
	2100											70	69	6	H ⊕									
	2300	65	90	WSW 4	5 H	160 ⊕	69	66	ESE 6	12	160 ⊕	67	79	6	H ⊕			0.04	0.07	-	10	0	0	4.1
	0100	64	93	WSW 5	7	160 ⊕	70	61	E 1	15	150 ⊕	69	78	6	H ⊕			0.05	0.07	-	12	0	0	3.2
9-8	2000	69	76	WSW 8	15+	160 ⊕	81	23	ESE 5	15+	180 ⊕					560	520	0.02	0.06	0.01	8	0.01	0.01	3.9
	2100											73	56	15	O									
	2300	70	66	S 6	15+	130 ⊕	75	45	ESE 5	15+	O	73	57	15	H ⊕			0.07	0.07	0.01	10	0.01	0.01	4.7
	0100	70	63	WNW 6	15+	O	73	43	E 7	15+	O	73	56	15	O			0.07	0.07	0.01	10	0.01	0.01	4.0
9-10	2000	75	64	WSW 8	15+	160 ⊕	82	34	C	15+	140 ⊕					520	Surface	0.01	0.06	0.01	12	0.01	0.01	3.6
	2100											80	34	10	O									
	2300	73	73	SSE 4	15+	O	77	35	E 3	15+	140 ⊕	78	46	10	O			0.06	0.06	0.01	15	0.01	0.01	4.3
	0100	71	79	S 7	15+	O	76	36	ESE 4	15	O	77	55	10	O			0.07	0.05	0.01	16	0.01	0.01	4.3
9-11	2000	65	74	WSW 6	12	O	81	47	ESE 4	15+	O					620	Surface	0.02	0.05	-	9	0	0.01	2.7
	2100											80	56	10	O									
	2300	68	87	WSW 5	10	O	78	54	ESE 7	15	O	78	64	9	O			0.03	0.06	0.06	12	0	0	-
	0100	68	90	NNE 5	10	O	76	60	ESE 5	15	O	77	69	7	O			0.05	0.07	0.07	13	0	0	-
9-12	2000	74	74	W 7	15	O	86	40	ESE 4	15	O					720	Surface	0	0.05	0.04	10	0	0	3.1
	2100											81	56	8	O									
	2300	73	84	SSW 4	15	O	80	52	C	12	O	80	58	8	O			0	0.08	0.03	13	0	0	6.1
	0100	72	84	WSW 4	15+	O	77	56	C	10	O	79	59	8	O			0.05	0.07	0.02	16	0	0	4.6
9-13	2000	72	79	WSW 8	15	O	84	41	ESE 5	15+	9 ⊕					690	1180	0	0.05	-	8	0	0.01	2.7
	2100											77	67	10	O									
	2300	71	84	SW 6	10	O	74	66	ESE 11	15	O	72	72		O			0	0.05	0.02	8	0	0.02	2.4
	0100	70	90	N 6	7	O	71	66	ESE 4	10	O	71	91	6	O			0	0.05	0.01	8	0	0.03	2.2
9-17	2000	68	76	WSW 7	8	O	69	71	ESE 7	7	O			6	O	620	1740	0	0.03	0.06	7	0	0.06	2.4
	2100											67	81	6	O									
	2300	66	90	W 7	6 H	O	65	78	SE 3	5 H	O	67	85	6	O			0	0.04	-	8	0	0.04	2.7
	0100	64	93	WSW 7	7	O	64	78	C	5 H	O	66	93					0	0.04	0.01	8	0	0.04	2.2

(Continued on page 33)

		Los Angeles International Airport					Burbank Airport					Downtown Los Angeles		Test Range		Inversion* Ht.	Inversion* Ft.	Contaminants, Downtown Los Angeles						
Date	Time	Temp °F	R.H. %	Wind Knots	Vsby* Miles	Cloud* & Height	Temp °F	R.H. %	Wind Knots	Vsby* Miles	Cloud* & Height	Temp °F	R.H. %	Vsby* Miles	Cloud* & Height	1700 hours	0300 hours	NO ppm	NO_2 ppm	Oxidant ppm	CO ppm	SO_2 ppm	O_3 ppm	K_m*
9-18	2000	66	87	WSW 6	10	11 ◍	67	75	SSE 7	10	O				L ◍	1080	Surface	0	0.02	0.02	7	0	0.06	1.6
	2100											67	83	6	O									
	2300	65	87	W 6	10	O	64	81	W 5	8	O	66	90	6	O			0	0.03	-	8	0	0.04	1.4
	0100	64	90	WSW 7	10	O	63	73	C	8	O	64	92	6	O			0	0.03	0.01	8	0	0.04	1.5
9-21	2000	Not on record.																0	0.02	0.02	5	0	0.02	1.1
	2100											65	83	6	L ◍									
	2300											64	82	6	L ⊕			0	0.02	-	4	0	0.04	1.5
	0100											65	75	6	L ◍			0	0.02	-	4	0	0.02	1.0
9-22	2000	65	84	WSW 8	9	O	67	63	ENE 6	7	O			7	O	1740	Surface	0	0.03	-	5	0	0.03	1.0
	2100											66	63	6	O									
	2300	64	87	W 5	8	O	63	72	C	6 H	O	65	72	5	O			0	0.03	-	5	0	0.02	1.7
	0100	63	87	W 4	5 HK	O	62	75	NW 3	6 H	O	63	75	4	O			0.01	0.05	-	6	0	0.01	2.4

TABLE 2

WEATHER CONDITIONS

Weather Type	Dates	Remarks
No cloud, moderate haze, visibilities estimated 4 to 8 miles	8-10	None
	8-12	None
	8-15	None
	8-16	Light fog with visibilities less than 3 miles at end of test period.
	8-17	None
	8-18	Visibility decreased from 8 to 4 miles during test period.
	8-19	Light fog observed in the vicinity of source near end of test period at which time the relative humidity was above 90% in downtown Los Angeles.
	8-23	None
	8-30	None
	9-6	None
	9-13	Visibility rapidly decreasing near end of test period.
	9-17	None
	9-18	None
	9-22	Visibility decreased from 8 to 4 miles during test period.
No cloud, light haze, visibilities 8 to 15+ miles	8-11	Visibility estimated 15 miles.
	8-14	Visibility estimated 10 miles.
	8-31	Visibility estimated 15 miles
	9-1	Visibility increased during test period.
	9-4	Visibility greater than 15 miles, light East winds.
	9-5	Visibility estimated 12 miles.
	9-10	Visibility estimated 10 miles. Downtown L.A. relative humidity less than 54%.

TABLE 2 (continued)

Weather Type	Dates	Remarks
	9-11	Visibility decreased during test period.
	9-12	Visibility estimated 8 miles.
Variable cloud over range	8-21	Variable low stratus, visibility increased from 6 to 10 miles during test period.
	8-22	Scattered to broken low stratus during most of test period. Visibility estimated 8 miles.
	8-26	Broken to overcast low stratus during last part of test period. Visibility decreased during test period.
	8-27	Low overcast appeared at end of test period. Visibility decreased from 10 to 3 miles during test period.
	9-7	High scattered cloud (16,000 ft). Visibility estimated 6 miles.
	9-8	High scattered cloud (13,000 ft). Visibility estimated 15 miles.
	9-21	Broken to overcast low stratus. Visibility estimated 8 miles.

TABLE 3

RESPONSE FLUCTUATIONS, ARRAY NO. 4
GRIFFITH PARK STATION, 20 SEPTEMBER

Flash No	Normalized Response of Photomultiplier-Filter Combination, μ amps				Percent Difference from A-1 Response		
	A-1	A-2	C-1	C-2	A-2	C-1	C-2
1	0.880	0.855	0.640	0.796	-3.1	-30.2	-10.6
2	0.840	0.806	1.120	0.796	-4.3	+35.2	- 5.5
3	0.820	0.822	0.520	0.687	+0.3	-37.7	-16.7
4	0.840	0.822	0.720	1.043	-2.3	-15.0	+25.5
5	0.840	0.822	0.600	1.043	-2.3	-30.2	+25.5
6	0.840	0.822	0.920	0.714	-2.3	+10.1	-15.9
7	0.840	0.822	0.800	0.934	-2.3	- 5.0	+11.8
8	0.740	0.789	1.200	0.604	+6.2	+57.9	-17.1
9	0.800	0.789	1.160	0.824	-1.4	+45.3	+ 3.0
10	0.760	0.756	0.640	0.659	-0.5	-15.0	-12.7
11	0.760	0.789	0.520	0.796	+3.6	-30.2	+4.5
12	0.760	0.756	1.160	0.961	-0.5	+50.3	+25.3
13	0.740	0.756	0.800	0.714	+2.0	+ 7.5	- 3.3
14	0.700	0.740	0.520	0.769	+5.0	-22.6	+ 8.7
15	0.760	0.773	0.600	0.576	+1.6	-20.1	-23.2
Average of Absolute Difference					2.5	27.5	13.9

TABLE 4

SUMMARY OF ATTENUATION COEFFICIENTS

Test Area	Atten. Coefficient Miles^{-1}	Wavelength μ 0.40	0.50	0.77	0.88
Nev. Test Site Feb., Overcast	σ_t	0.064	0.061	0.035	0.043
	σ_{tau}	0.043	0.020	-0.003	-0.007
	$\sigma_t - \sigma_{tau}$	0.021	0.041	0.038	0.036
Nev. Test Site Feb., 5/10 coverage	σ_t	0.105	0.080	0.078	0.064
	σ_{tau}	0.061	0.047	0.055	0.047
	$\sigma_t - \sigma_{tau}$	0.044	0.033	0.023	0.017
Nev. Test Site Feb., clear skies	σ_t	0.091	0.062	0.070	0.030
	σ_{tau}	0.051	0.029	0.044	0.013
	$\sigma_t - \sigma_{tau}$	0.040	0.033	0.026	0.017
Nev. Test Site May, clear skies	σ_t	0.096	0.105	0.110	0.081
	σ_{tau}	0.036	0.060	0.084	0.058
	$\sigma_t - \sigma_{tau}$	0.060	0.045	0.026	0.023
Los Angeles, Calif. August and September Central Half, all values	σ_t	0.71-1.12	0.52-0.88	0.44-0.78	0.07-0.33
	σ_{tau}	0.36-0.68	0.32-0.58	0.32-0.57	0.02-0.28
	$\sigma_t - \sigma_{tau}$	0.35-0.44	0.20-0.30	0.12-0.21	0.05
San Francisco, Calif. clear skies	$\sigma_t - \sigma_{tau}$	.09* (λ=0.55μ)			
San Francisco, Calif. Overcast	$\sigma_t - \sigma$ tau	.19* (λ=0.55μ)			
San Joaquin Valley, Calif., Clear skies	$\sigma_t - \sigma$ tau	.12**			

* Calculated from ratio of irradiance received from a 4π source by a flat receiver to that received by a collimated receiver at a distance of 7 miles. (See text).

**Calculated from ratio of "scattered-in" radiation to total radiation at a distance of 12,000 ft after correction for effect of increasing the half-angle field of view from 45 to 90 degrees.

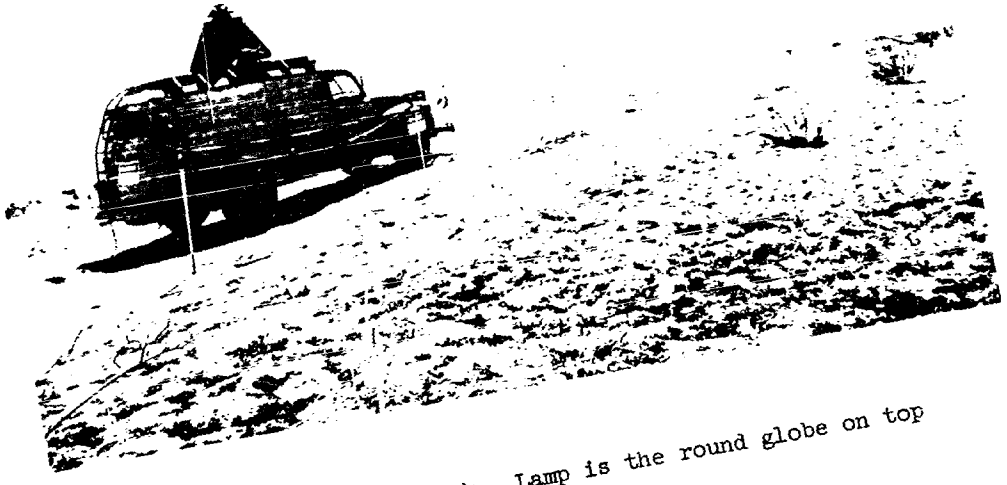

Fig. 1 Light source truck. Lamp is the round globe on top of the truck.

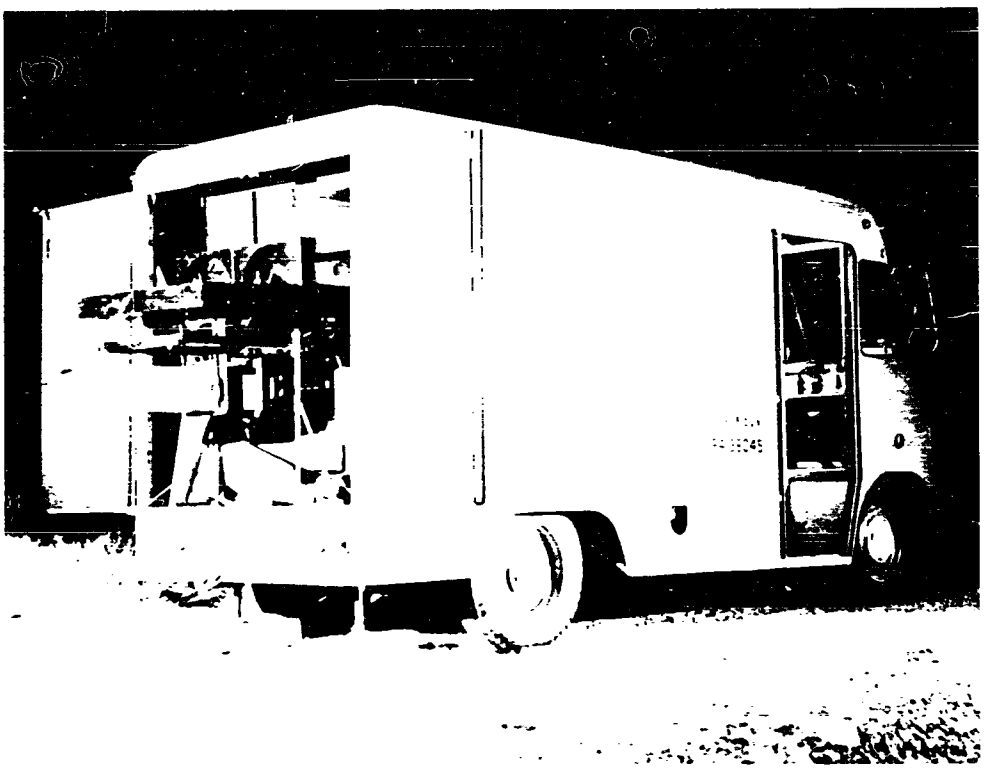

Fig. 2 Observation truck with field-of-view device in operating position. Round tube beneath field of view device is part of the triggering circuit.

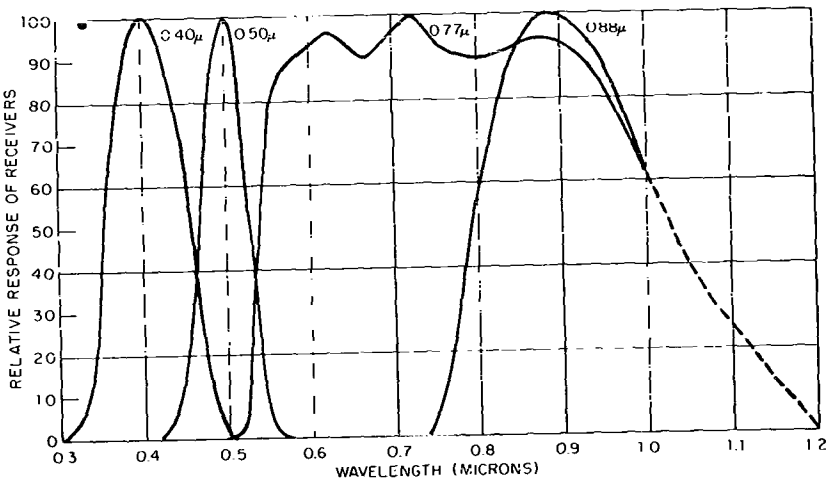

Fig. 3 Curves showing product of photomultiplier-filter combination and flashlamp output versus wavelength.

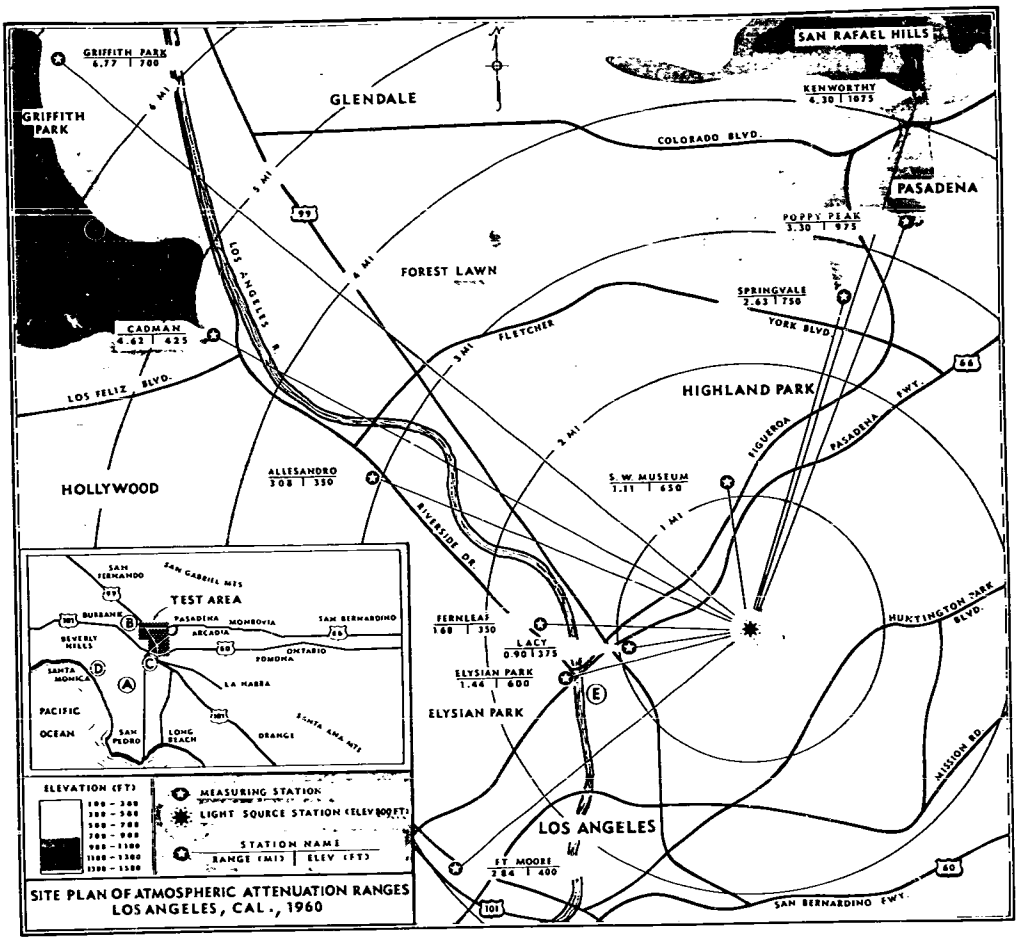

Fig. 4 Map of atmospheric attenuation test area. Figures beneath name of measuring station show distance in miles from light source, and elevation in feet.

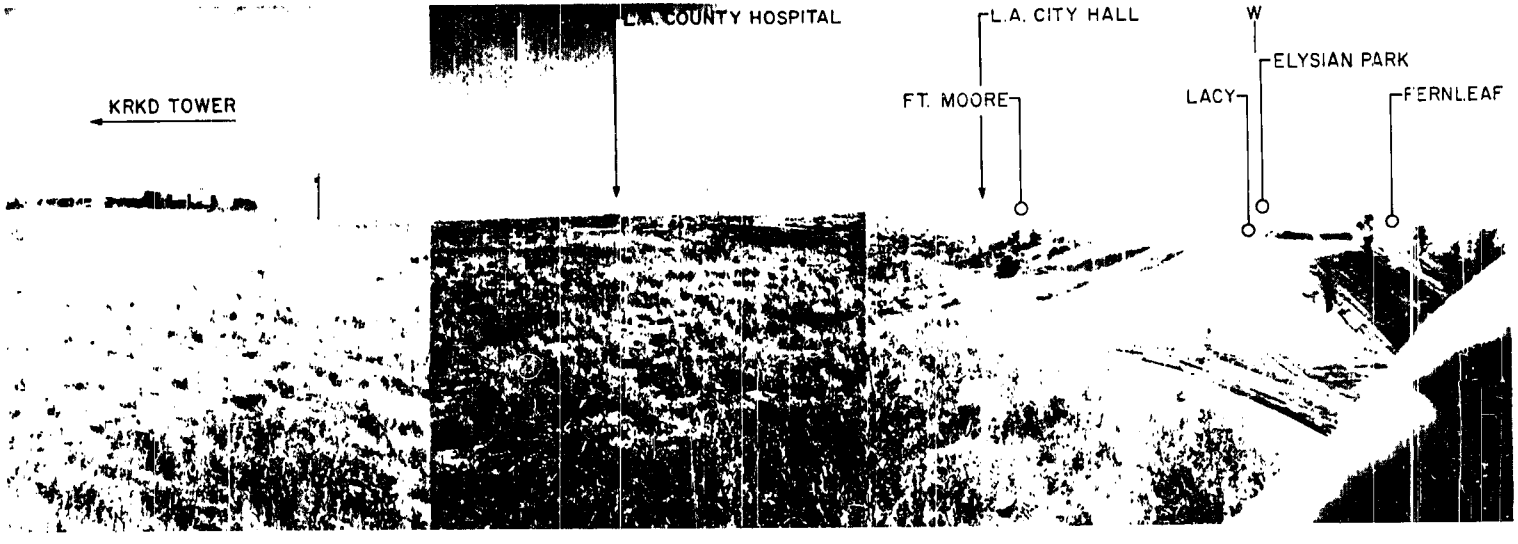

Fig. 5 Panoramic view of test area from light source location. (Continued in Fig. 6.)

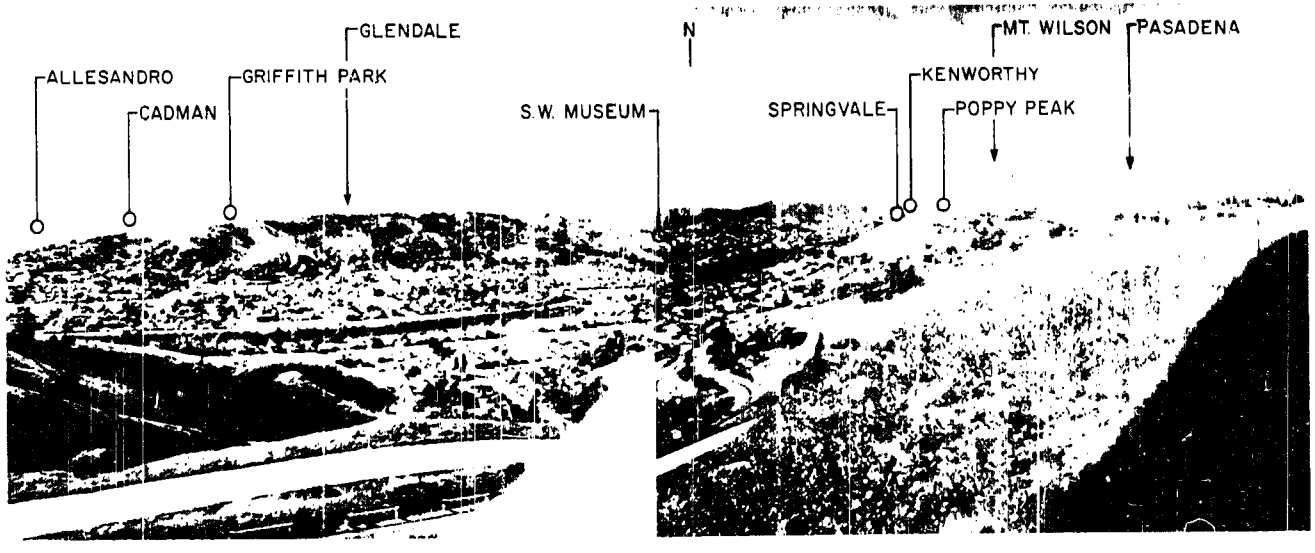

Fig. 6 Panoramic view from light source. (Continued from Fig. 5.)

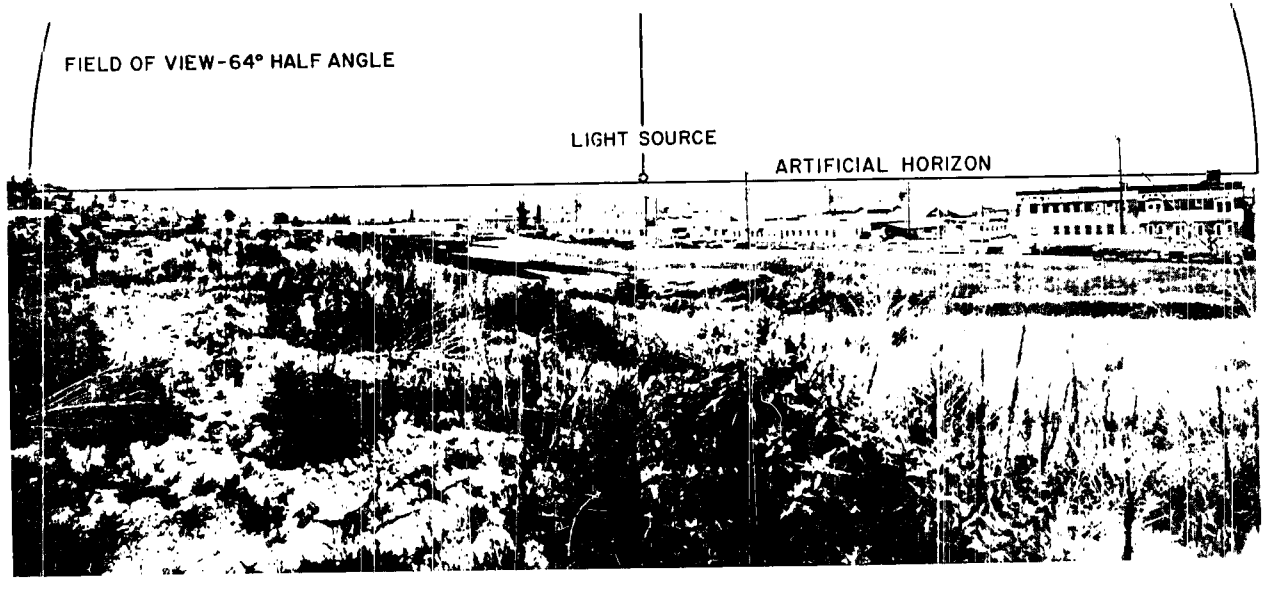

Fig. 7 Range view from Lacy receiving station, looking toward light source. Arc shows the 64-deg half-angle field-of-view as seen by photomultiplier above the artificial horizon.

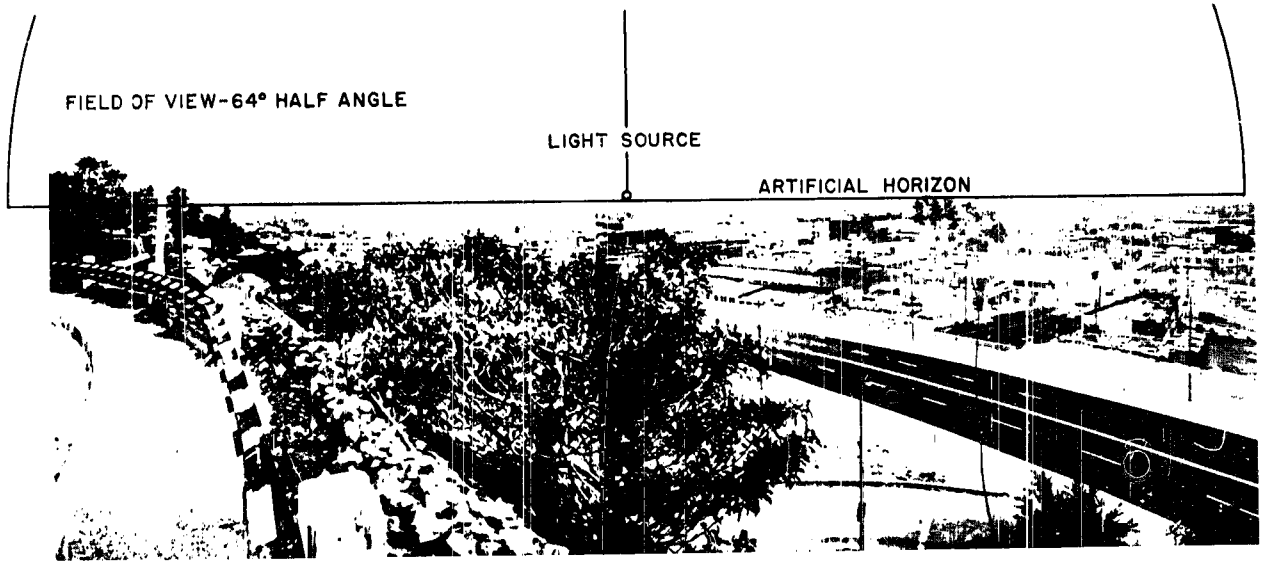

Fig. 8 Range view from Ft. Moore receiving station.

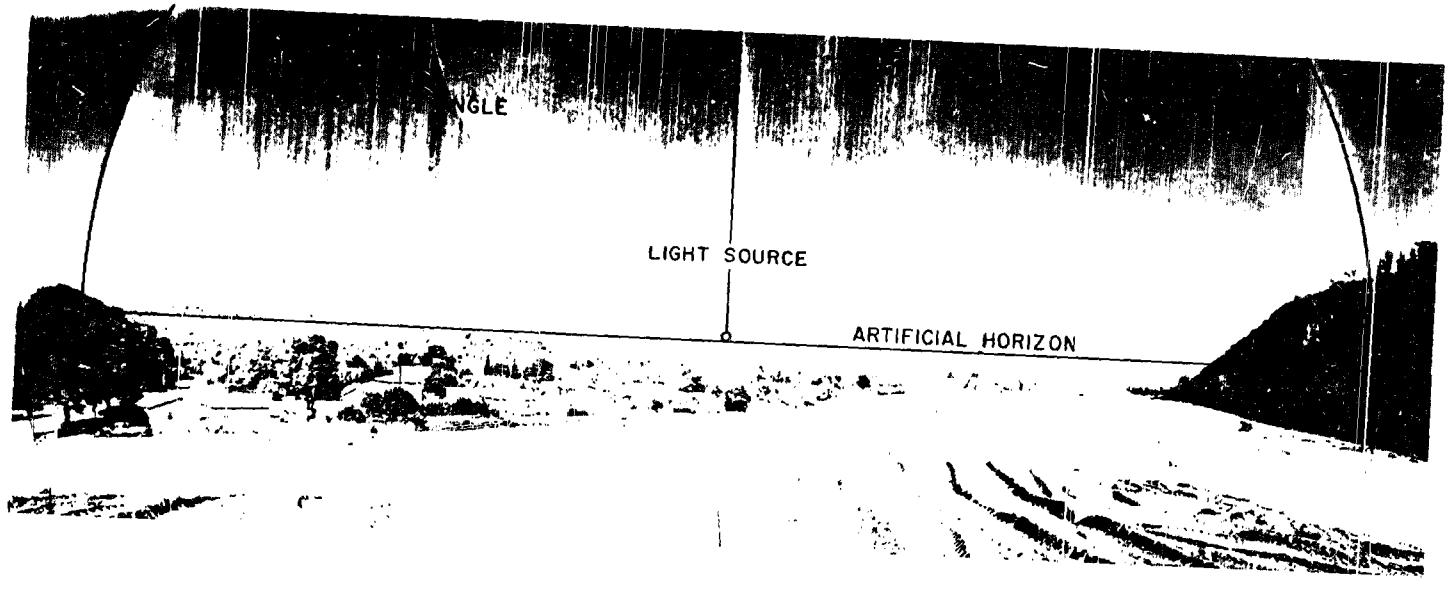

Fig. 9 Range view from Fernleaf receiving station.

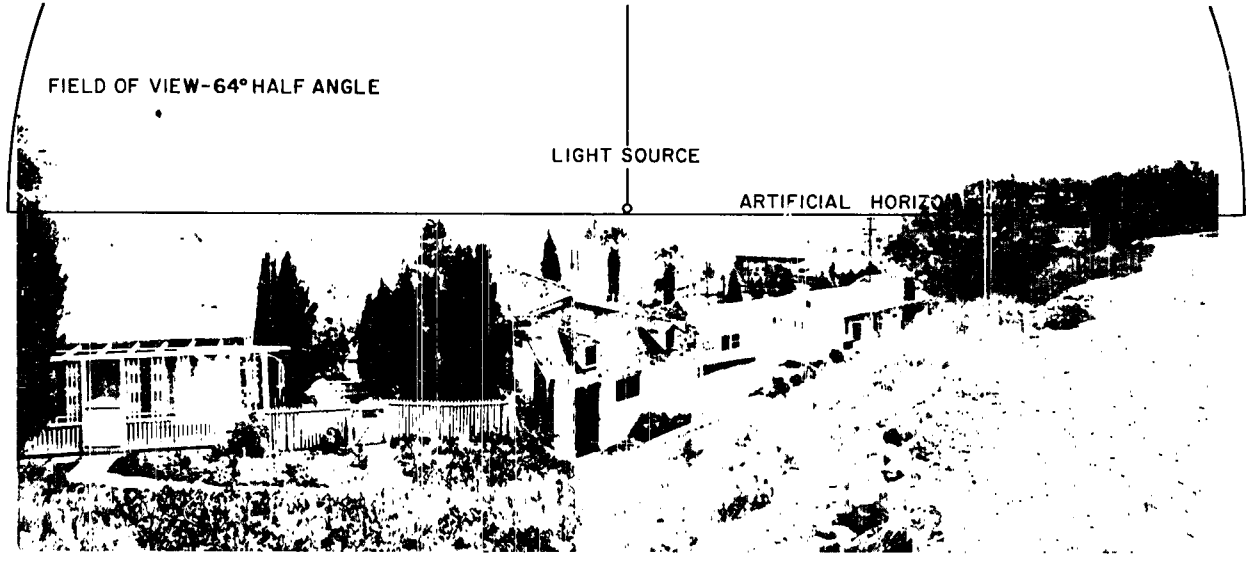

Fig. 10 Range view from Allesandro receiving station.

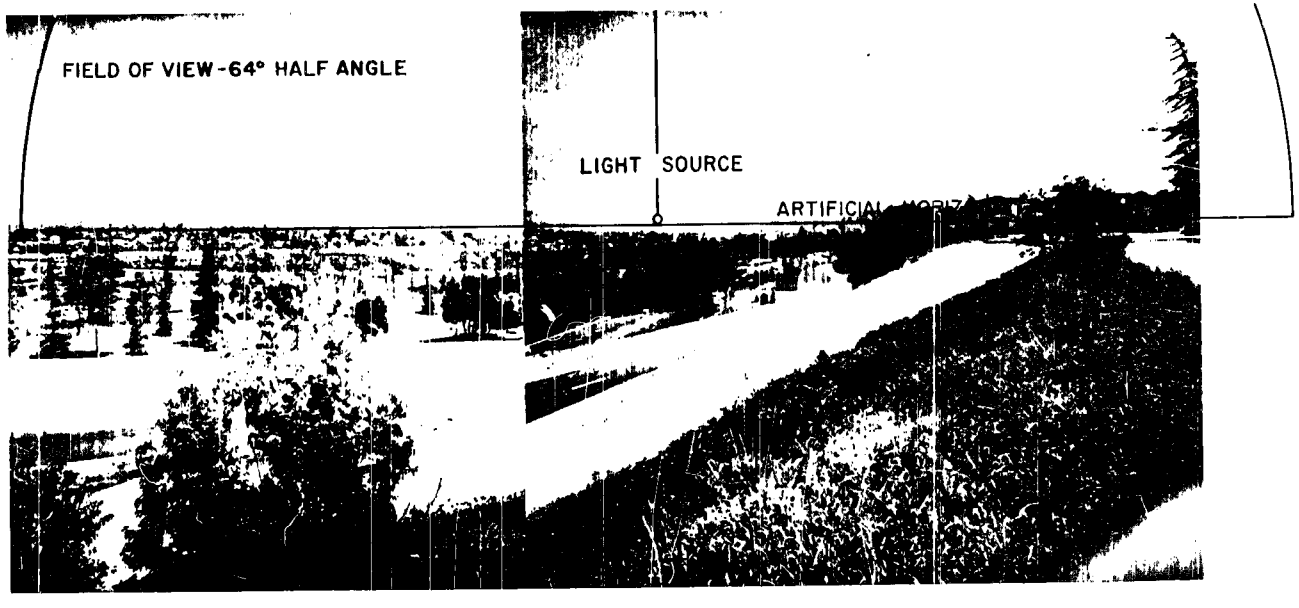

Fig. 11 Range view from Cadman receiving station.

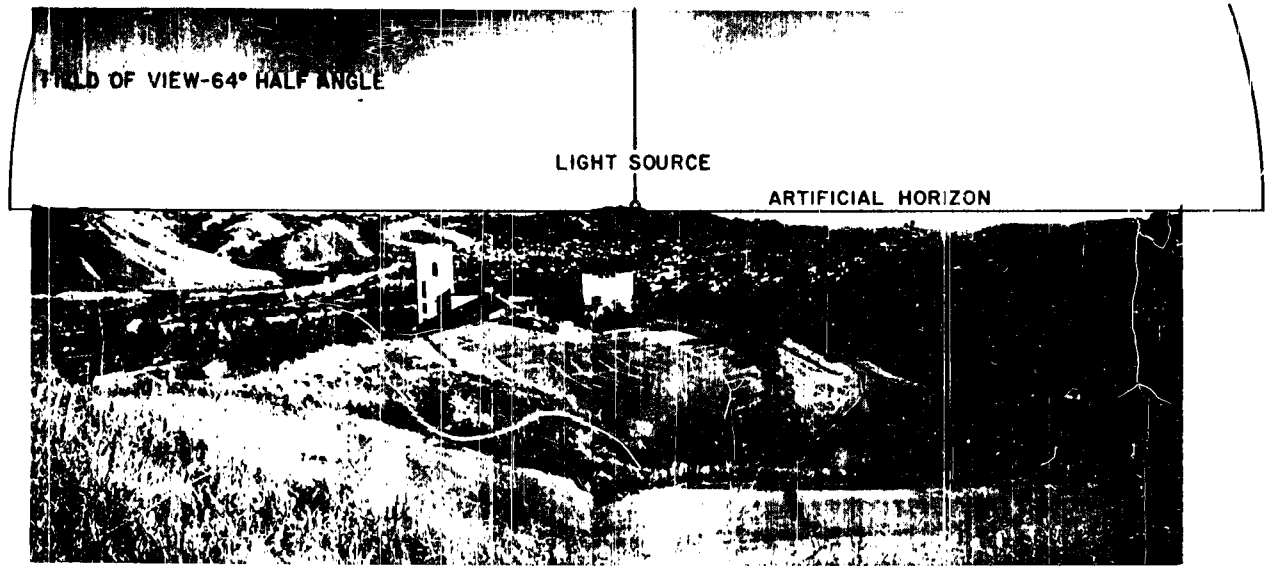

Fig. 12 Range view from Southwest Museum receiving station.

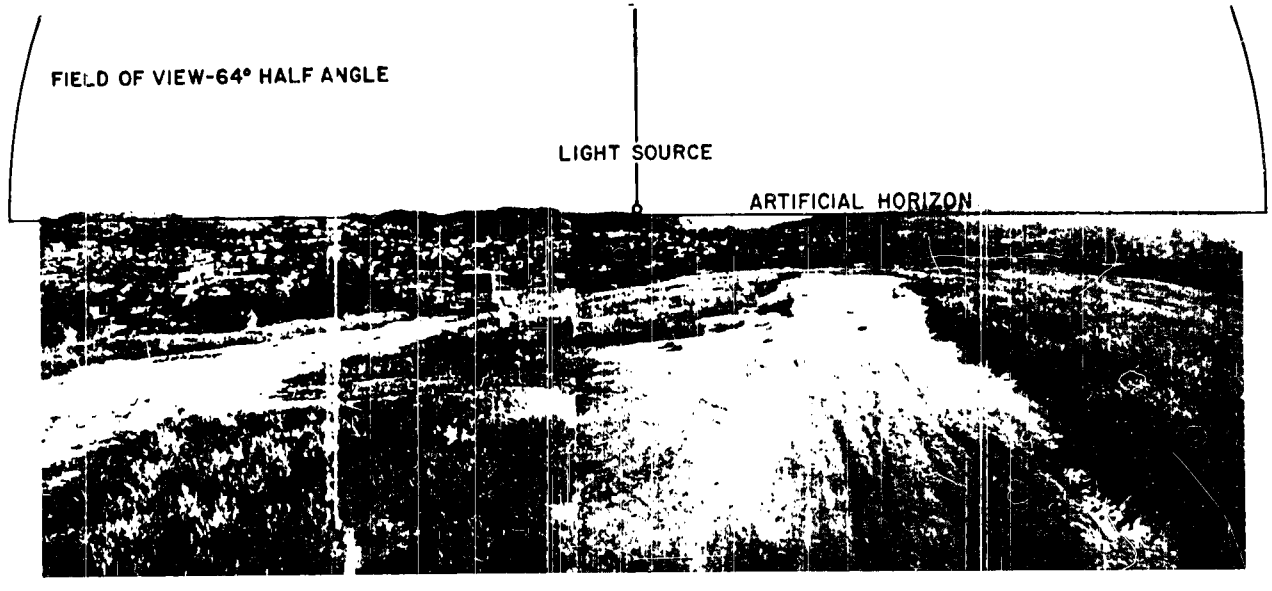

Fig. 13 Range view from Springvale receiving station.

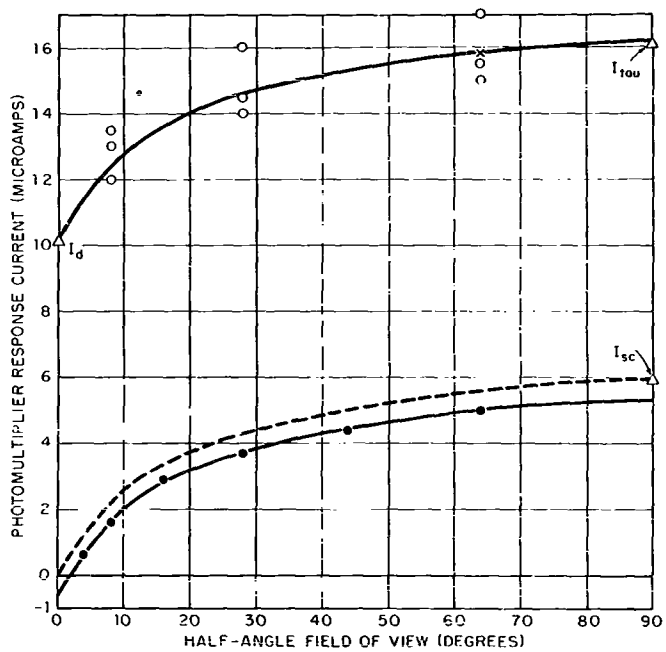

Fig. 14 Typical curves of photomultiplier response versus field-of-view. See text for complete explanation. The plotted points represent experimental data except for the X, which is the average of the three plotted values, and the triangles which are explained in the text.

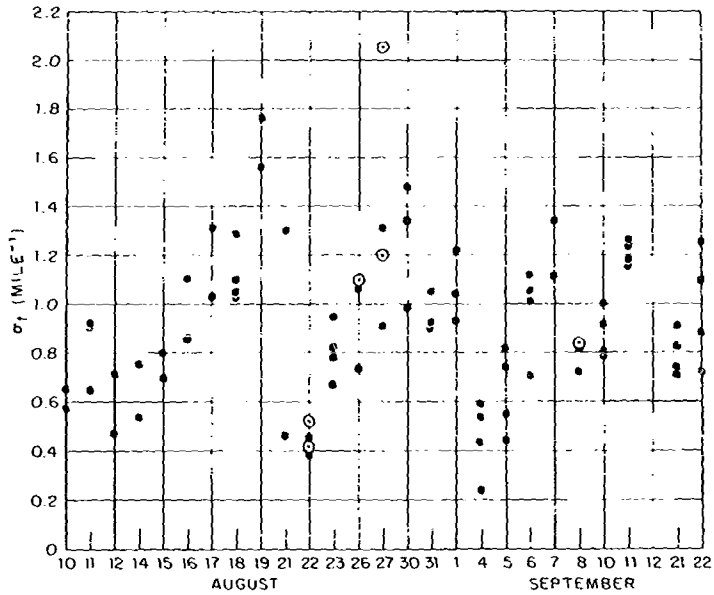

Fig. 15 Individual σ_t values for each test day, $\lambda = 0.40\mu$. Encircled points obtained with cloud overhead.

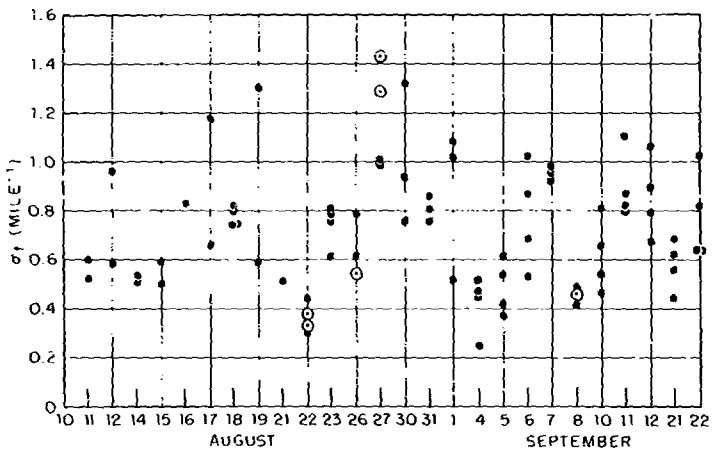

Fig. 16 Individual σ_t values for each test day, $\lambda = 0.50\mu$. Encircled points obtained with cloud overhead.

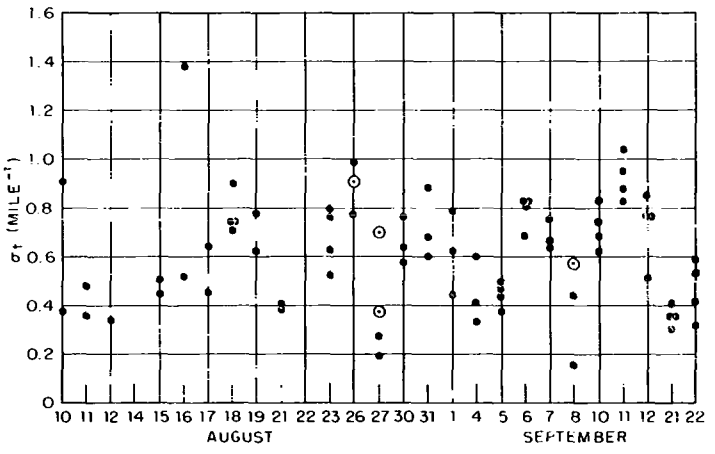

Fig. 17 Individual σ_t values for each test day, $\lambda = 0.77\mu$. Encircled points obtained with cloud overhead.

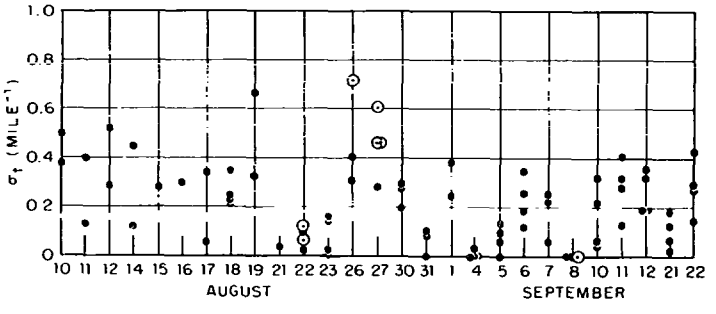

Fig. 18 Individual σ_t values for each test day, $\lambda = 0.88\mu$. Encircled points obtained with cloud overhead.

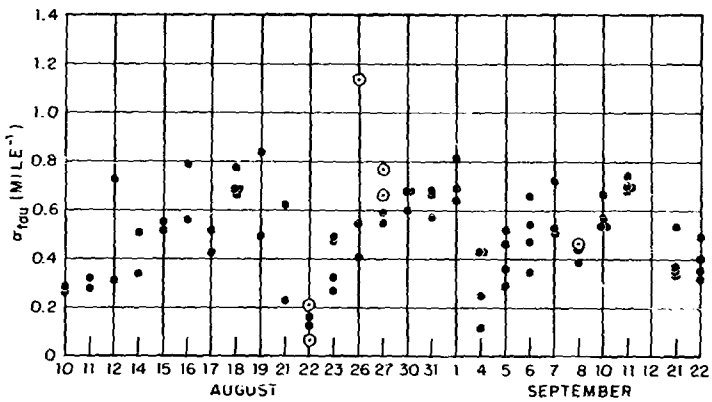

Fig. 19 Individual σ_{tau} values for each test day, $\lambda = 0.40\mu$. Encircled points obtained with cloud overhead.

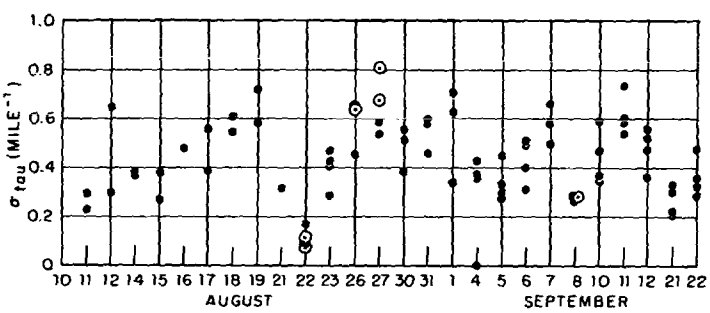

Fig. 20 Individual σ_{tau} values for each test day, $\lambda = 0.50\mu$. Encircled points obtained with cloud overhead.

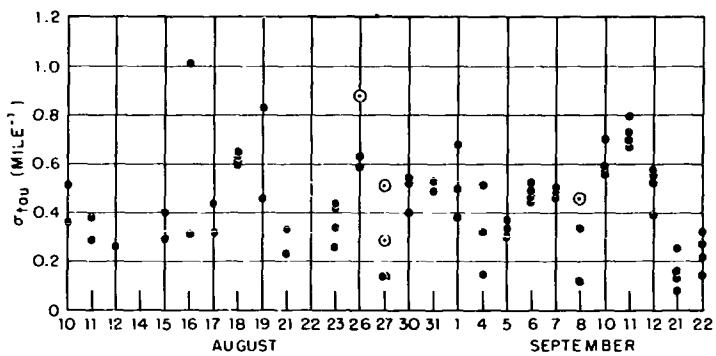

Fig. 21 Individual σ_{tau} values for each test day, $\lambda = 0.77\mu$. Encircled points obtained with cloud overhead.

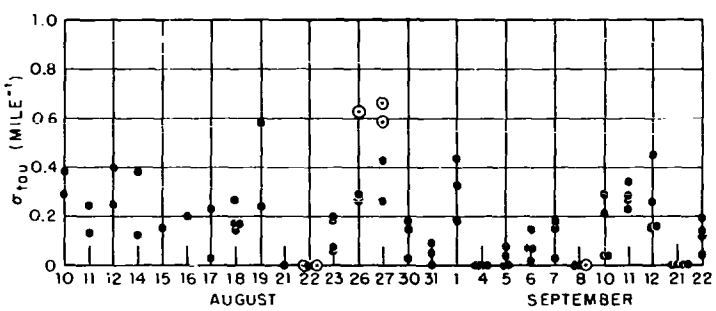

Fig. 22 Individual σ_{tau} values for each test day, $\lambda = 0.88\mu$. Encircled points obtained with cloud overhead.

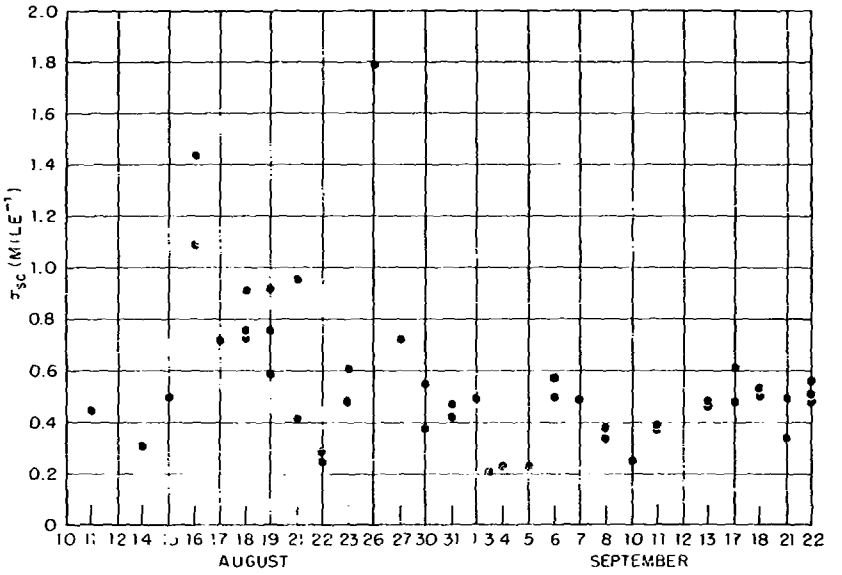

Fig. 23 Individual σ_{sc} values for each test day, $\lambda = 0.40\mu$.

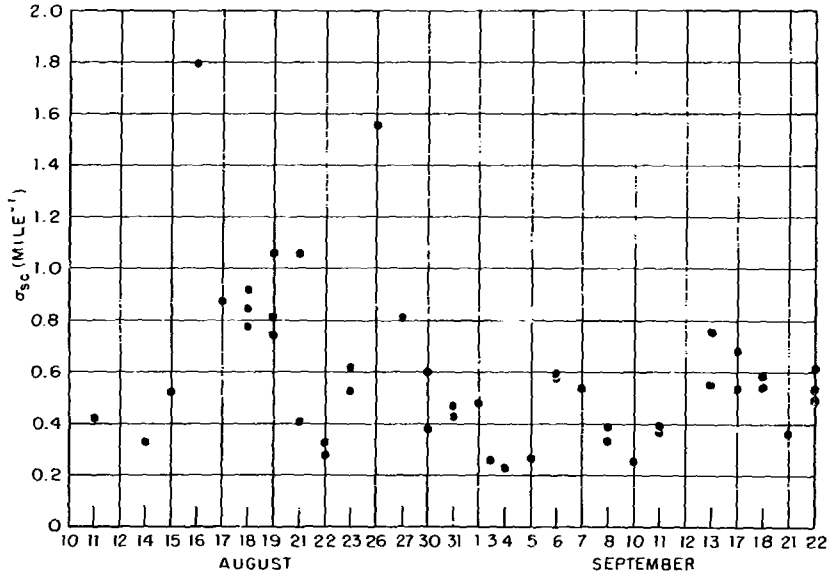

Fig. 24 Individual σ_{sc} values for each test day, $\lambda = 0.45\mu$.

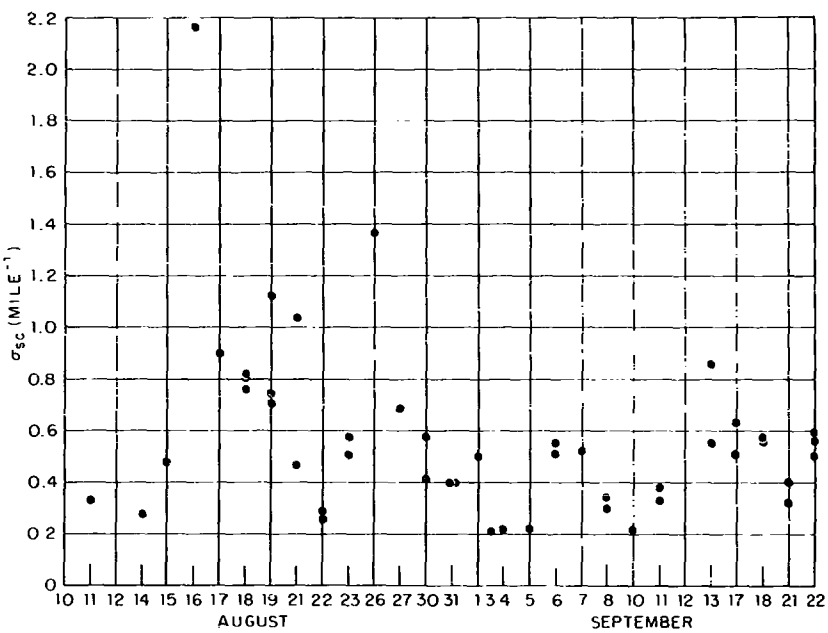

Fig. 25 Individual σ_{sc} values for each test day, $\lambda = 0.50\mu$.

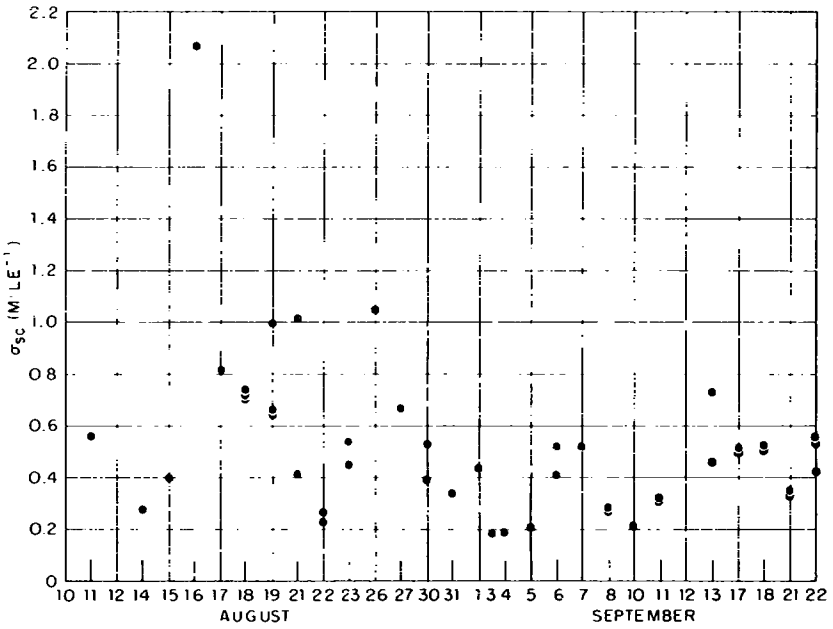

Fig. 26 Individual σ_{sc} values for each test day, λ = 0.55u.

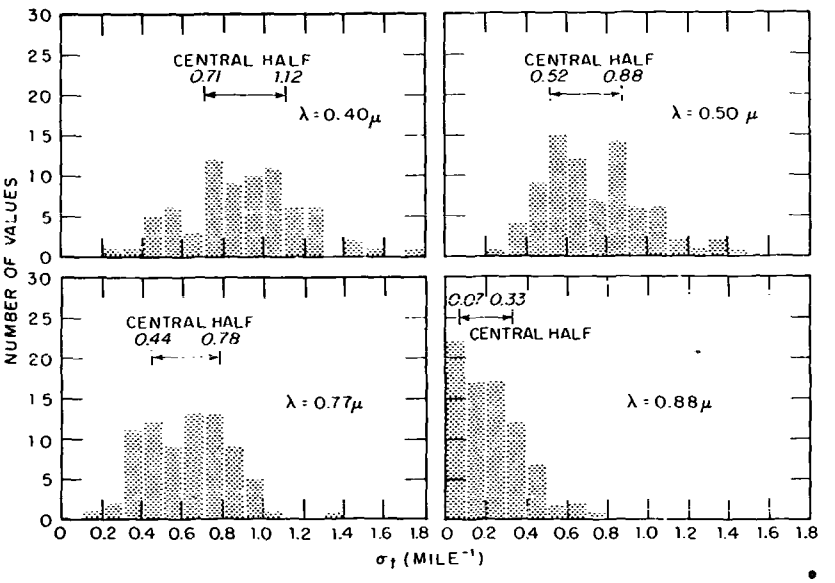

Fig. 27 Frequency distribution of all experimental σ_t values for the four wavelengths.

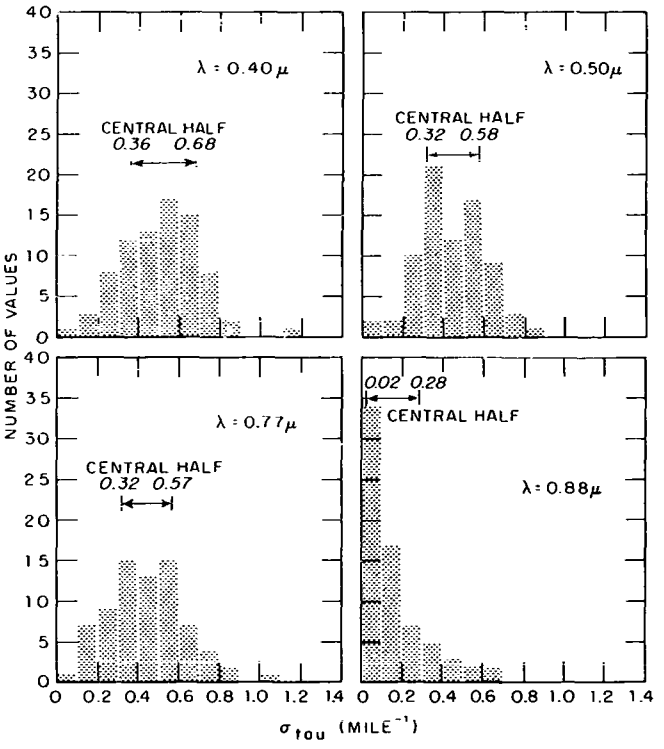

Fig. 28 Frequency distribution of all experimental σ_{tau} values for the four wavelengths.

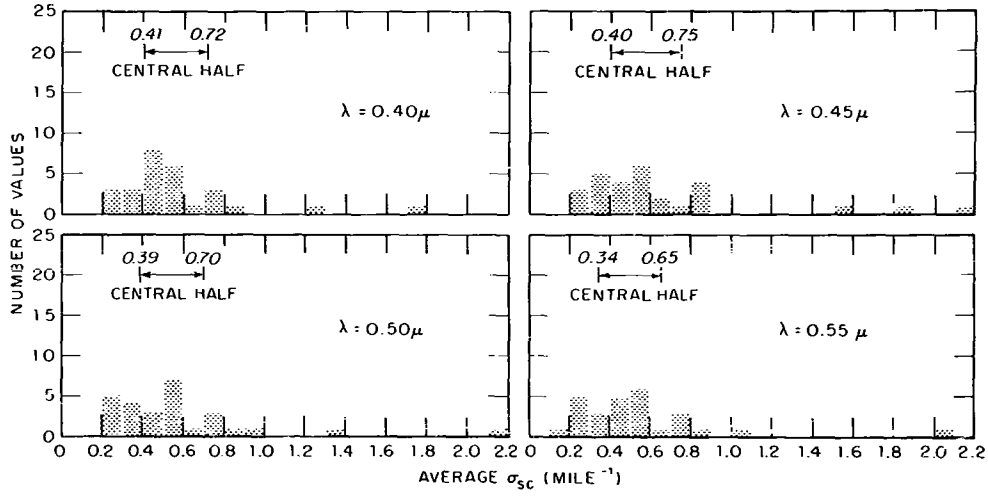

Fig. 29 Frequency distribution of all experimental σ_{sc} values for the four wavelengths.

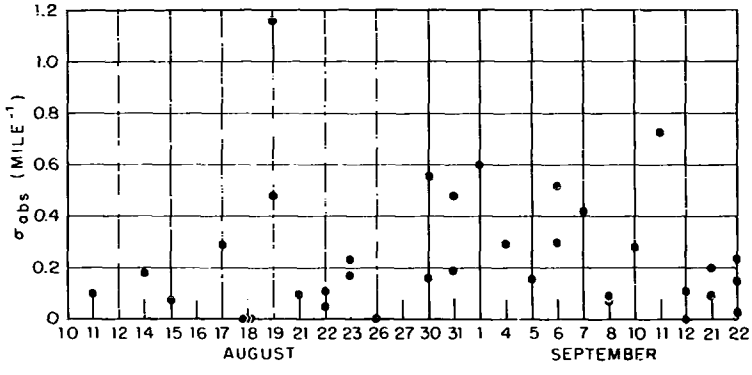

Fig. 30 Individual σ_{abs} values for each test day (λ = 0.50μ).

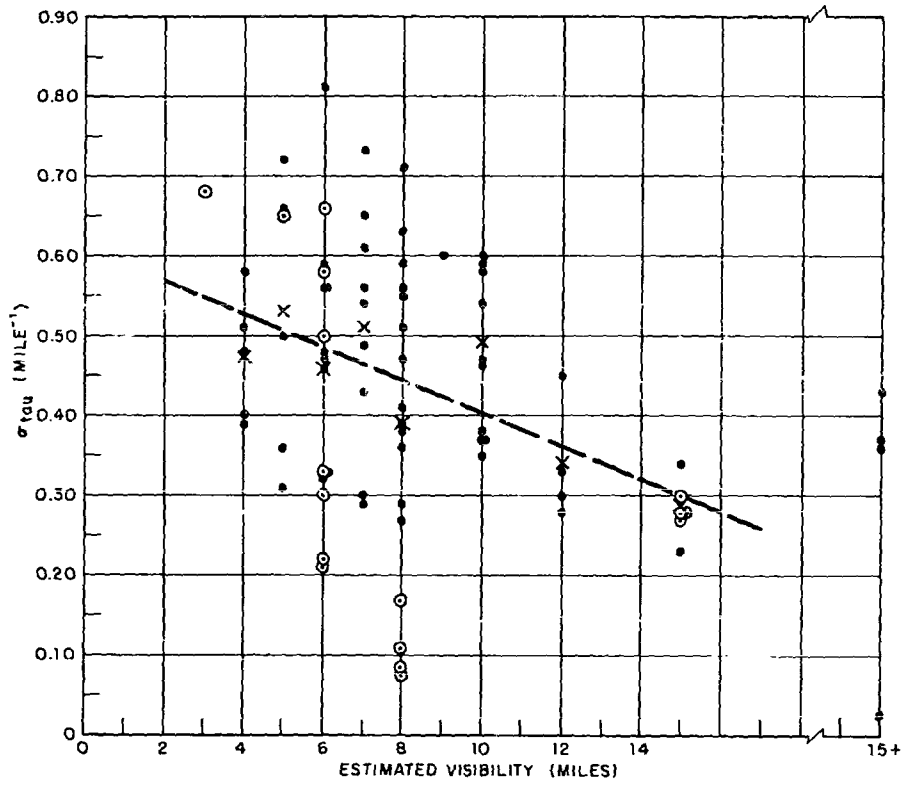

Fig. 31 Individual σ_{tau} values versus estimated range visibility. Encircled points are for data taken with clouds overhead. The dashed line has been drawn to fit the average values which are plotted as X.

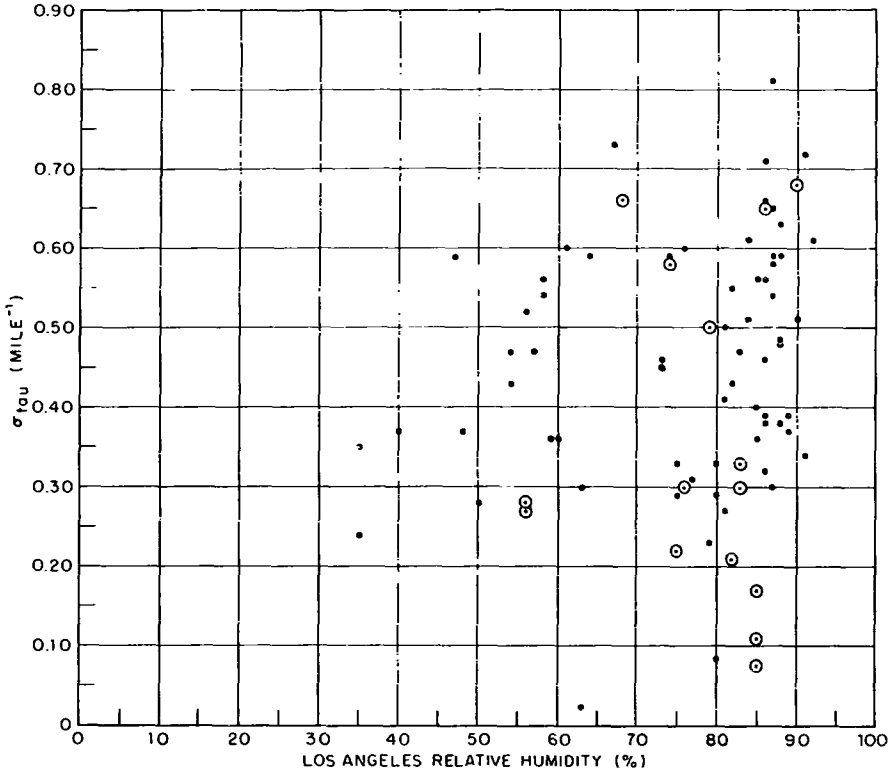

Fig. 32 Individual σ_{tau} values versus surface relative humidity at Los Angeles for wavelength 0.50μ. Encircled points are for data taken with clouds overhead.

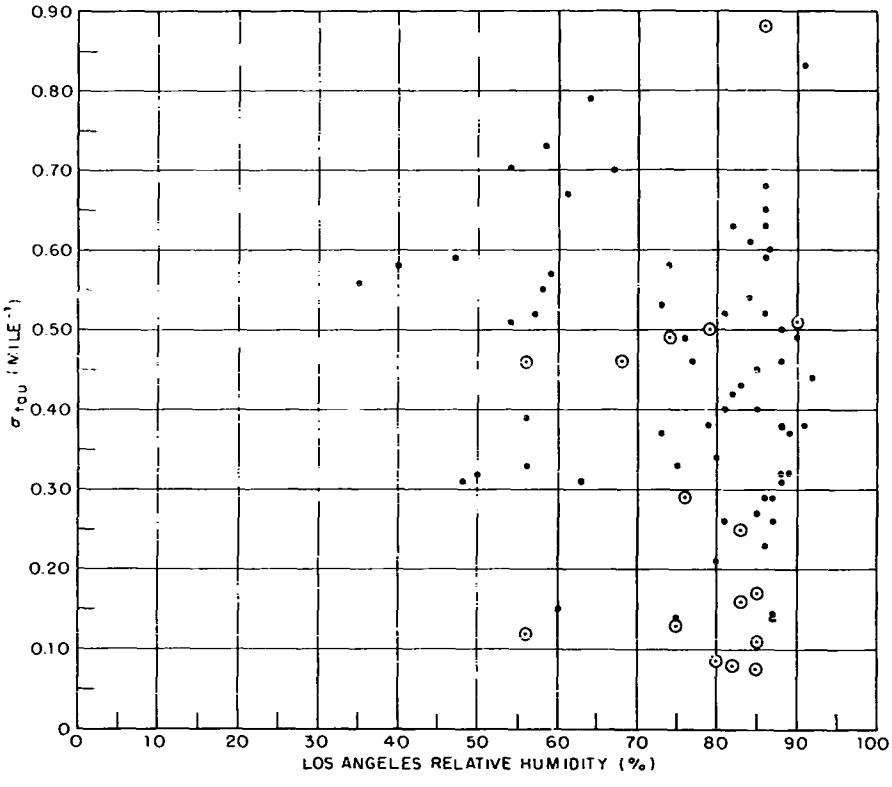

Fig. 33 Individual σ_{tau} values versus surface relative humidity at Los Angeles for wavelength 0.77μ. Encircled points are for data taken with clouds overhead.

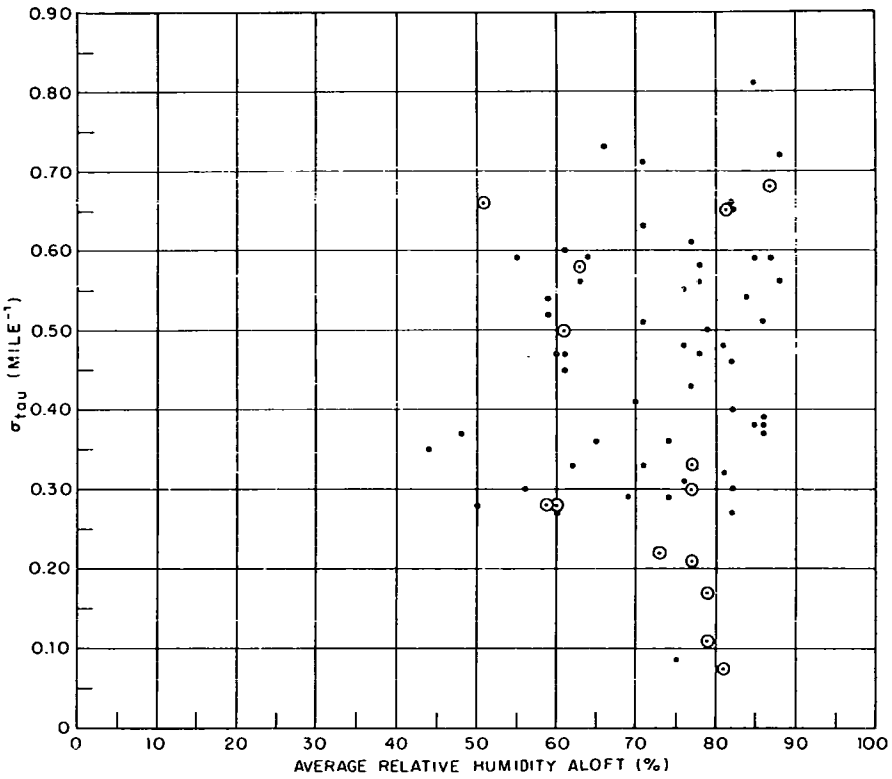

Fig. 34 Individual σ_{tau} values versus relative humidity aloft for wavelength 0.50μ. Encircled points are for data taken with clouds overhead.

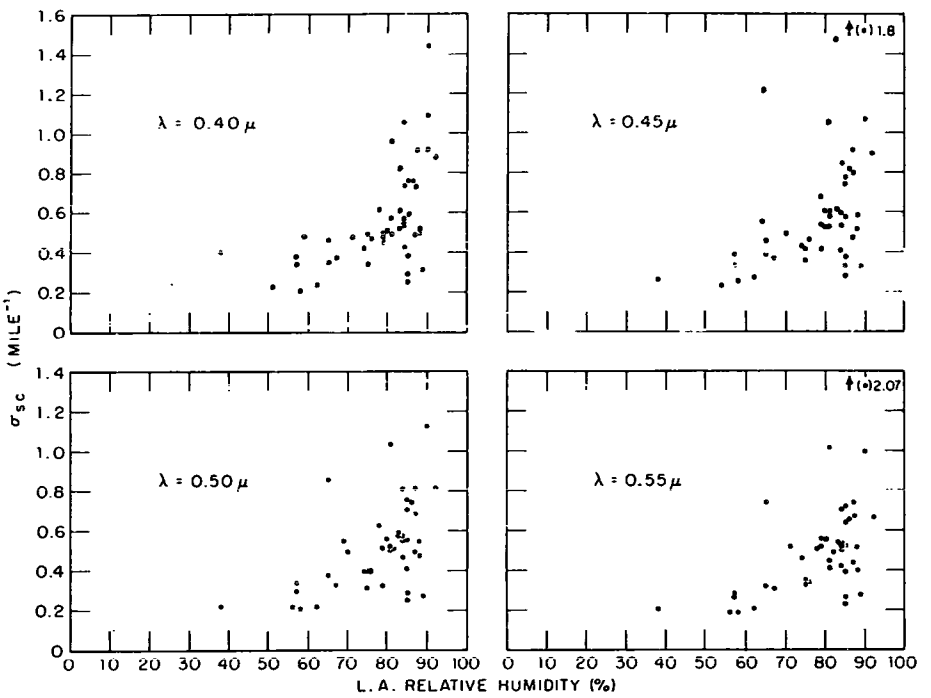

Fig. 35 Individual σ_{sc} values versus surface relative humidity in Los Angeles for four different wavelengths.

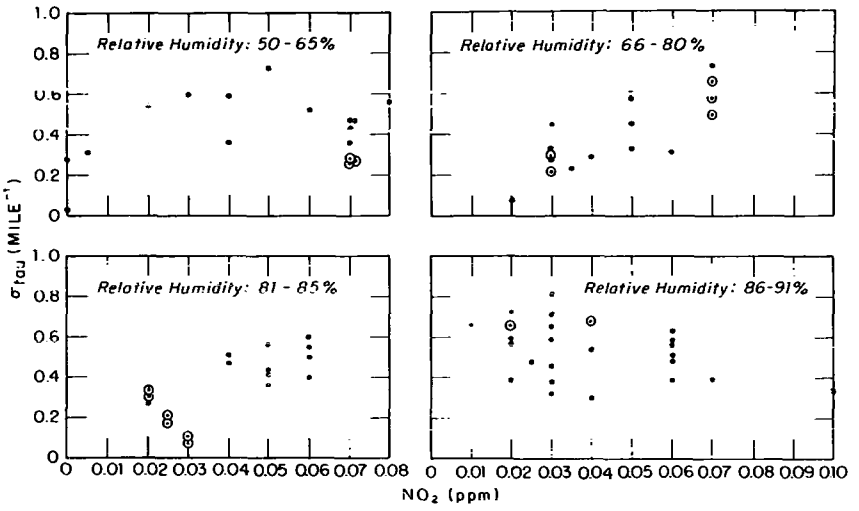

Fig. 36 Individual σ_{tau} values at wavelength 0.50μ versus NO_2 content for four different ranges of relative humidity in downtown Los Angeles. Encircled points are for data taken with clouds overhead.

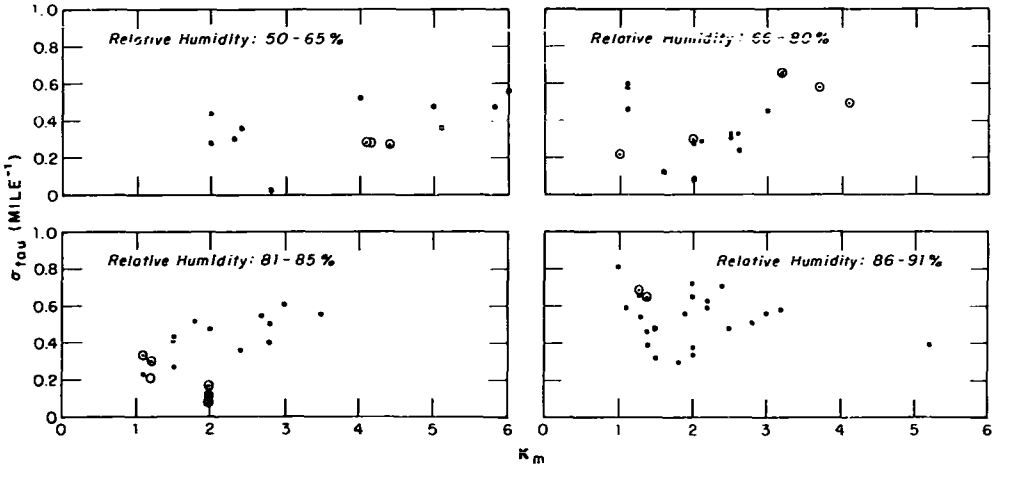

Fig. 37 Individual σ_{tau} values at wavelength 0.50μ versus K_m readings for four different ranges of relative humidity in downtown Los Angeles. Encircled points are for data taken with clouds overhead.

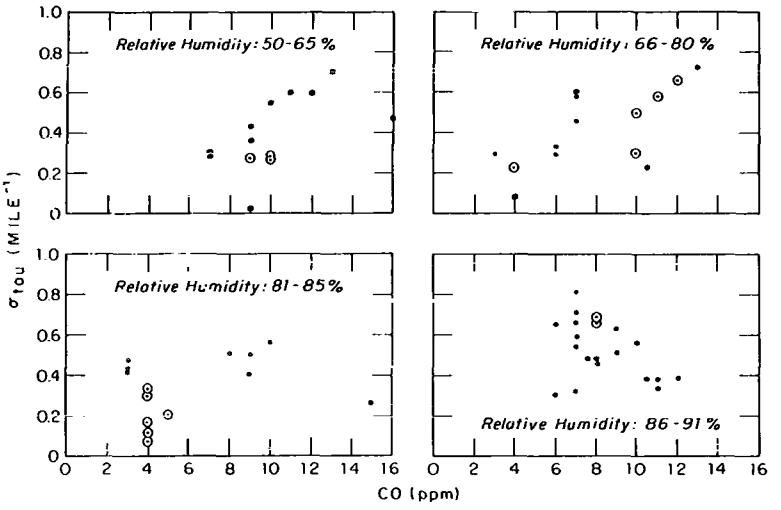

Fig. 38 Individual σ_{tau} values at wavelength 0.50μ versus CO content for four different ranges of relative humidity in downtown Los Angeles. Encircled points are for data taken with clouds overhead.

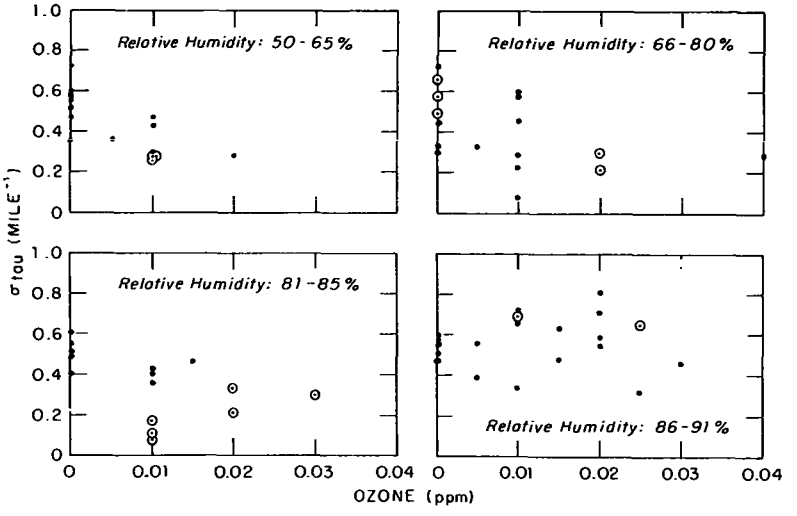

Fig. 39 Individual σ_{tau} values at wavelength 0.50μ versus ozone content for four different ranges of relative humidity in downtown Los Angeles. Encircled points are for data taken with clouds overhead.

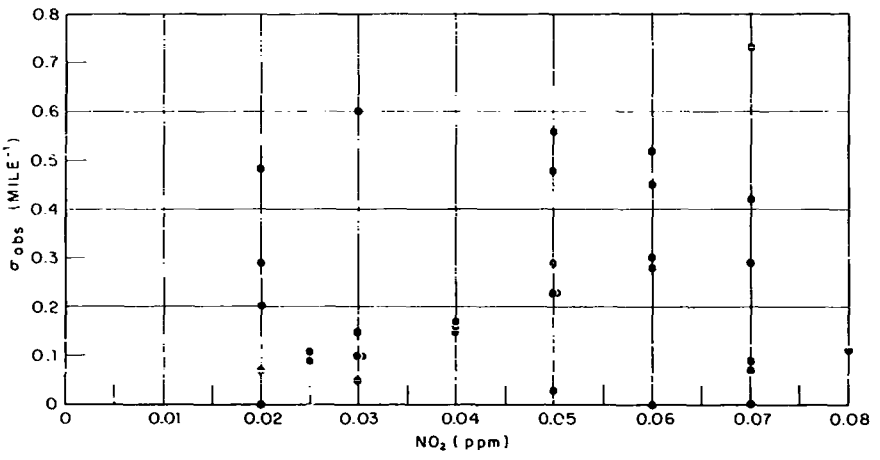

Fig. 40 Individual σ_{abs} values versus NO_2 content at wavelength 0.50μ.

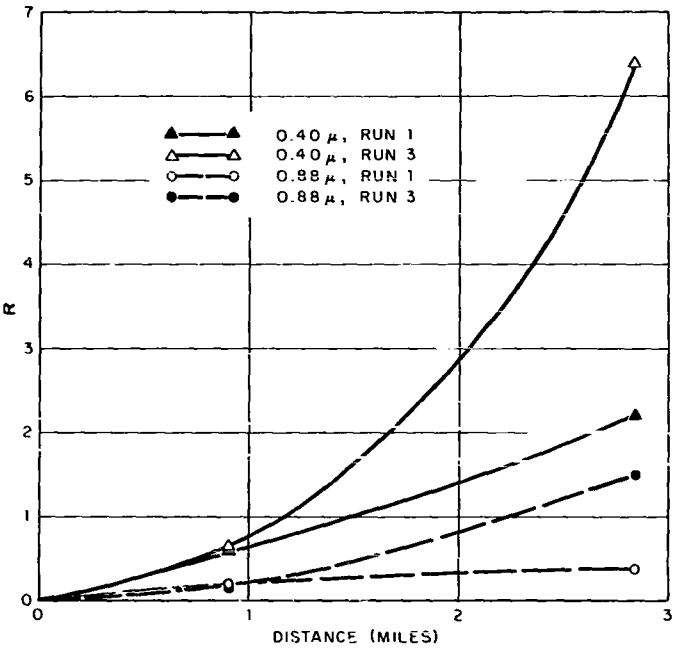

Fig. 41 Plots of R versus D for two wavelengths on 30 August 1960. Approximately 3 hours time differential between runs 1 and 3.

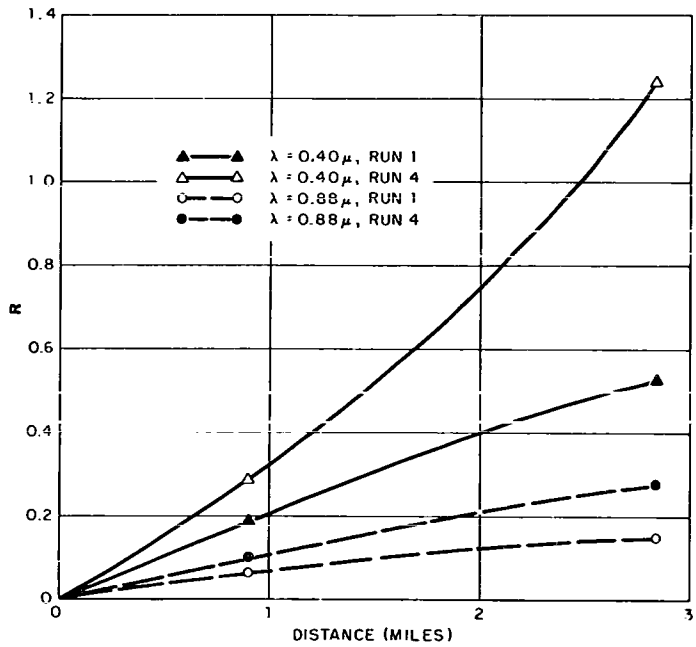

Fig. 42 Plots of R versus D for two wavelengths on 5 September 1960. Approximately 3-1/2 hours time differential between runs 1 and 4.

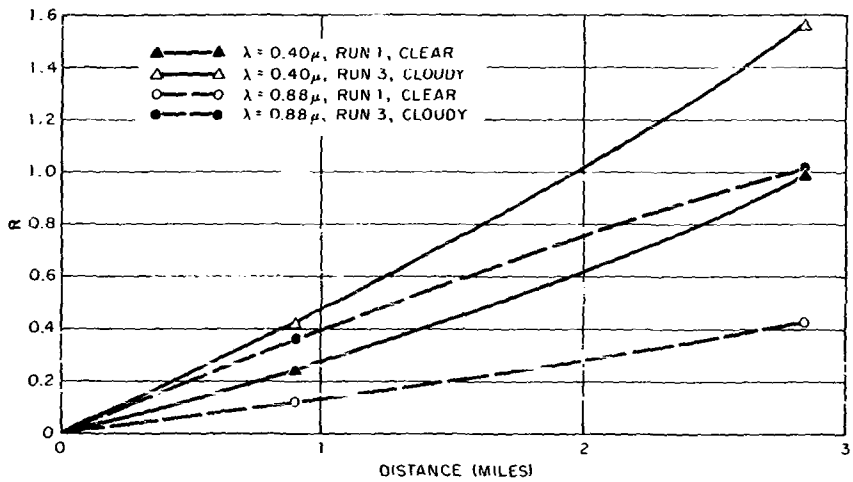

Fig. 43 Plots of R versus D for two wavelengths on 22 August 1960. See text for discussion of differences between runs 1 and 3.

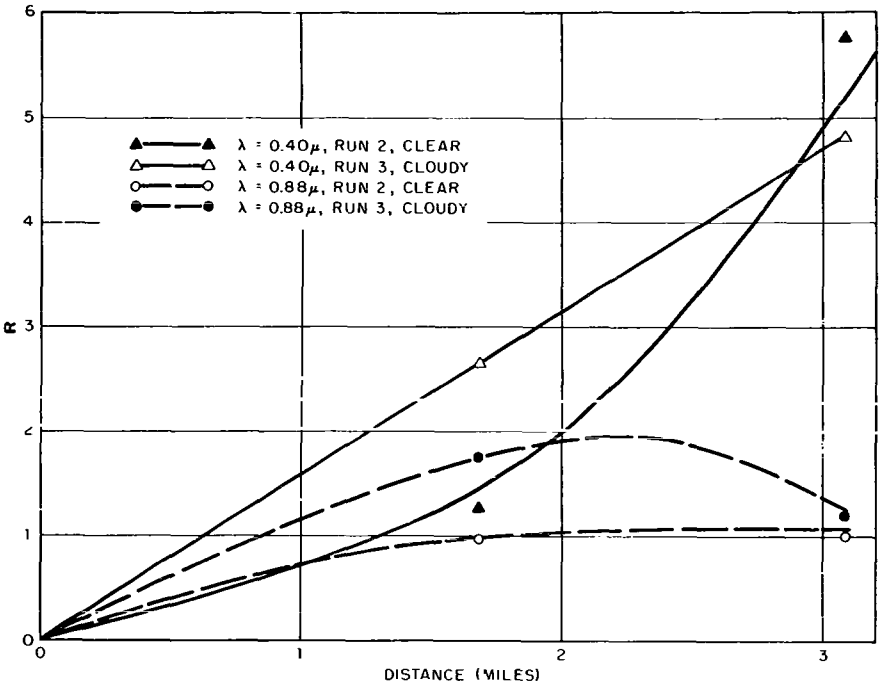

Fig. 44 Plots of R versus D for two wavelengths on 27 August 1960. See text for discussion of differences between runs 2 and 3.

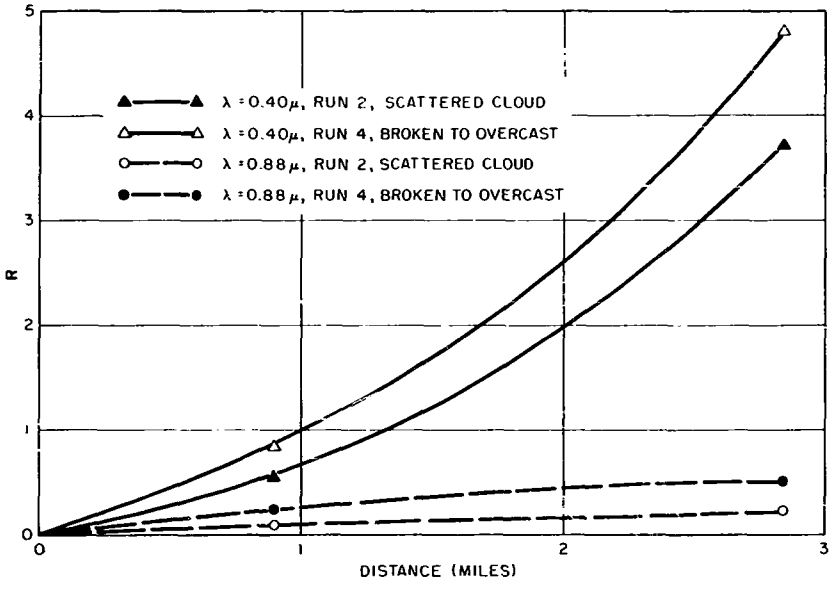

Fig. 45 Plots of R versus D for two wavelengths on 7 September 1960. See text for discussion of differences between runs 2 and 4.

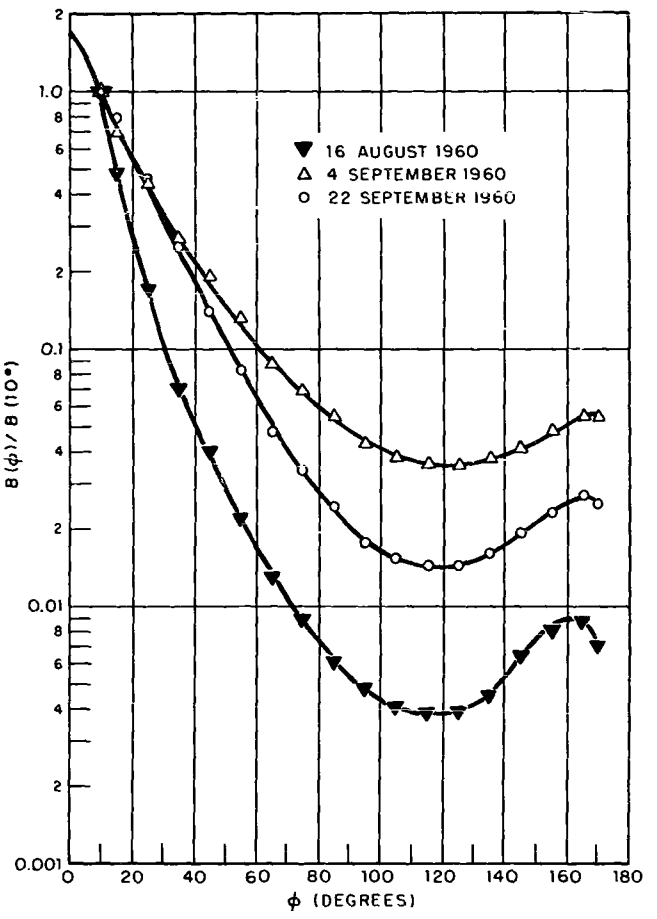

Fig. 46 Semilog plot of $B(\phi)/B(10^{\circ})$ versus ϕ for three different nights--all at wavelength 0.50μ. See text for description of the meteorological conditions during each night.

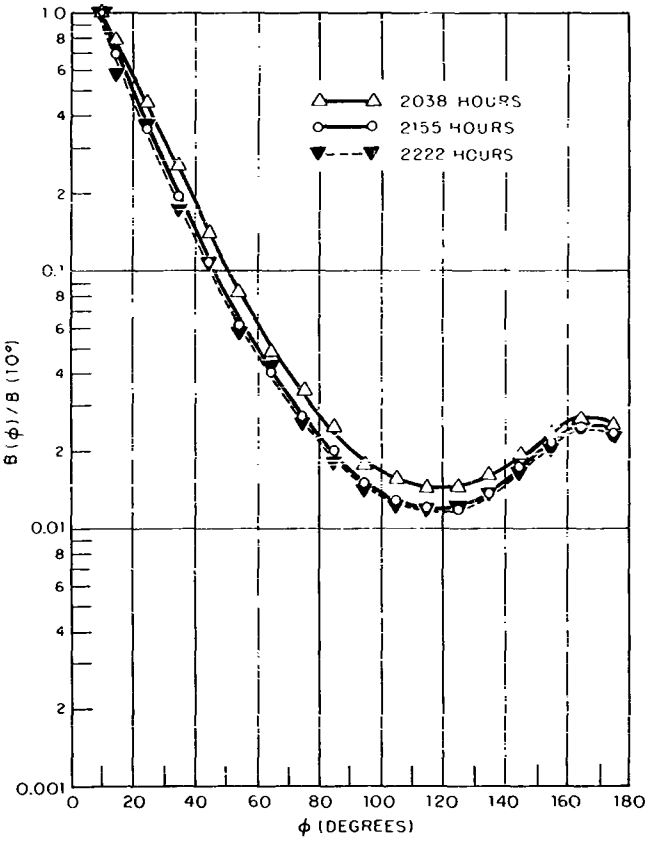

Fig. 47 Semilog plot of $B(\emptyset)/B(10^{o})$ versus $\emptyset$ for three different times during one night--all at wavelength 0.50μ. See text for description of the meteorological conditions existing during each run.

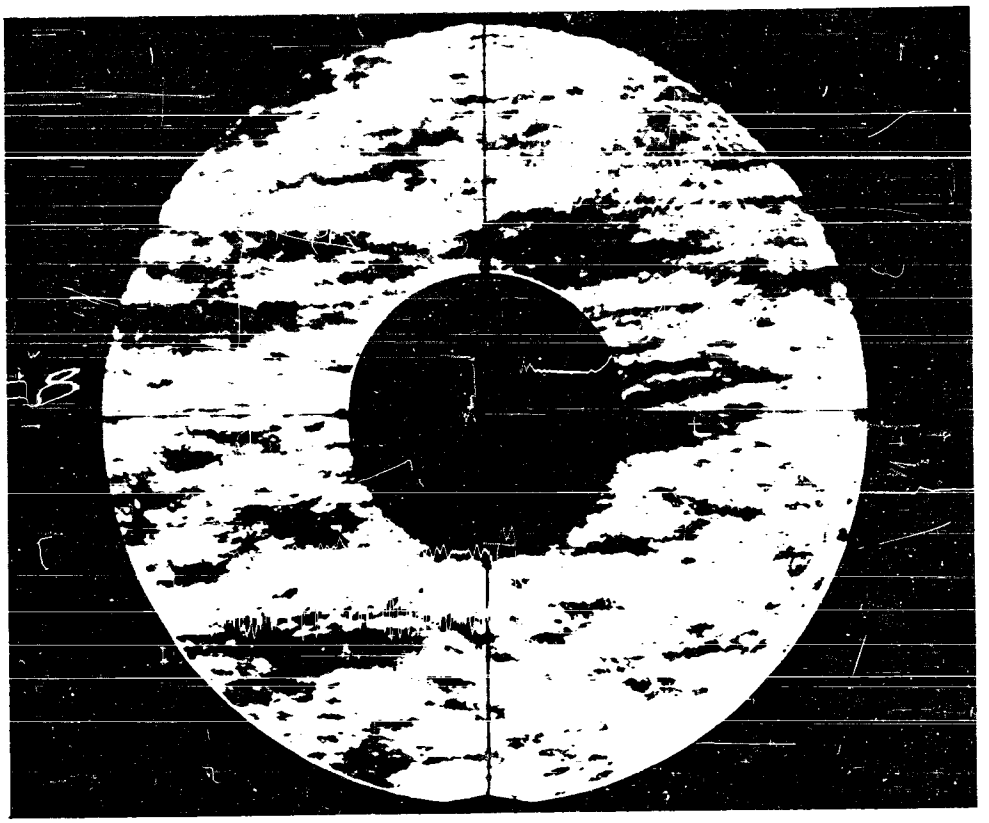

Fig. 48 Shadow bands produced by atmospheric striations in a photograph of Sirius taken with the 200-inch telescope at the Palomar Observatory.

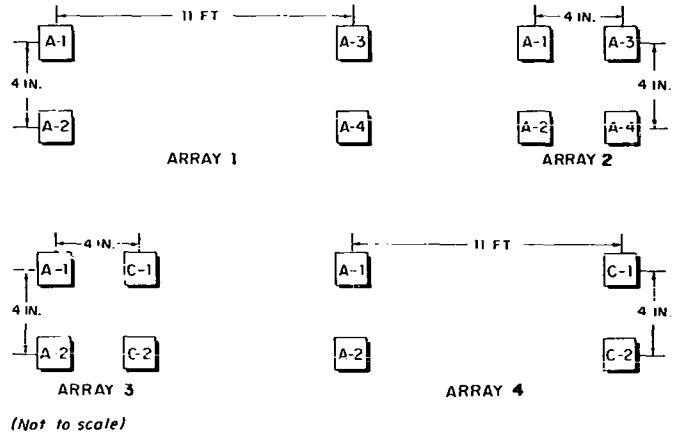

Fig. 49 Diagram of photomultiplier arrays used in transmission variability studies. A and C designate photomultiplier-filter combinations with maximum responses to lamp at wavelengths 0.40μ and 0.77μ, respectively.

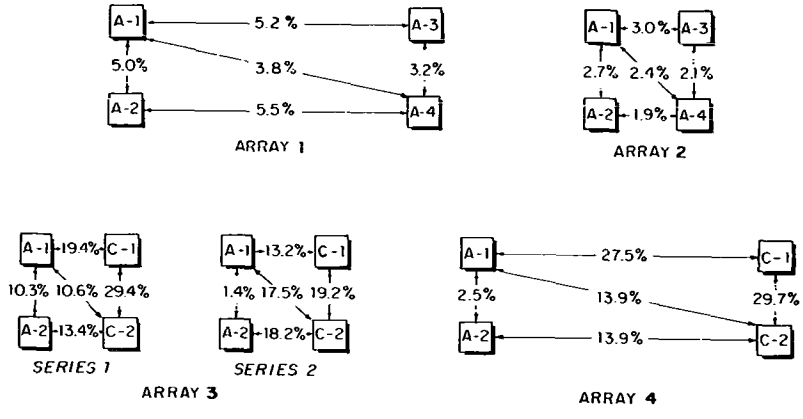

Fig. 50 Average differences between normalized responses of four photomultiplier-filter arrays at Griffith Park station 20 September 1960. A and C designate photomultiplier-filter combinations with maximum responses to lamp at wavelengths 0.40μ and 0.77μ, respectively.

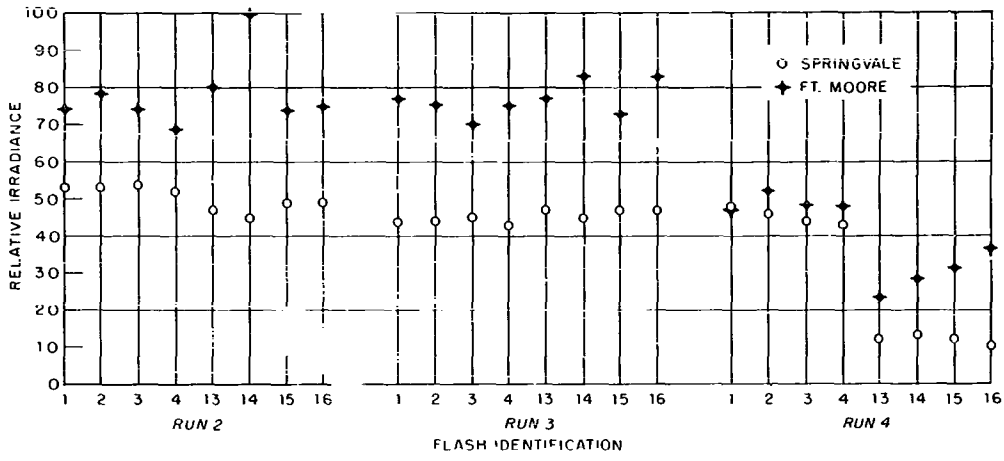

Fig. 51 Comparisons of calculated irradiances at two different stations for identical lamp flashes, 13 September 1960, wavelength 0.40μ. See text for description of corrections made for difference between the two station distances from the source.

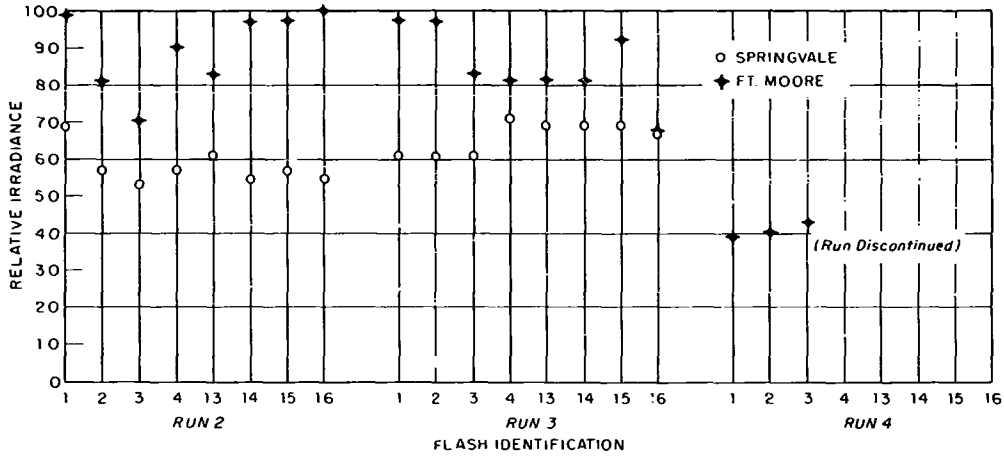

Fig. 52 Comparisons of calculated irradiances at two different stations for identical lamp flashes, 13 September 1960, wavelength 0.50μ. See text for description of corrections made for difference between the two station distances from the source.

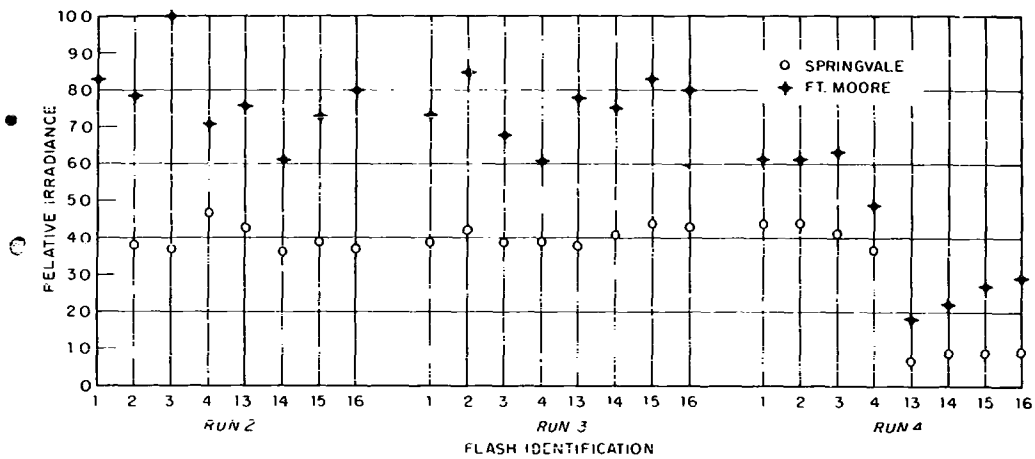

Fig. 53 Comparisons of calculated irradiances at two different stations for identical lamp flashes, 13 September 1960, wavelength 0.77μ. See text for description of corrections made for difference between the two station distances from the source.

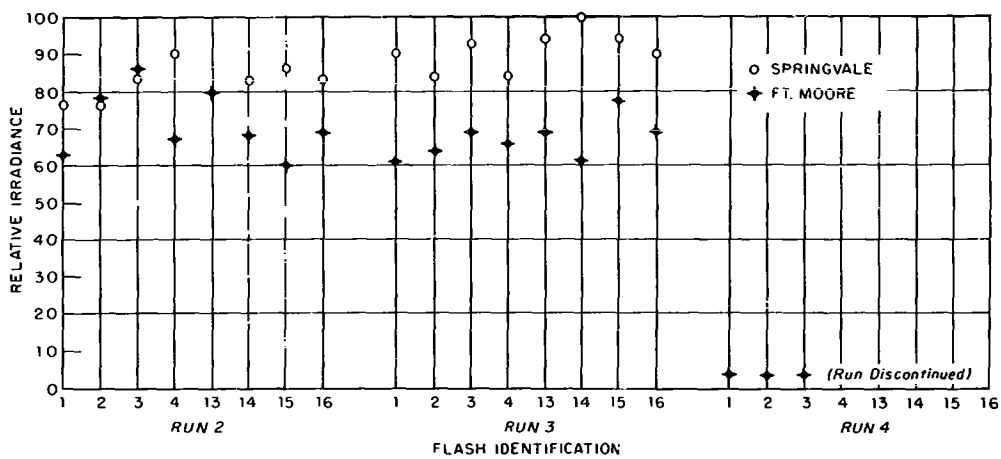

Fig. 54 Comparisons of calculated irradiances at two different stations for identical lamp flashes, 13 September 1960, wavelength 0.88μ. See text for description of corrections made for difference between the two station distances from the source.

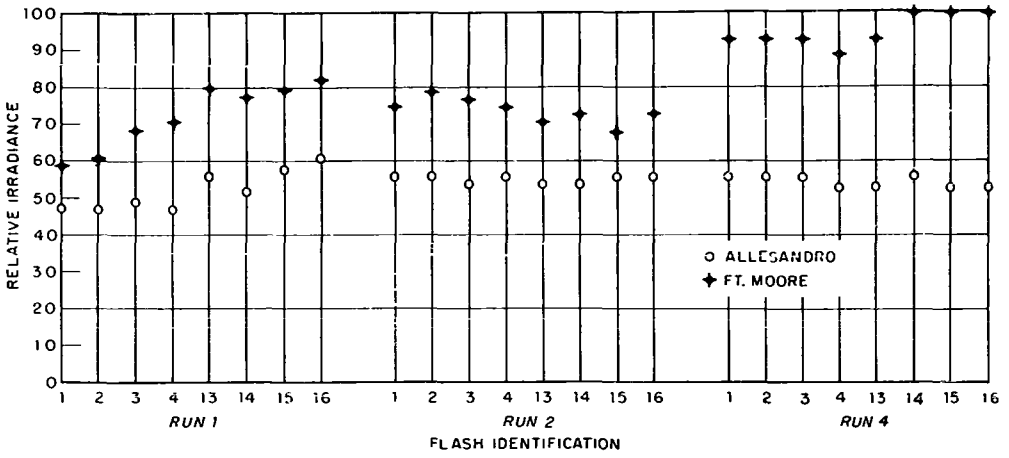

Fig. 55 Comparisons of calculated irradiances at two different stations for identical lamp flashes, 17 September 1960, wavelength 0.40μ. See text for description of corrections made for difference between the two station distances from the source.

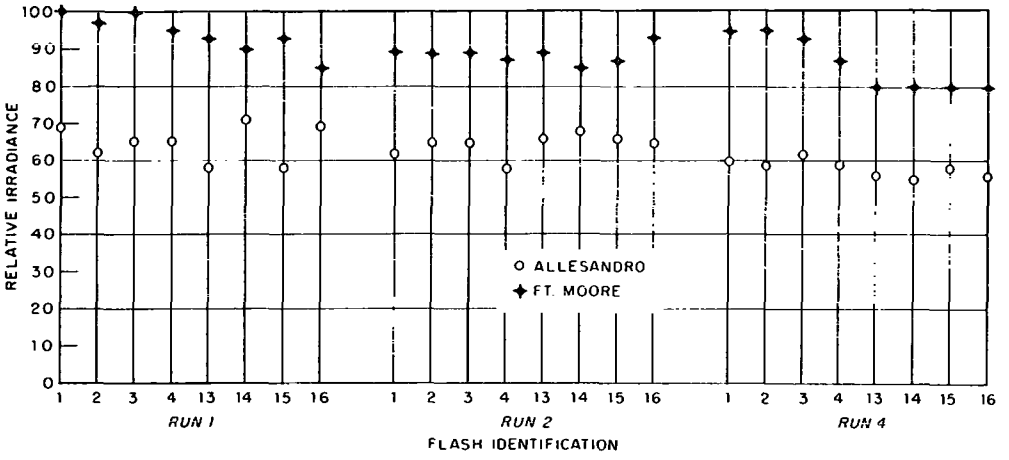

Fig. 56 Comparisons of calculated irradiances at two different stations for identical lamp flashes, 17 September 1960, wavelength 0.50μ. See text for description of corrections made for difference between the two station distances from the source.

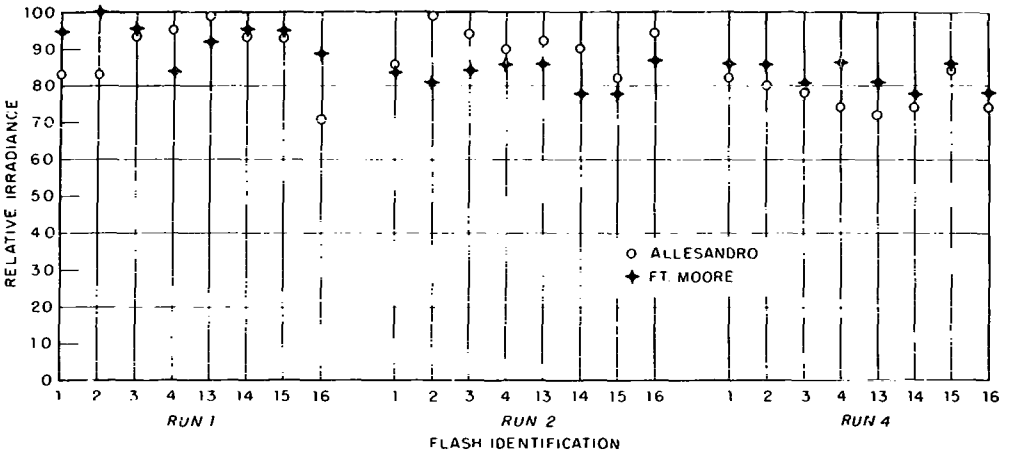

Fig. 57 Comparisons of calculated irradiances at two different stations for identical lamp flashes, 17 September 1960, wavelength 0.77μ. See text for description of corrections made for difference between the two station distances from the source.

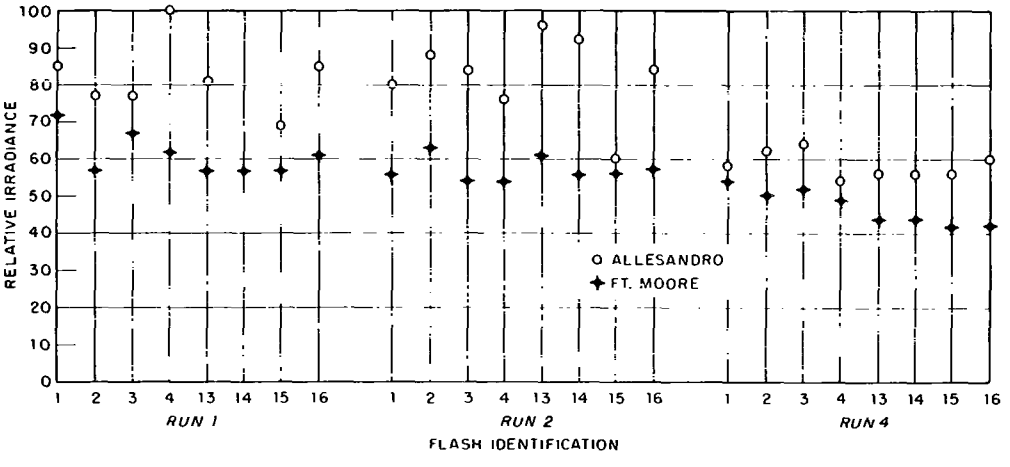

Fig. 58 Comparisons of calculated irradiances at two different stations for identical lamp flashes, 17 September 1960, wavelength 0.88μ. See text for description of corrections made for difference between the two station distances from the source.

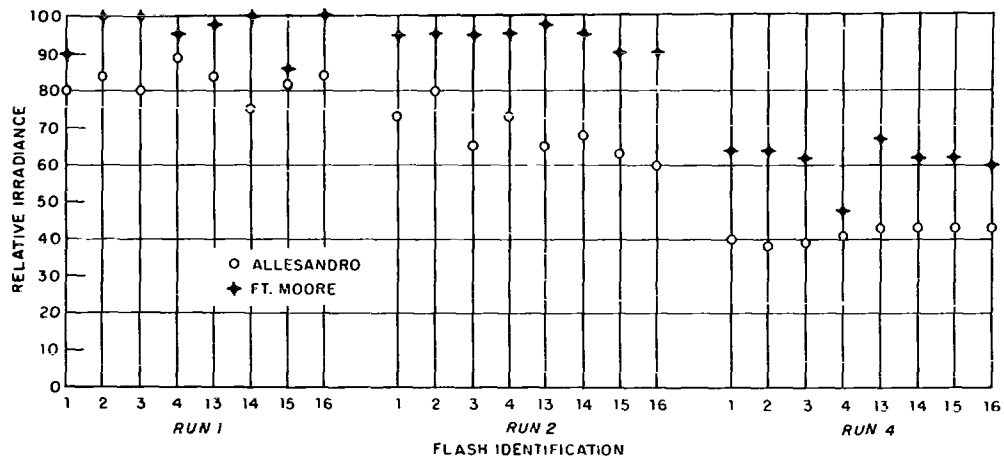

Fig. 59 Comparisons of calculated irradiances at two different stations for identical lamp flashes, 18 September 1960, wavelength 0.40μ. See text for description of corrections made for difference between the two station distances from the source.

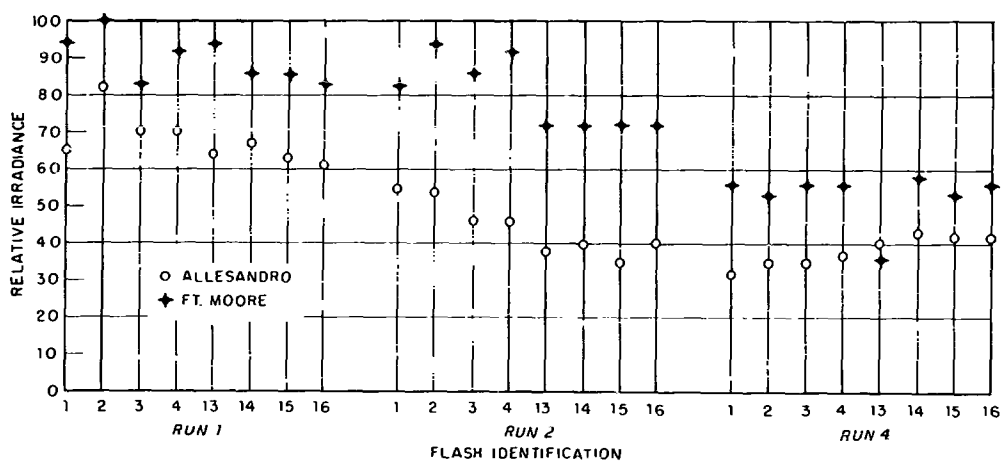

Fig. 60 Comparisons of calculated irradiances at two different stations for identical lamp flashes, 18 September 1960, wavelength 0.50μ. See text for description of corrections made for difference between the two station distances from the source.

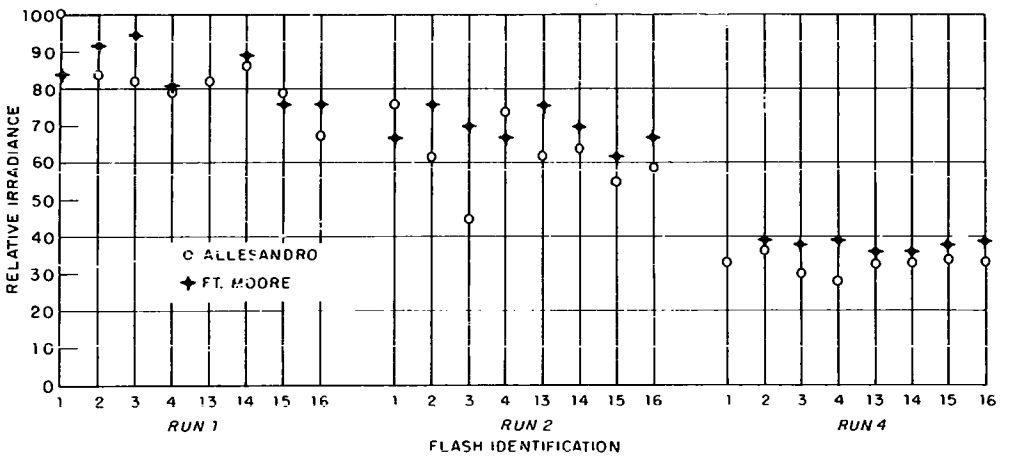

Fig. 61 Comparisons of calculated irradiances at two different stations for identical lamp flashes, 18 September 1960, wavelength 0.77μ. See text for description of corrections made for difference between the two station distances from the source.

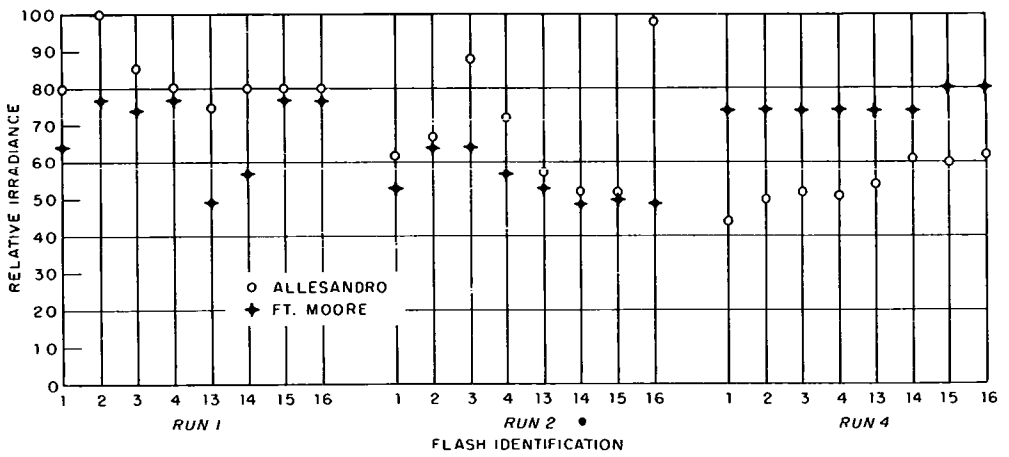

Fig. 62 Comparisons of calculated irradiances at two different stations for identical lamp flashes, 18 September 1960, wavelength 0.88μ. See text for description of corrections made for difference between the two station distances from the source.

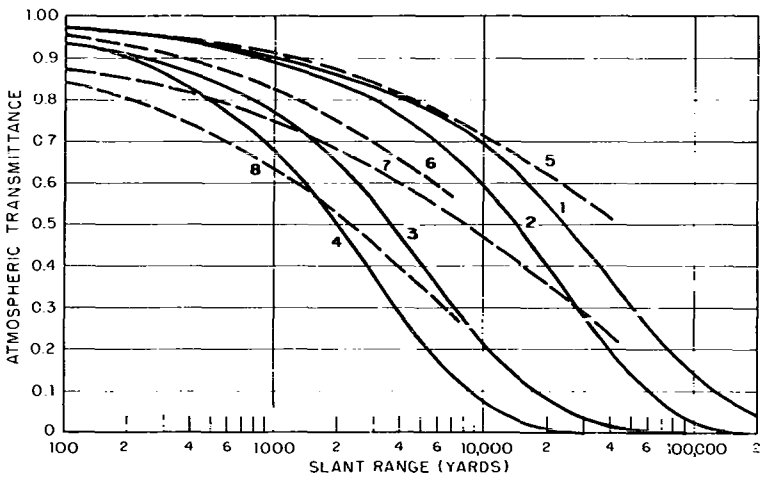

Fig. 63 Plot of atmospheric transmittance versus slant range for various sources and atmospheres. Solid curves are for aureoled transmission of radiation from a black body 4π radiator at $6000^{\circ}K$ with atmospheres as follows: 1 and 2, Nevada desert, visibility 65 and 35 miles, respectively; 3 and 4, Los Angeles, California, during period August-September for visibilities 12 and 6 miles, respectively. Dashed curves are from Figures 3-5A and 3-5B of TM 23-200[27] as follows: 5 and 6 are for air bursts, visibilities 50 and 10 miles, respectively; 7 and 8 are for surface bursts, visibilities 50 and 10 miles, respectively.

REFERENCES

1. Gibbons, M. G., et al, "Experimental Study of the Effect of Field of View on Transmission Measurements," USNRDL-TR-236, 1958.

2. Gibbons, M. G. et al., "Ground to Air Transmissions of Visible and Near Infrared Radiation from a 4-Pi Source," USNRDL-TR-357, 1959.

3. Gibbons, M. G. et al., "Transmission and Scattering Properties of a Nevada Desert Atmosphere," USNRDL-TR-439, 1959.

4. Gibbons, M. G. et al., "Transmission and Scattering Properties of a Nevada Desert Atmosphere under Cloudy Conditions," USNRDL-TR-461, 1960.

5. Carlson, F. E. and Pritchard, D. A., "Characteristics and Applications of Flashtubes," Illuminating Engineering 42 235 (1947).

6. Pritchard, B. S. and Elliott, W. G., "Two Instruments for Atmospheric Optics Measurements," J. Opt. Soc. Am. 50 191 (1960).

7. ASTM Method, D 1704-59T.

8. Middleton, W. E. K., Vision Through the Atmosphere, Univ. of Toronto Press 1952, page 105.

9. Hall, T. C., Jr., and Blacet, F. E., "Separation of the Absorption Spectra of NO_2 and N_2O_4 in the Range of 2400-5000A," J. Chem. Phys. 20, 1745 (1952).

10. Dixon, J. K., "The Absorption Coefficient of Nitrogen Dioxide in Visible Spectrum," J. Chem. Phys. 8, 157 (1940).

11. Inn, Edward, C. Y., and Tanaka, Yoshio, "Absorption Coefficient of Ozone in the Ultraviolet and Visible Regions," J. Opt. Soc. Am. 43, 870 (1953).

12. Hulburt, E. O., "Explanation of the Brightness and Color of the Sky, Particularly the Twilight Sky," J. Opt. Soc. Am. 43, 113 (1953)

13. Hitchcock, L. B., Faith, W. L., Neiburger, M., Renzetti, N. A., and Rogers, L. H., "Air Pollution Saturation in Los Angeles, an Aeromatic Survey," Proceedings of the Third National Air Pollution Symposium, 12 (1955).

14. Chambers, L. A., Foter, M. J., and Cholak, J., "A Comparison of Particulate Loadings in the Atmosphere of Certain American Cities," Proceedings of the Third National Air Pollution Symposium, 24 (1955).

15. Magill, P. L., "Techniques Employed in the Analysis of Los Angeles Smog," Proceedings of the First National Air Pollution Symposium, 61 (1949).

16. Waldram, J. M., "Measurement of the Photometric Properties of the Upper Atmosphere," Quart. J. Roy. Meteorol. Soc. 71, 319 (1945).

17. Hulburt, E. O., "Optics of Atmospheric Haze," J. Opt. Soc. Am. 31 467 (1941).

18. Goldstein, Emmanuel, "The Measurement of Fluctuating Radiation Components in Sky and Atmosphere, Part 2," NRL Report 3710, July 1950.

19. Siedentopf, H. and Wisshak, F., "Die Szintillation der Strahlung Terrestricher Lichtquellen und ihr Gang mit der Tageszeit," Optik 3, 430.

20. Duclaux, J., "Propagation de la lumiere dans l"atmosphere," J. de Phys, et le Radium, 6, 49 (1935).

21. Yates, H. W., and Taylor, J. H. "Infrared Transmission of the Atmosphere," NRL Report 5453, June 1960.

22. Middleton, W. E. K., Vision Through the Atmosphere, Univ. of Toronto Press 1952, page 27.

23. Middleton, W. E. K., Vision Through the Atmosphere, Univ. of Toronto Press 1952 (Fig. 3-8, page 39 "after Fortzik").

24. Dunkleman, L., NRL Report 4031, "Horizontal Attenuation of Ultraviolet and Visible Light by the Lower Atmosphere," September 1952.

25. TM 23-200 OPNAV Instruction 03400.1B Capabilities of Atomic Weapons, November 1957 edition, pp. 3-15 and 3-16 (Confidential).

26. Gibbons, M. G., "Wavelength Dependence of the Scattering Coefficient for Infrared Radiation in Natural Haze," J. Opt. Soc. Am. 48, 122 (1958).

27. Sinclair, D., "Proceedings of the U. S. Technical Conference on Air Pollution," (McGraw-Hill Book Co., Inc., New York, 1952) Chap. 18.

DISTRIBUTION

Copies

NAVY

1-3	Chief, Bureau of Ships (Code 335)
4	Chief, Bureau of Ships (Code 320)
5	Chief, Bureau of Naval Weapons (RRMA-11)
6-7	Chief, Bureau of Yards and Docks (Code 74)
8	Chief, Bureau of Yards and Docks (Code E-400)
9	Chief of Naval Operations (Op-07T)
10	Chief of Naval Research (Code 104)
11-13	Director, Naval Research Laboratory (Code 2021)
14	Office of Naval Research (Code 422)
15-29	Office of Naval Research FPO, New York
30	CO, Office of Naval Research Branch Office, SF
31	CO, U.S. Naval Civil Engineering Laboratory
32	Commander, Naval Air Material Center, Philadelphia
33	Naval Medical Research Institute
34	U.S. Naval Postgraduate School, Monterey
35	CO, Naval Nuclear Ordnance Evaluation Unit (Code 4011)
36	Commander, Naval Ordnance Laboratory, Silver Spring
37	Office of Patent Counsel, San Diego

ARMY

38	Chief of Research and Development (Atomic Division)
39	Chief of Research and Development (Life Science Div.)
40	Chief of Engineers (ENGMC-EB)
41	Chief of Engineers (ENGMC-DE)
42	Chief of Engineers (ENGRD-S)
43	CG, Ballistic Research Laboratories
44	Chief Chemical Officer (Director for Safety)
45	CG, Chemical Corps Res. and Dev. Command
46	Hq., Chemical Corps Materiel Command
47	President, Chemical Corps Board
48	CO, Chemical Corps Training Command
49	Commandant, Chemical Corps Schools (Library)
50	Chemical Committee, Army Infantry School, Fort Benning
51	CO, Chemical Research and Development Laboratories
52	Commander, Chemical Corps Nuclear Defense Laboratory

53	Hq., Army Environmental Hygiene Agency
54	CG, Aberdeen Proving Ground
55	Office of Chief Signal Officer (SIGRD-8B)
56	Director, Walter Reed Army Medical Center
57	CG, Quartermaster Res. and Eng. Command
58	Hq., Dugway Proving Ground
59-61	The Surgeon General (MEDNE)
62	CO, Army Signal Res. and Dev. Laboratory
63	CG, Army Electronic Proving Ground
64	CG, Engineer Res. and Dev. Laboratory
65	Director, Office of Special Weapons Development
66	CO, Office of Ordnance Research
67	CO, Watertown Arsenal
68	CG, Ordnance Tank-Automotive Command
69	CO, Ordnance Materials Research Office, Watertown
70	CO, Frankford Arsenal
71	CG, Ordnance Missile Command

AIR FORCE

72	Assistant Chief of Staff, Intelligence (AFCIN-3B)
73-78	Commander, Aeronautical Systems Division (ASAPRD-NS)
79	Directorate of Civil Engineering (AFOCE-ES)
80	Director, USAF Project RAND
81-82	Commandant, School of Aerospace Medicine, Brooks AFB
83	Office of the Surgeon (SUP3.1), Strategic Air Command
84	Commander, Special Weapons Center, Kirtland AFB
85	Director, Air University Library, Maxwell AFB
86-87	Commander, Technical Training Wing, 3415th TTG
88	Commander, Electronic Systems Division (CRZT)

OTHER DOD ACTIVITIES

89-91	Chief, Defense Atomic Support Agency (Library)
92	Commander, FC/DASA, Sandia Base (FCDV)
93	Commander, FC/DASA, Sandia Base (FCTG5, Library)
94	Commander, FC/DASA, Sandia Base (FCWT)
95-114	Armed Services Technical Information Agency
115	Director, Armed Forces Radiobiology Research Institute

OCD

116-125	Office of Civil Defense, Battle Creek
126	Office of Civil Defense, Washington

AEC ACTIVITIES AND OTHERS

127	Research Analysis Corporation
128	Texas Instruments, Inc. (Mouser)

129	Aerojet General, Azusa
130	Aerojet General, San Ramon
131	Alco Products, Inc.
132	Allis-Chalmers Manufacturing Co., Milwaukee
133	Allis-Chalmers Manufacturing Co., Washington
134	Allison Division, GMC
135-136	Argonne Cancer Research Hospital
137-146	Argonne National Laboratory
147	Armour Research Foundation
148	Atomic Bomb Casualty Commission
149	AEC Scientific Representative, France
150	AEC Scientific Representative, Japan
151-153	Atomic Energy Commission, Washington
154-157	Atomic Energy of Canada, Limited
158-161	Atomics International
162-163	Babcock and Wilcox Company
164-165	Battelle Memorial Institute
166-169	Brookhaven National Laboratory
170	Carnegie Institute of Technology
171	Chicago Patent Group
172	Columbia University (Havens)
173	Columbia University (SOO-187)
174	Combustion Engineering, Inc.
175	Combustion Engineering, Inc. (NRD)
176-177	Convair Division, Fort Worth
178	Convair-General Dynamics Corporation, San Diego
179-183	Defence Research Member
184-186	duPont Company, Aiken
187	duPont Company, Wilmington
188	Edgerton, Germeshausen and Grier, Inc., Las Vegas
189	Franklin Institute of Pennsylvania
190-191	General Atomic Division
192-193	General Electric Company (ANPD)
194-199	General Electric Company, Richland
200	General Electric Company, St. Petersburg
201	General Nuclear Engineering Corporation
202	Gibbs and Cox, Inc.
203	Glasstone, Samuel
204-205	Goodyear Atomic Corporation
206	Hughes Aircraft Company, Culver City
207-208	Iowa State University
209-210	Jet Propulsion Laboratory
211-213	Knolls Atomic Power Laboratory
214	Lockheed Aircraft Corporation
215-216	Los Alamos Scientific Laboratory (Library)
217	Lovelace Foundation
218	Maritime Administration
219	Marquard Corporation
220	Martin Company

221	Massachusetts Institute of Technology (Profio)
222	Massachusetts Institute of Technology (Thompson)
223-224	Midwestern Universities Research Association
225	Mound Laboratory
226	NASA, Langley Research Center
227	NASA, Lewis Research Center
228	National Bureau of Standards (Library)
229-230	National Bureau of Standards (Taylor)
231	National Lead Company of Ohio
232	New Brunswick Area Office
233	New York Operations Office
234	New York University (Fisher)
235	New York University (Richtmeyer)
236	Nuclear Materials and Equipment Corporation
237	Nuclear Metals, Inc.
238	Oak Ridge Institute of Nuclear Studies
239	Patent Branch, Washington
240	Pennsylvania State University (Blanchard)
241-244	Phillips Petroleum Company
245	Power Reactor Development Company
246-248	Pratt and Whitney Aircraft Division
249	Princeton University (White)
250-251	Public Health Service, Washington
252	Public Health Service, Las Vegas
253	Public Health Service, Montgomery
254	Rand Corporation (Deirmendjian)
255	Purdue University
256	Rensselaer Polytechnic Institute
257	Sandia Corporation, Albuquerque
258	Sandia Corporation, Livermore
259	States Marine Lines, Inc.
260	Stevens Institute of Technology
261	Sylvania Electric Products, Inc.
262	Scripts Institute (Duntley)
263	Technical Research Group
264	Tennessee Valley Authority
265	Texas Nuclear Corporation
266-267	Union Carbide Nuclear Company (ORGDP)
268-272	Union Carbide Nuclear Company (ORNL)
273	Union Carbide Nuclear Company (Paducah Plant)
274-275	United Nuclear Corporation (NDA)
276	U.S. Coast and Geodetic Survey, Washington
277	U.S. Geological Survey, Denver
278	U.S. Geological Survey, Menlo Park
279	U.S. Geological Survey, Naval Gun Factory
280	U.S. Geological Survey, Washington
281-282	University of California Lawrence Radiation Lab., Berkeley
283-286	University of California Lawrence Radiation Lab., Livermore
287	University of California, Los Angeles

288	University of California, San Francisco
289-290	University of Michigan (Churchill)
291	University of Puerto Rico
292	University of Rochester (Atomic Energy Project)
293-294	University of Rochester (Marshak)
295	University of Rochester (Stewart)
296	University of Washington (Geballe)
297	University of Washington (Rohde)
298-301	Westinghouse Bettis Atomic Power Laboratory
302-303	Westinghouse Electric Corporation
304	Yale University (Breit)
305	Yale University (Schultz)
306	Yankee Atomic Electric Company
307-331	Technical Information Service, Oak Ridge

USNRDL

332-375	USNRDL, Technical Information Division

DISTRIBUTION DATE: 25 May 1962

Naval Radiological Defense Laboratory
USNRDL-TR-554
TRANSMISSION AND SCATTERING PROPERTIES OF THE LOS ANGELES, CALIFORNIA ATMOSPHERE IN AUGUST AND SEPTEMBER 1960 by E.R. Schleiger, J.R. Nichols, and F.I. Laughridge
10 October 1961 100 p. tables illus. 27 refs.
UNCLASSIFIED

Measurements of peak irradiances have been made in Los Angeles, California, nighttime atmospheres at distances from 0.90 to 6.77 statute miles from a Xenon flashlamp radiating uniformly in all directions. The measurements were made at
(over)

1. Atmosphere - Radiation-scattering determination.
2. Infrared radiation - Urban areas.
3. Thermal radiation - Attenuation.
I. Schleiger, E.R.
II. Nichols, J.R.
III. Laughridge, F.I.
IV. Title.

UNCLASSIFIED

wavelengths 0.40, 0.50, 0.77 and 0.88μ (microns) with receiver fields of view up to 64 degrees half-angle. From these data attenuation coefficients were calculated for collimated transmission and aureoled transmission (4π source and flat receiver facing the source). Also calculated for aureoled transmission were values of R, the ratio of "scattered-in" radiation to direct radiation received by the flat receiver at various distances from the source. Angular scattering diagrams and attenuation coefficients for scattering were measured for radiation of wavelengths 0.40, 0.45, 0.50 and 0.55μ. Relations between these optical characteristics of the atmosphere and meteorological characteristics such as visibility, relative humidity, and contaminant contents were examined. Investigations of transmission variability with respect to both time and space were made. Curves were prepared from these and other experimental data showing transmittances of four typical atmospheres as a function of range for the case of flat receivers and radiation from a 4π black body source at 6000 degrees K.

UNCLASSIFIED

Naval Radiological Defense Laboratory
USNRDL-TR-554
TRANSMISSION AND SCATTERING PROPERTIES OF THE LOS ANGELES, CALIFORNIA ATMOSPHERE IN AUGUST AND SEPTEMBER 1960 by E.R. Schleiger, J.R. Nichols, and F.I. Laughridge
10 October 1961 100 p. tables illus. 27 refs.
UNCLASSIFIED

Measurements of peak irradiances have been made in Los Angeles, California, nighttime atmospheres at distances from 0.90 to 6.77 statute miles from a Xenon flashlamp radiating uniformly in all directions. The measurements were made at
(over)

1. Atmosphere - Radiation-scattering determination.
2. Infrared radiation - Urban areas.
3. Thermal radiation - Attenuation.
I. Schleiger, E.R.
II. Nichols, J.R.
III. Laughridge, F.I.
IV. Title.

UNCLASSIFIED

wavelengths 0.40, 0.50, 0.77 and 0.88μ (microns) with receiver fields of view up to 64 degrees half-angle. From these data attenuation coefficients were calculated for collimated transmission and aureoled transmission (4π source and flat receiver facing the source). Also calculated for aureoled transmission were values of R, the ratio of "scattered-in" radiation to direct radiation received by the flat receiver at various distances from the source. Angular scattering diagrams and attenuation coefficients for scattering were measured for radiation of wavelengths 0.40, 0.45, 0.50 and 0.55μ. Relations between these optical characteristics of the atmosphere and meteorological characteristics such as visibility, relative humidity, and contaminant contents were examined. Investigations of transmission variability with respect to both time and space were made. Curves were prepared from these and other experimental data showing transmittances of four typical atmospheres as a function of range for the case of flat receivers and radiation from a 4π black body source at 6000 degrees K.

UNCLASSIFIED

Naval Radiological Defense Laboratory
USNRDL-TR-554
TRANSMISSION AND SCATTERING PROPERTIES OF THE LOS ANGELES, CALIFORNIA ATMOSPHERE IN AUGUST AND SEPTEMBER 1960 by E.R. Schleiger, J.R. Nichols, and F.I. Laughridge
10 October 1961 100 p. tables illus. 27 refs.
UNCLASSIFIED

Measurements of peak irradiances have been made in Los Angeles, California, nighttime atmospheres at distances from 0.90 to 6.77 statute miles from a Xenon flashlamp radiating uniformly in all directions. The measurements were made at
(over)

1. Atmosphere - Radiation-scattering determination.
2. Infrared radiation - Urban areas.
3. Thermal radiation - Attenuation.

I. Schleiger, E.R.
II. Nichols, J.R.
III. Laughridge, F.I.
IV. Title.

UNCLASSIFIED

wavelengths 0.40, 0.50, 0.77 and 0.88μ (microns) with receiver fields of view up to 64 degrees half-angle. From these data attenuation coefficients were calculated for collimated transmission and aureoled transmission (4π source and flat receiver facing the source). Also calculated for aureoled transmission were values of R, the ratio of "scattered-in" radiation to direct radiation received by the flat receiver at various distances from the source. Angular scattering diagrams and attenuation coefficients for scattering were measured for radiation of wavelengths 0.40, 0.45, 0.50 and 0.55μ. Relations between these optical characteristics of the atmosphere and meteorological characteristics such as visibility, relative humidity, and contaminant contents were examined. Investigations of transmission variability with respect to both time and space were made. Curves were prepared from these and other experimental data showing transmittances of four typical atmospheres as a function of range for the case of flat receivers and radiation from a 4π black body source at 6000 degrees K.

UNCLASSIFIED

Naval Radiological Defense Laboratory
USNRDL-TR-554
TRANSMISSION AND SCATTERING PROPERTIES OF THE LOS ANGELES, CALIFORNIA ATMOSPHERE IN AUGUST AND SEPTEMBER 1960 by E.R. Schleiger, J.R. Nichols, and F.I. Laughridge
10 October 1961 100 p. tables illus. 27 refs.
UNCLASSIFIED

Measurements of peak irradiances have been made in Los Angeles, California, nighttime atmospheres at distances from 0.90 to 6.77 statute miles from a Xenon flashlamp radiating uniformly in all directions. The measurements were made at
(over)

1. Atmosphere - Radiation-scattering determination.
2. Infrared radiation - Urban areas.
3. Thermal radiation - Attenuation.

I. Schleiger, E.R.
II. Nichols, J.R.
III. Laughridge, F.I.
IV. Title.

UNCLASSIFIED

wavelengths 0.40, 0.50, 0.77 and 0.88μ (microns) with receiver fields of view up to 64 degrees half-angle. From these data attenuation coefficients were calculated for collimated transmission and aureoled transmission (4π source and flat receiver facing the source). Also calculated for aureoled transmission were values of R, the ratio of "scattered-in" radiation to direct radiation received by the flat receiver at various distances from the source. Angular scattering diagrams and attenuation coefficients for scattering were measured for radiation of wavelengths 0.40, 0.45, 0.50 and 0.55μ. Relations between these optical characteristics of the atmosphere and meteorological characteristics such as visibility, relative humidity, and contaminant contents were examined. Investigations of transmission variability with respect to both time and space were made. Curves were prepared from these and other experimental data showing transmittances of four typical atmospheres as a function of range for the case of flat receivers and radiation from a 4π black body source at 6000 degrees K.

UNCLASSIFIED

Naval Radiological Defense Laboratory
USNRDL-TR-554
TRANSMISSION AND SCATTERING PROPERTIES OF THE LOS ANGELES, CALIFORNIA ATMOSPHERE IN AUGUST AND SEPTEMBER 1960 by E.R. Schleiger, J.R. Nichols, and F.I. Laughridge
10 October 1961 100 p. tables illus. 27 refs.
UNCLASSIFIED

Measurements of peak irradiances have been made in Los Angeles, California, nighttime atmospheres at distances from 0.90 to 6.77 statute miles from a Xenon flashlamp radiating uniformly in all directions. The measurements were made at
(over)

1. Atmosphere - Radiation-scattering determination.
2. Infrared radiation - Urban areas.
3. Thermal radiation - Attenuation.
I. Schleiger, E.R.
II. Nichols, J.R.
III. Laughridge, F.I.
IV. Title.

UNCLASSIFIED

wavelengths 0.40, 0.50, 0.77 and 0.88μ (microns) with receiver fields of view up to 64 degrees half-angle. From these data attenuation coefficients were calculated for collimated transmission and aureoled transmission (4π source and flat receiver facing the source). Also calculated for aureoled transmission were values of R, the ratio of "scattered-in" radiation to direct radiation received by the flat receiver at various distances from the source. Angular scattering diagrams and attenuation coefficients for scattering were measured for radiation of wavelengths 0.40, 0.45, 0.50 and 0.55μ. Relations between these optical characteristics of the atmosphere and meteorological characteristics such as visibility, relative humidity, and contaminant contents were examined. Investigations of transmission variability with respect to both time and space were made. Curves were prepared from these and other experimental data showing transmittances of four typical atmospheres as a function of range for the case of flat receivers and radiation from a 4π black body source at 6000 degrees K.

UNCLASSIFIED

Naval Radiological Defense Laboratory
USNRDL-TR-554
TRANSMISSION AND SCATTERING PROPERTIES OF THE LOS ANGELES, CALIFORNIA ATMOSPHERE IN AUGUST AND SEPTEMBER 1960 by E.R. Schleiger, J.R. Nichols, and F.I. Laughridge
10 October 1961 100 p. tables illus. 27 refs.
UNCLASSIFIED

Measurements of peak irradiances have been made in Los Angeles, California, nighttime atmospheres at distances from 0.90 to 6.77 statute miles from a Xenon flashlamp radiating uniformly in all directions. The measurements were made at
(over)

1. Atmosphere - Radiation-scattering determination.
2. Infrared radiation - Urban areas.
3. Thermal radiation - Attenuation.
I. Schleiger, E.R.
II. Nichols, J.R.
III. Laughridge, F.I.
IV. Title.

UNCLASSIFIED

wavelengths 0.40, 0.50, 0.77 and 0.88μ (microns) with receiver fields of view up to 64 degrees half-angle. From these data attenuation coefficients were calculated for collimated transmission and aureoled transmission (4π source and flat receiver facing the source). Also calculated for aureoled transmission were values of R, the ratio of "scattered-in" radiation to direct radiation received by the flat receiver at various distances from the source. Angular scattering diagrams and attenuation coefficients for scattering were measured for radiation of wavelengths 0.40, 0.45, 0.50 and 0.55μ. Relations between these optical characteristics of the atmosphere and meteorological characteristics such as visibility, relative humidity, and contaminant contents were examined. Investigations of transmission variability with respect to both time and space were made. Curves were prepared from these and other experimental data showing transmittances of four typical atmospheres as a function of range for the case of flat receivers and radiation from a 4π black body source at 6000 degrees K.

UNCLASSIFIED

Naval Radiological Defense Laboratory
USNRDL-TR-554
TRANSMISSION AND SCATTERING PROPERTIES OF THE LOS ANGELES, CALIFORNIA ATMOSPHERE IN AUGUST AND SEPTEMBER 1960 by E.R. Schleiger, J.R. Nichols, and F.I. Laughridge
10 October 1961 100 p. tables illus. 27 refs.
UNCLASSIFIED

Measurements of peak irradiances have been made in Los Angeles, California, nighttime atmospheres at distances from 0.90 to 6.77 statute miles from a Xenon flashlamp radiating uniformly in all directions. The measurements were made at
(over)

1. Atmosphere - Radiation-scattering determination.
2. Infrared radiation - Urban areas.
3. Thermal radiation - Attenuation.
I. Schleiger, E.R.
II. Nichols, J.R.
III. Laughridge, F.I.
IV. Title.

UNCLASSIFIED

Naval Radiological Defense Laboratory
USNRDL-TR-554
TRANSMISSION AND SCATTERING PROPERTIES OF THE LOS ANGELES, CALIFORNIA ATMOSPHERE IN AUGUST AND SEPTEMBER 1960 by E.R. Schleiger, J.R. Nichols, and F.I. Laughridge
10 October 1961 100 p. tables illus. 27 refs.
UNCLASSIFIED

Measurements of peak irradiances have been made in Los Angeles, California, nighttime atmospheres at distances from 0.90 to 6.77 statute miles from a Xenon flashlamp radiating uniformly in all directions. The measurements were made at
(over)

1. Atmosphere - Radiation-scattering determination.
2. Infrared radiation - Urban areas.
3. Thermal radiation - Attenuation.
I. Schleiger, E.R.
II. Nichols, J.R.
III. Laughridge, F.I.
IV. Title.

UNCLASSIFIED

wavelengths 0.40, 0.50, 0.77 and 0.88μ (microns) with receiver fields of view up to 64 degrees half-angle. From these data attenuation coefficients were calculated for collimated transmission and aureoled transmission (4π source and flat receiver facing the source). Also calculated for aureoled transmission were values of R, the ratio of "scattered-in" radiation to direct radiation received by the flat receiver at various distances from the source. Angular scattering diagrams and attenuation coefficients for scattering were measured for radiation of wavelengths 0.40, 0.45, 0.50 and 0.55μ. Relations between these optical characteristics of the atmosphere and meteorological characteristics such as visibility, relative humidity, and contaminant contents were examined. Investigations of transmission variability with respect to both time and space were made. Curves were prepared from these and other experimental data showing transmittances of four typical atmospheres as a function of range for the case of flat receivers and radiation from a 4π black body source at 6000 degrees K.

UNCLASSIFIED

wavelengths 0.40, 0.50, 0.77 and 0.88μ (microns) with receiver fields of view up to 64 degrees half-angle. From these data attenuation coefficients were calculated for collimated transmission and aureoled transmission (4π source and flat receiver facing the source). Also calculated for aureoled transmission were values of R, the ratio of "scattered-in" radiation to direct radiation received by the flat receiver at various distances from the source. Angular scattering diagrams and attenuation coefficients for scattering were measured for radiation of wavelengths 0.40, 0.45, 0.50 and 0.55μ. Relations between these optical characteristics of the atmosphere and meteorological characteristics such as visibility, relative humidity, and contaminant contents were examined. Investigations of transmission variability with respect to both time and space were made. Curves were prepared from these and other experimental data showing transmittances of four typical atmospheres as a function of range for the case of flat receivers and radiation from a 4π black body source at 6000 degrees K.

UNCLASSIFIED

UNCLASSIFIED

Defense Threat Reduction Agency
45045 Aviation Drive
Dulles, VA 20166-7517

CPWC/TRC

May 6, 1999

MEMORANDUM FOR DEFENSE TECHNICAL INFORMATION CENTER
ATTN: OCQ/MR WILLIAM BUSH

SUBJECT: DOCUMENT REVIEW

The Defense Threat Reduction Agency's Security Office has reviewed and declassified or assigned a new distribution statement:

- AFSWP-1069, AD-341090, STATEMENT A — RD waiting for reply
- DASA-1151, AD-227900, STATEMENT A
- DASA-1355-1, AD-336443, STATEMENT A
- DASA-1298, AD-285252, STATEMENT A
- DASA-1290, AD-444208, STATEMENT A
- DASA-1271, AD-276892, STATEMENT A
- DASA-1279, AD-281597, STATEMENT A
- DASA-1237, AD-272653, STATEMENT A
- DASA-1246, AD-279670, STATEMENT A
- DASA-1245, AD-419911, STATEMENT A
- DASA-1242, AD-279671, STATEMENT A
- DASA-1256, AD-280809, STATEMENT A
- DASA-1221, AD-243886, STATEMENT A
- DASA-1390, AD-340311, STATEMENT A — FRD
- ~~DASA-1283, AD-717097, STATEMENT A~~ OK
- DASA-1285-5, AD-443589, STATEMENT A
- DASA-1714, AD-473132, STATEMENT A
- DASA-2214, AD-854912, STATEMENT A
- DASA-2627, AD-514934, STATEMENT A
- DASA-2651, AD-514615, STATEMENT A
- ~~DASA-2536, AD-876697, STATEMENT A~~
- DASA-2722T-V3, AD-518506, STATEMENT A
- DNA-3042F, AD-525631, STATEMENT A
- DNA-2821Z-1, AD-522555, STATEMENT A

If you have any questions, please call me at 703-325-1034.

Ardith Jarrett

ARDITH JARRETT
Chief, Technical Resource Center